Study on Improvement of Water Dispersibility of Terpenoids Using Nanoencapsulation Technology with Sub- and Supercritical Fluids

ZHANG Yelin

Study on Improvement of Water Dispersibility of Terpenoids Using Nanoencapsulation Technology with Sub- and Supercritical Fluids

2023

ZHANG Yelin

Graduate School of Engineering

Nagoya University

Contents

Chapter 1 Introduction

1.1 Introduction of terpenoids

Primary and secondary metabolites are the main classification of the organic compounds used for plants, animals, fungi and bacteria [1]. Basic living activities are adjusted by primary metabolites, and the secondary metabolites often cited as the "natural compounds" are responsible for the maintenance of various additional activities in plants, animals, fungi and bacteria [1]. As shown in **Table 1.1**, terpenes or terpenoids are categorized in secondary metabolites. Terpenes are derived from many assembled isoprene units (C_5H_8), and terpenoid refers to terpene with functional groups and oxidized methyl group [2]. The classification of terpenes by the number of isoprene units was shown in **Figure 1.1**. Broadly speaking, isoprenoids or terpenoids are used as the general term for terpenes and terpenoids.

It is reported that around 55,000 types of terpenoids with different structures and biological effects have been found and it is the vastest classification of compounds occurred in nature with the hugest diversities [3-5]. Previous researches have reported that terpenoids possess various physiological effects depending on its structures, such as anti-inflammatory, antibacterial, anticancer and anticonvulsant [3, 4, 6]. Moreover, it is noted that compared with the synthesized drugs with strong side effects, the naturally-derived compounds are considered as alternative drugs for diseases with less side effects [4]. Thus, terpenoids with various structures and biological effects are been universally studied. However, it is reported that the majority of found terpenoids are unstable and insoluble in water, and in order to use it in pharmaceutical areas, encapsulation technology is often considered to improve its physiochemical properties.

Table 1.1 Classification of organic compounds of naturally-occurring compounds and its roles in living things [1, 5, 7].

	Roles in living things	Classification
Primary metabolites	Growth, development, production growth	Proteins, carbohydrates, lipids, nucleic acids
Secondary metabolites	Maintenance of various activities (Such as activities responsible for aroma, flavor, and color of plants)	Terpenoids, alkaloids, shikimates, polyketides

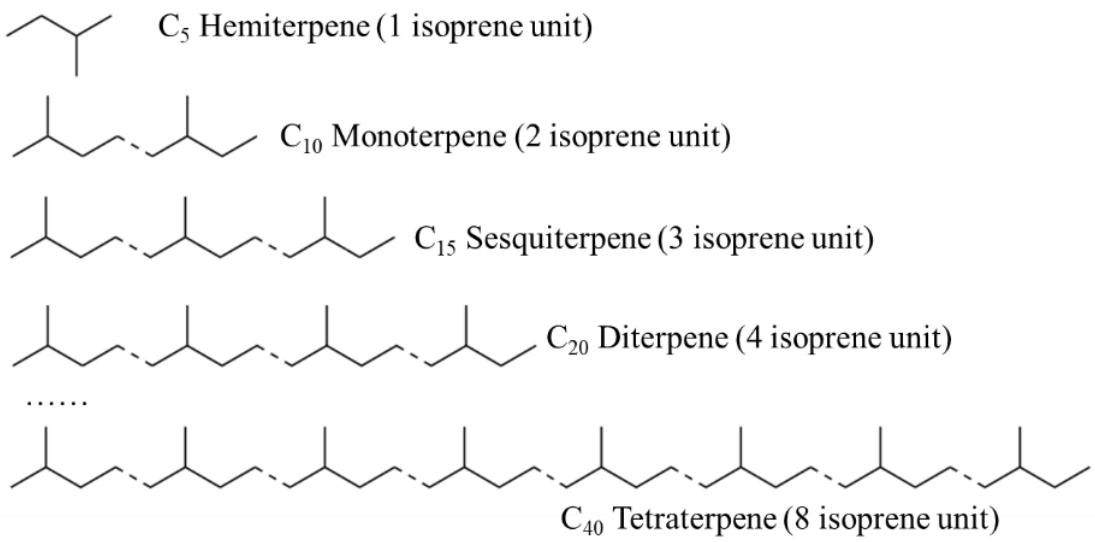

Figure 1.1 The classification of terpenes by the number of isoprene units [2].

1.2 Nanoencapsulation technology

As mentioned previously, to utilize water-insoluble and unstable compounds in pharmaceutical, food and cosmetic industries, the encapsulation technology is commonly used. Encapsulation technology is a technology that encapsulates the core material bioactive compounds) into the shell of wall material (such as polymer, emulsifier) to mask its unpleasant taste or odor, improve the water-solubility and the stability of core compounds, or to get the controlled release of main materials [8]. Micro / nano-encapsulation is an encapsulation technology being able to produce particles in micro-level or nano-level size. It is proposed that particles produced by nanotechnology is in range of 1–1000 nm [9]. Encapsulation can enhance the stability of core compounds during various storage conditions (such as light, temperature, pH, and oxygen) [10]. Many researches have reported that the encapsulation of water-insoluble compounds with wall materials can enhance its vitro solubility of main compounds in various environments [11-13]. It is reported that thin wall material or highly-loaded core compounds can lead to fast release of core compounds and less protection of core compounds [14].

Generally, the common size of prepared capsules by encapsulation are distributed in 1–1000 μm, but some technology can produce capsules with average size ranging from approximately 5 nm to 1000 nm, such as capsules of emulsifier (nanoemulsions) with particle size of 5–20 nm, capsules of liposome with particle size of 100–1000 nm [14-17]. The emulsifier-based nanoemulsions are called as nanodispersions [18]. Moreover, size reduction of produced capsules can improve its aqueous solubility and further improve its bioavailability in human body [19].

According to preparation mechanism, encapsulation technology can be classified into 3 types: chemical, physico-chemical, and physical as shown in **Table 1.2** [8, 17]. Compared with the conventional methods such as spray drying technology, freeze drying technology, encapsulation technology using subcritical or supercritical fluids are attracting attentions. Some researchers have addressed the problems about the hardness to control the size of produced microcapsules prepared by freeze-drying and spray-drying [20, 21]. Contrary to these methods, encapsulation technology using supercritical

fluids can finely tailor the size and uniformness of produced capsules by adjusting the parameters (temperature, pressure, flow rate, etc.) slightly [20, 22].

Table 1.2 Classification of encapsulation technology [8, 17].

Classification	Methods
Chemical	In situ polymerization
	Liposomes
Physico-chemical	Coacervation
	Sol-gel encapsulation
Physical	Emulsification
	Freeze drying
	Spray drying
	Fluidized bed coating
	Encapsulation by sub/supercritical fluid

1.3 Supercritical and subcritical fluids

In 1822, Baron Charles Cagniard de la Tour, as an French engineering and physicist found critical point in his experiments using cannon barrel [23]. Until the 1950s, supercritical fluid was started to be considered as a solvent in industrial processing. In 1982, the application of supercritical carbon dioxide (SC-CO_2) in the extraction of fresh hops in Germany is reported to be the first industrial use of supercritical fluid [24, 25]. Gradually, SC-CO_2 is being utilized into the separation of nicotine from tobaccos and caffeine from coffee beans, and processing of various spices, medicines or even waste water.

It can be found out that in diverse supercritical fluids, SC-CO_2 is a commonly used one in food and pharmaceutical industries. It is greatly related with its relatively low critical points as shown in **Table 1.3** and **Figure 1.2**, non-flammable, and relatively inert properties of CO_2. Moreover, compared with common organic solvents, by adjusting temperature and pressure of CO_2 system, the density of CO_2 can be easily adjusted in a broad scale as shown in **Figure 1.3**. Subsequently, the solubility of solute in SC-CO_2 can be greatly adjusted, and this property can be used to separate solutes from SC-CO_2 or to separate different solutes with different solubilities in SC-CO_2 by slight decomposition. However, due to the low molecular weight and low polarity of CO_2,

SC-CO_2 shows limits in dissolving large molecular compounds or polar compounds. Furthermore, to get high process efficiency, SC-CO_2 with the pressure set in range of 50–100 MPa is gradually investigated, and it is reported that the solubilities of large molecular compounds such as curcumin and carotene in SC-CO_2 are markedly improved around 50 MPa [26]. Conversely, the apparatus cost increases greatly as operation pressure increases.

Gradually, "subcritical fluids" which are pressurized solvents with temperature higher than boiling point and lower than critical temperature, are begun to be studied because of their good solvent power [27]. Subcritical water is the commonly investigated subcritical fluid, but the use of it in unstable and easily-decomposed compounds is limited as high pressure and temperature are normally required which could lead to high decomposition rate of these compounds. Therefore, for production of food, cosmetics, and medicine, the use of ethyl acetate and ethanol is prospective due to its low toxicity and high solubility towards these compounds.

Table 1.3 Critical temperature and pressure of some common solvents [28, 29].

Solvent	Molecular formula	Critical temperature (°C)	Critical pressure (MPa)
Carbon dioxide	CO_2	31.0	7.4
Water	H_2O	374.0	21.8
Methane	CH_4	-82.6	4.6
Propane	$CH_3CH_2CH_3$	96	4.3
Dimethyl ether	CH_3OCH_3	127.9 ± 2.0	5.4 ± 0.3
Methanol	CH_3OH	240.2	8.2
Ethanol	CH_3CH_2OH	240.8	6.3
Ethyl acetate	$CH_3COOCH_2CH_3$	356.9 ± 20.0	4.0 ± 0.2

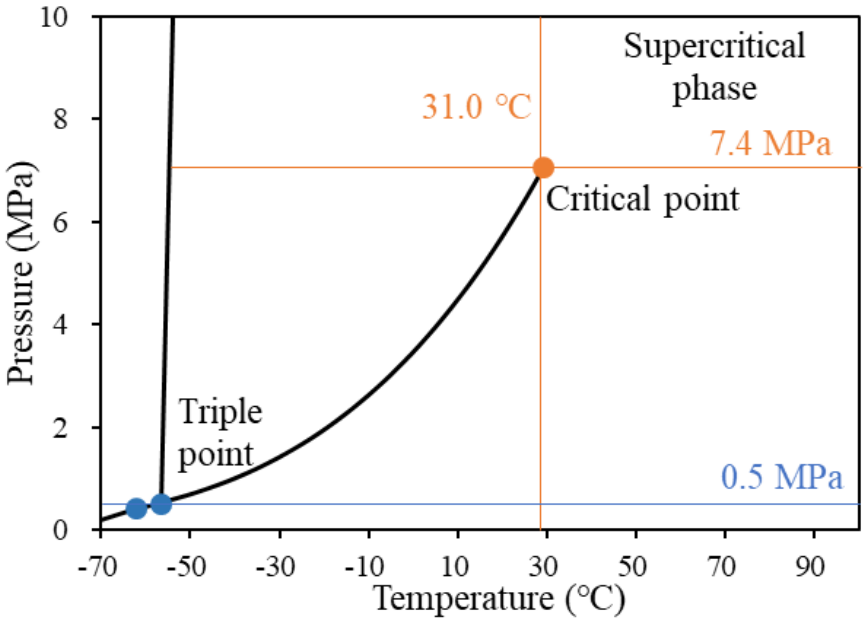

Figure 1.2 Phase diagram of CO_2.

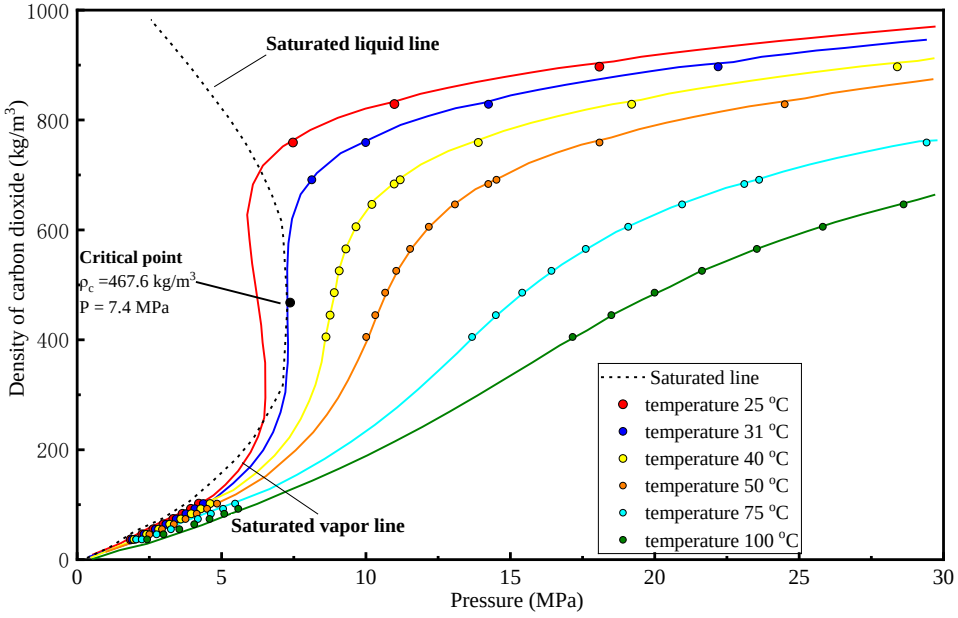

Figure 1.3 Variation of carbon dioxide density with pressure and temperature.

1.4 Purpose of this research

The main purpose is to improve the water dispersibility of two-type terpenoids by nanoencapsulation technology using subcritical and supercritical fluids. The exact research objectives are as follows:

1. To optimize the extraction conditions of getting SCG extract rich in diterpenes using ethanol-modified SC-CO_2, and to encapsulate SCG extract rich in diterpenes into nanoparticles of hydrophilic polymer to improve its water dispersibility in Chapter 2;

2. To simplify the production processes of producing *Z*-isomer-rich β-carotene nanodispersions by adding *Z*-isomerization-accelerating catalyst using ultrasound-assisted SC-CO_2 in Chapter 3;

3. To develop a continuous production system to prepare *Z*-isomer-rich β-carotene nanodispersions by a swirl-type mixer using subcritical ethyl acetate as the dissolving solvent in Chapter 4.

References:

[1] Charles, S. S., A Fragrant Introduction to Terpenoid Chemistry. The Royal Society of Chemistry: 2003.

[2] Perveen, S., Introductory Chapter: Terpenes and Terpenoids. In *Terpenes and Terpenoids*, Shagufta, P.; Areej, A.-T., Eds. IntechOpen: London, 2018; pp 1 - 12.

[3] Prakash, V., TERPENOIDS AS SOURCE OF ANTI-INFLAMMATORY COMPOUNDS. *Asian Journal of Pharmaceutical and Clinical Research,* **2017**, *10* (3), 68-76.

[4] Del Prado-Audelo, M. L.; Cortés, H.; Caballero-Florán, I. H.; González-Torres, M.; Escutia-Guadarrama, L.; Bernal-Chávez, S. A.; Giraldo-Gomez, D. M.; Magaña, J. J.; Leyva-Gómez, G., Therapeutic Applications of Terpenes on Inflammatory Diseases. *Frontiers in Pharmacology,* **2021**, *12*, 60-77.

[5] Destinney Cox-Georgian; Niveditha Ramadoss; Chathu Dona; Basu, C., *Therapeutic and Medicinal Uses of Terpenes*. Medicinal Plants. 2019 Nov 12:333-59. doi: 10.1007/978-3-030-31269-5_15.

[6] Serrano Vega R. J.; Campos Xolalpa N.; Castro Alonso J. A.; González Pérez C.; Pérez Ramos J.; S., P. G., Terpenes from Natural Products with Potential Anti-Inflammatory Activity. In *Terpenes from Natural Products with Potential Anti-Inflammatory Activity*, Shagufta, P.; Areej, A.-T., Eds. IntechOpen: London, 2018; pp 61 - 77.

[7] Eastman, R. H. Isoprenoid. https://www.britannica.com/science/isoprenoid (accessed September 26, 2022).

[8] Peanparkdee, M.; Iwamoto, S.; Yamauchi, R., MICROENCAPSULATION: A REVIEW OF APPLICATIONS IN THE FOOD AND PHARMACEUTICAL INDUSTRIES. *Reviews in Agricultural Science,* **2016**, *4*, 56-65.

[9] Paredes, A. J.; Asensio, C. M.; Llabot, J. M.; Allemandi, D. A.; Palma, S. D., Nanoencapsulation in the food industry: manufacture, applications and characterization. *Journal of Food Bioengineering and Nanoprocessing,* **2016**, *1* (1), 56-79.

[10] Domínguez, R.; Pateiro, M.; Munekata, P. E. S.; McClements, D. J.; Lorenzo, J. M., Encapsulation of Bioactive Phytochemicals in Plant-Based Matrices and Application as Additives in Meat and Meat Products. *Molecules (Basel, Switzerland),* **2021**, *26* (13).

[11] Varona, S.; Fernández, J.; Rossmann, M.; Braeuer, A., Solubility of Paracetamol and Polyvinylpyrrolidone in Mixtures of Carbon Dioxide, Ethanol, and Acetone at Elevated Pressures. *Journal of Chemical & Engineering Data,* **2013**, *58* (4), 1054-1061.

[12] El-Gazayerly, O. N., Characterization and Evaluation of Tenoxicam Coprecipitates. *Drug Development and Industrial Pharmacy,* **2000**, *26* (9), 925-930.

[13] Mura, P.; Faucci, M. T.; Manderioli, A.; Bramanti, G.; Parrini, P., Thermal Behavior and Dissolution Properties of Naproxen From Binary and Ternary Solid Dispersions. *Drug Development and Industrial Pharmacy,* **1999**, *25* (3), 257-264.

[14] Van Tran, V.; Moon, J.-Y.; Lee, Y.-C., Liposomes for delivery of antioxidants in cosmeceuticals: Challenges and development strategies. *Journal of Controlled Release,* **2019**, *300*, 114-140.

[15] Choudhury, N.; Meghwal, M.; Das, K., Microencapsulation: An overview on concepts, methods, properties and applications in foods. *Food Frontiers,* **2021**, *2* (4), 426-442.

[16] Ozkan, G.; Franco, P.; De Marco, I.; Xiao, J.; Capanoglu, E., A review of microencapsulation methods for food antioxidants: Principles, advantages, drawbacks and applications. *Food Chemistry,* **2019**, *272*, 494-506.

[17] Mehta, N.; Kumar, P.; Verma, A. K.; Umaraw, P.; Kumar, Y.; Malav, O. P.; Sazili, A. Q.; Domínguez, R.; Lorenzo, J. M., Microencapsulation as a Noble Technique for the Application of Bioactive Compounds in the Food Industry: A Comprehensive Review. *Applied Sciences,* **2022**, *12* (3), 1424.

[18] 1. Nanodispersions – general introduction. In *Nanodispersions*, De Gruyter: Berlin, Boston, 2015; pp 1-10.

[19] Hussain, K.; Qamar, A.; Bukhari, N. I.; Hussain, A.; Shehzadi, N.; Qamar, S.; Parveen, S., Impact of Particle-Size Reduction on the Solubility and Antidiabetic Activity of Extracts of Leaves of *Vinca rosea*. *TURKISH JOURNAL OF PHARMACEUTICAL SCIENCES,* **2019**, *16* (3), 335-339.

[20] Klettenhammer, S.; Ferrentino, G.; Morozova, K.; Scampicchio, M., Novel Technologies Based on Supercritical Fluids for the Encapsulation of Food Grade Bioactive Compounds. *Foods,* **2020**, *9* (10), 1395.

[21] Bernard F. Gibbs; Selim Kermasha; Inteaz Alli; Mulligan, C. N., Encapsulation in the food industry: a review. *International Journal of Food Sciences and Nutrition,* **1999**, *50* (3), 213-224.

[22] Soh, S. H.; Lee, L. Y., Microencapsulation and Nanoencapsulation Using Supercritical Fluid (SCF) Techniques. *Pharmaceutics,* **2019**, *11* (1), 21.

[23] Yasuhiko, A., *Fundamentals and Applications of Supercritical Fluids*. TECHNOSYSTEM Co.,Ltd.: 2002.

[24] Phelps, C. L.; Smart, N. G.; Wai, C. M., Past, Present, and Possible Future Applications of Supercritical Fluid Extraction Technology. *Journal of Chemical Education,* **1996**, *73* (12), 1163.

[25] Beckman, E. J., Supercritical and near-critical CO_2 in green chemical synthesis and processing. *The Journal of Supercritical Fluids,* **2004**, *28* (2), 121-191.

[26] Motonobu, G., 躍進する超臨界流体技術—新しいプロセスの原理とその実用化. CORONA PUBLISHING CO., LTD.: **2014**.

[27] Srinivas, K.; King, J. W.; Monrad, J. K.; Howard, L. R.; Hansen, C. M., Optimization of Subcritical Fluid Extraction of Bioactive Compounds Using Hansen Solubility Parameters. *Journal of Food Science,* **2009**, *74* (6), E342-E354.

[28] The Engineering Toolbox. https://www.engineeringtoolbox.com/ (accessed Spetember 6, 2022).

[29] National Institute of Standards and Technology. https://www.nist.gov/ (accessed September 6, 2022).

Chapter 2 Extraction of diterpenes from spent coffee grounds and encapsulation into polyvinylpyrrolidone particles using supercritical carbon dioxide

2.1 Introduction

2.1.1 Diterpenes in spent coffee grounds

The global popularity of coffee drink can contribute to its special flavor and caffeine content. It is reported that the annual coffee consumption amount was 167.23 million bags (60 kilograms per bag) [1]. What comes with the popularity of coffee drinks is the greatly increasing amount of coffee beans side-product—spent coffee grounds (SCGs), and it is reported that based on the weight of coffee beans, SCG accounts for ~45%–50% [2]. Normally, SCGs are dumped into landfills, but it is reported that it could lead to soil pollution due to the presence of caffeine, tannins in it [3]. What's more, except the greenhouse gas—methane, SCG also produces carbon dioxide approximately 1.6-fold that produced by black tea [4]. Even though a huge amount of SCGs was generated annually, there is no established system to recycle and dispose of them yet.

It is reported that SCG can be used to dye paper, clothes, or retouch furniture due to the mordanting effect of tannins with wool fabrics [5]. Except the research about the direct use of SCG, notable number of lipids, flavonoids, polyphenols and diterpenes in SCG are reported, and the possibility to use these compound is attractive to various areas [2]. For instance, during processes of handling and storing food products, polyphenols with antioxidant ability can be used to inhibit the propagation reaction in oxidation reaction and leads a vital part in food industry [6]. SCG is considered to be a crucial source of polyphenols [7]. The compound extracted from SCG accounts for 10–27.8 wt.% of SCG weight, and it depends on the species of coffee beans, as well as roasting and coffee brewing methods [7-10]. Triglycerides (~75.2 wt.%) and diterpenes (~18.5 wt.%) is the main contents of SCG extract [11-13]. The naturally-existed diterpenes in coffee bean are cafestol and kahweol and these two compounds are categorized as pentacyclic diterpene alcohols [14]. In coffee beans, most cafestol and kahweol existed in esterified state, such

as cafestol or kahweol esters, and only a very small ratio of diterpenes exists as free diterpenes [14]. Various derivatives of cafestol and kahweol in SCGs have been revealed in previous studies [15]. Indeed, in coffee beans, cafestol and kahweol are reported to be the major contents effective in preventing chronic diseases [16]. The contents of cafestol and kahweol contents extracted from SCGs by various methods are listed in **Table 2.1.1**. It can be found that cafestol content varies from 9.43 to 32.06 mg/g SCG extract, and the kahweol content varies from 6.22 to 47.57 mg/g SCG extract, which indicates that the contents of cafestol and kahweol are strongly dependent on the sources of the SCG [7, 9, 17]. Cafestol and kahweol exhibit anti-inflammatory, antioxidative, anticancer, and chemo-protective activities. Thus, they are reported to be highly prospective to be used in functional foods and multitarget medicines [2, 18, 19]. Moreover, cafestol and kahweol from the SCG can be used as anti-aging products in the cosmetic industry because of their antioxidant activities.

Table 2.1.1 SCG extraction yield wt.%, cafestol content and kahweol content (mg/g SCG extract) in SCG by various extraction methods.

Extraction	Solvent/ conditions	Extraction yield* (g/g SCG extract)	Cafestol content*(mg/g SCG extract)	Kahweol content*(mg/g SCG extract)	Reference
Soxhlet	Hexane	26.4	9.43	6.22	[7]
SC-CO_2	40 ℃/ 9.8 MPa	1.48	13.99	7.70	[7]
SC-CO_2	80 ℃/ 25 MPa	6.95	17.87	16.87	[8]
SC-CO_2	55 ℃/ 14 MPa	4.61	32.06	47.57	[9]

* Extraction yield, cafestol content and kahweol content were calculated under dry SCG weight.

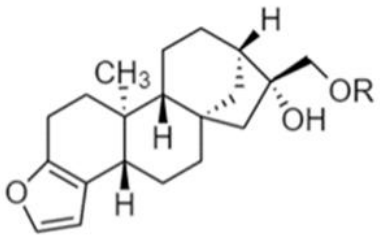

R=H: Cafestol **1**
R= fatty acid: Cafestol esters **2**

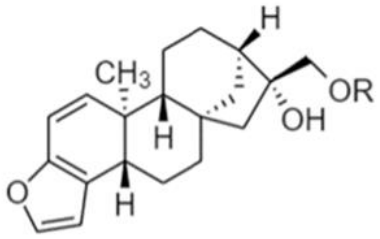

R=H: Kahweol **3**
R=fatty acid: Kahweol esters **4**

Figure 2.1.1 Main two-type diterpenes in coffee beans: (**1**) Cafestol, (**2**) Cafestol esters, (**3**) Kahweol, (**4**) Kahweol esters.

2.1.2 Extraction using ethanol modified supercritical carbon dioxide

Plant is regarded as a source of numerous compounds with bioactive activities in nature. The method of extracting plant essence by hot water is considered as the traditional extraction method which has been developed since ancient times. Nowadays, the plant-derived bioactive compounds still play a crucial role in pharmaceutical, food and cosmetic industries. Generally, extraction technology can be approximately categorized into pressing extraction, solvents extraction, microwave or ultrasound-assisted extraction [20]. The solvent extraction can be further divided into organic solvents extraction, and sub/supercritical extraction like subcritical ethanol extraction. Normally, extraction using *n*-hexane or petroleum ether was considered as a standard way to measure total amounts of bioactive components in plants and is commonly utilized to extract diterpenes from coffee beans [14].

However, for the industries of food, cosmetics and medicine, the utilization of these organic solvents is strictly limited. In contrast, SC-CO_2 has been declared as a safe and environmentally friendly solvent by various government constitutes [21]. In addition to the moderate critical point of CO_2, which exhibits changeable density and high diffusivity in large range and, is a good substitute for these organic solvents. Moreover, thanks to the low boiling point of carbon oxidate, SC-CO_2 can be effortlessly separated from final products. In addition, the changeable density relating with the solvent power

of SC-CO_2 gives its high selectivity toward certain compounds compared with conventional organic solvents. It is reported that compared with the extraction results of petroleum ether 30% more pyrethrin is extracted by SC-CO_2 [22]. Moreover, extract obtained by SC-CO_2 extraction showed higher antioxidant activities than those got by Soxhlet extraction or ultrasound-assisted extraction [23]. Therefore, SC-CO_2 is considered as a superior substitute to conventional organic solvents towards the extraction of plant-derived compounds used for food, cosmetic, and pharmaceutical industries without polluting the environment and final products.

As mentioned previously, to improve the performance of SC-CO_2 extraction process, ethanol is commonly used modifier to increase polarity of extraction solvents [24, 25]. Normally, modifier inhibits higher polarity than SC-CO_2. Araújo et al. reported that ethanol addition can enhance coffee oil recovery amount compared with SC-CO_2 and pressurized ethanol at the same pressure and temperature [26].

2.1.3 Encapsulation by supercritical anti-solvent crystallization

Like essential oils, the hydrophobicity of SCG extract containing diterpenes might limit its utilization in various areas [27]. Moreover, it is revealed by Speer et al. that cafestol and kahweol in the SCG extract are sensitive to acids, light, and heat; in particular, kahweol is unstable when it exists as a free diterpene [14]. Encapsulation technology using SC-CO_2 was used to improve dispersibility in water and stability of valuable contents in SCG extract in this study. It is noted that encapsulating oil with edible hydrophilic polymers can improve its water dispersibility and the bioavailability [27, 28].

Owing to its high solvability in water, polyvinylpyrrolidone (PVP) is broadly applied in the encapsulation of plant-derived oils. In this research, hydrophilic PVP was chosen as the wall material to encapsulate SCG extract. In PVP particles, intermolecular hydrogen bonds can be formed between the carbonyl groups of PVP, and hydroxyl groups in diterpenes, and the stability of these compounds can be enhanced [29, 30]. Supercritical antisolvent crystallization (SAS) technology was used to encapsulating the SCG extract into PVP particles. SAS is a widely used method for forming fine

particles, where SC-CO_2 is used as an antisolvent. Precisely speaking, by dispersing organic solvent drops containing solutes into SC-CO_2, owing to the high solvability of SC-CO_2 with various organic solvents, these two solvents dissolved in each other. Subsequently, the solvent power of mixed solvents for solutes will be greatly decreased and it leads to the fast supersaturation of the solutes in mixed solvents. Finally, solute precipitates from the system to form fine particles, and the organic solvents are brought out from the system together with SC-CO_2. Moreover, the particle shape and size can be regulated by tuning the operation conditions, such as pressure, temperature, types of organic solvents, concentration of solutes, and feed solution flow rate.

2.1.4 Response surface methodology

There are several studies that has reported about the extraction of coffee diterpenes and lipids from SCG using unmodified or ethanol-modified SC-CO_2 [7, 9, 11, 31]. However, a systematic extraction process preformed in a wider range of pressure and temperature is required to obtain an overall understanding of the SCG extraction performance. The response surface methodology (RSM) can optimize the extraction process using SC-CO_2 because of its ability to define the effect of single or combined independent variables on response variables [32]. It optimizes biochemical processes, such as that response surface contours are used to get the best experimental conditions to extract alkaline protease from *Bacillus mojavensis*, limonene from orange peel, and peanut skin oil from peanut skin [33-36].

2.1.5 Research objectives

In this research, the design of Box–Behnken design (BBD) was taken to investigate the influences of experimental conditions: temperature (40–80 °C), pressure (10–30 MPa), and ethanol ratio (0%–10% v/v) pertaining to the extraction yield wt.%, and total diterpene content (mg/g SCG extract) using SC-CO_2. Based on the experimental design, optimal operation conditions for SCG extraction yield and total diterpene (cafestol and kahweol) content using SC-CO_2 were predicted, separately.

The brief graph of research flow is shown in **Figure 2.1.2**. After the optimization of operation conditions of SCG extraction process, the SAS method is used to encapsulate SCG extract rich in diterpenes into PVP nanoparticles to improve its water dispersibility.

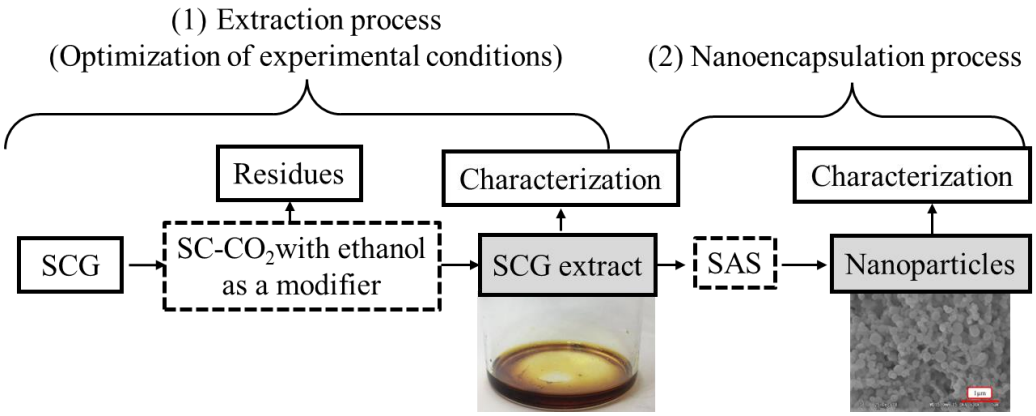

Figure 2.1.2 Process scheme: (1) Extraction process of SCG and optimization of experiment conditions; (2) Nanoncapsulation process for producing nanoparticles of SCG extract/PVP using SAS method.

2.2 Materials and methods

2.2.1 Materials and chemicals

SCGs were collected in a convenience store's vending machine in Japan, and the original coffee beans were regular commercial coffee beans provided by Ueshima Coffee Co., Ltd. (UCC, Tokyo, Japan). Polyvinylpyrrolidone (PVP; molecule weight: 29,000), gallic acid, and Folin-Ciocalteu's agent solution were produced by Sigma-Aldrich (St. Louis, MO, USA). Ethanol (> 99.5%), acetone (> 99.5%), hexane (> 99.9%), dimethyl ether (> 99.5%), methanol (> 99.7%), acetonitrile (> 99.8%), sodium chloride, sodium carbonate, and potassium hydroxide were produced by FUJIFILM Wako Pure Chemical Corporation (Osaka, Japan). Cafestol and kahweol standards were purchased from Cayman Chemical (MI, USA). Pure distillation water was used in all the procedures. Carbon dioxide (purity 99%) was produced by TOMOE Shokai, Inc. (Tokyo, Japan).

2.2.2 Extraction using ethanol modified supercritical carbon dioxide

The experimental apparatus used for semi-batch extraction process using SC-CO_2 with or without addition of ethanol as a modifier is shown in **Figure 2.2.1**. A freeze-drying machine (EYELA, FDU-1200, Tokyo, Japan) at a temperature of −45 °C was used to dry the SCG. Initially, 3 g of SCG was loaded in the middle of the stainless-steel extractor (volume: 10 mL; Thar Tech, Inc., PA, USA), and a certain number of small beads made of glass was placed on the two-end side of reactor to prevent SCG from escaping the extractor. The extractor was then connected to the system and preheated to certain temperature ranging in 40–80 °C by an oven (ST-110, ESPEC, Osaka, Japan). Liquid CO_2 was cooled by a chiller (EYELA Co. Ltd., Tokyo, Japan) and pumped in an up-flow mode into the extractor at 5 mL/min by the pump (PU-2080, JASCO, Tokyo, Japan). When CO_2 was pumped into the extraction system, ethanol in the range of 0%–10% v/v (0–0.5 mL/min) was pumped into the system using an ethanol pump (260D, Teledyne ISCO, NE, USA) and mixed with CO_2 in a solvent mixer (Swagelok, OH, USA). Accordingly, the mixed solvent was preheated to the desired temperature using a coil preheater. The pressure of the system was controlled within the range of 10–30 MPa using a pressure regulator in the back (BPR; AKICO Co. Ltd., Tokyo, Japan) and observed using a pressure gauge meter (MIGISHITA SEIKIMFG. Co. Ltd., Hyogo, Japan). After the desired pressure was achieved, the CO_2 and ethanol pumps were stopped simultaneously, and the extraction system was maintained at determined temperature and pressure for half an hour. After 30 min, the pumps were started again. The extraction process was maintained for 180 min, and the recovery vial for collecting the SCG extract after the BPR was changed every 60 min. Finally, both the pumps were stopped, and the pressure was slowly released through the BPR.

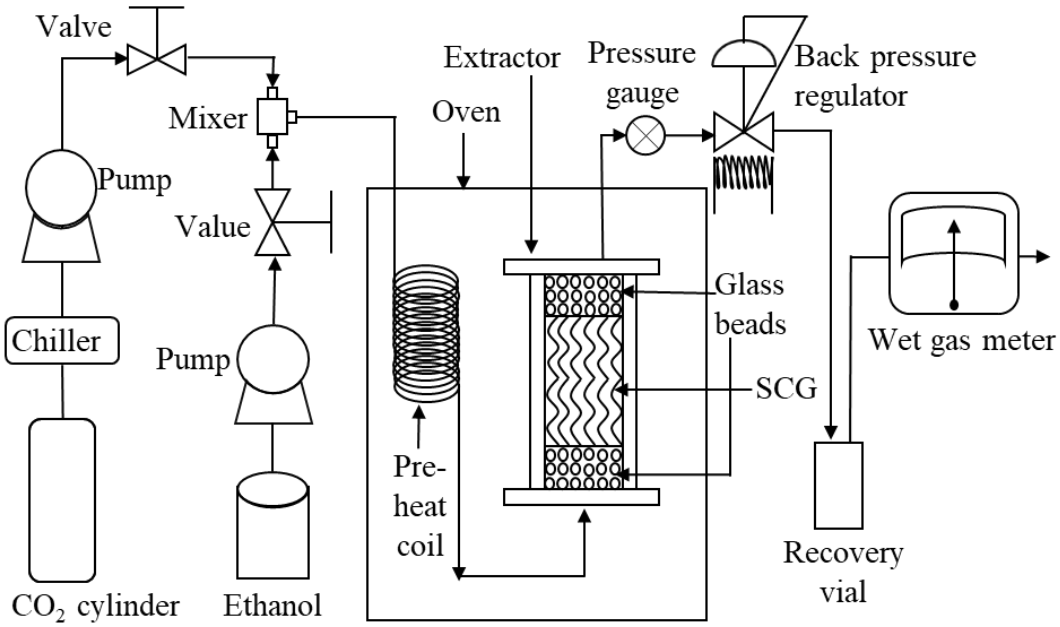

387

388 **Figure 2.2.1** Schematic diagram SC-CO_2 extraction with or without ethanol addition
389 as a modifier.

390

391 **2.2.3 Experimental design of extraction process**

392 The effects of independent variables—temperature (X_1), pressure (X_2), and ethanol
393 ratio (X_3)) on the dependent variables (extraction yield (Y_1), total diterpene content
394 (Y_2)) were investigated. The real and coded values of temperature (X_1), pressure (X_2),
395 and ethanol ratio (X_3) are listed in **Table 2.2.1**. Owing to the status of the pump, the
396 flow rate of pump for ethanol solution was fixed in 0.3 mL/min, but it was calculated
397 as 0.25 mL/min and coded as 0 in the Box–Behnken design (BBD). Fifteen runs of
398 experiments were conducted with 3 central points (**Table 2.2.2**). The total phenolic
399 content (TPC) in SCG extract was determined in every single run to help to determine
400 the components of the SCG extract. Unit of TPC is mg GAE/g SCG extract, referring
401 to similar antioxidant ability owned by this weight of gallic acid. How extraction yield
402 wt.% (Y_1) and the total diterpene content (mg/g SCG extract) were calculated were
403 shown in **equation (1)** and **(2),** respectively.

$$Extraction\ yield\ wt.\% = \frac{weight\ of\ SCG\ extract(g)}{weight\ of\ dry\ SCG\ (g)} \times 100\% \qquad \textbf{Equation (1)}$$

$$Total\ diterpenes\ content\ \left(\frac{mg}{g\ SCG\ etxract}\right) = \frac{(weight\ of\ cafestol + weight\ of\ kahweol)(mg)}{weight\ of\ \ SCG\ extract\ (g)} \qquad \textbf{Equation (2)}$$

Table 2.2.1 List of independent variables and the code of it in calculation.

Independent variables	Symbol	Code values		
		−1	0	1
		Real values		
Temperature (°C)	X_1	40	60	80
Pressure (MPa)	X_2	10	20	30
Ethanol ratio %v/v	X_3	0	5	10

Table 2.2.2 SCG extraction results using SC-CO_2 with ethanol as a modifier: extraction yield (wt.%, Y_1), total diterpene content consisting of cafestol content and kahweol content (mg/g SCG extract, Y_2), total polyphenolic content (TPC).

Run	X_1	X_2	X_3	Y_1	Y_2			TPC
					Cafestol	Kahweol	Diterpenes	
1	−1	−1	0	8.96	28.14	34.84	62.97	112.74
2	1	−1	0	12.26	32.90	41.40	74.30	139.50
3	−1	1	0	14.90	2.49	3.03	5.52	132.10
4	1	1	0	15.01	35.01	43.18	78.19	121.67
5	0	−1	−1	2.57	0.00	0.00	0.00	6.79
6	0	−1	1	14.41	25.76	31.78	57.54	137.64

7	0	1	−1	8.94	17.34	20.81	38.15	113.27
8	0	1	1	18.39	35.14	42.71	77.84	141.49
9	−1	0	−1	10.29	31.14	38.02	69.17	108.36
10	−1	0	1	17.59	1.80	2.21	4.01	135.01
11	1	0	−1	6.22	38.79	45.95	84.74	109.73
12	1	0	1	14.20	29.15	35.98	65.14	135.14
13	0	0	0	10.76	29.57	36.42	65.99	147.19
14	0	0	0	8.88	24.71	30.52	55.23	121.77
15	0	0	0	10.80	34.93	43.00	77.93	119.92
Soxhlet		*n*-hexane		15.42	2.73	3.38	6.11	-

2.2.4 Characterization of SCG extract

Saponification of the SCG extract

As mentioned previously, in coffee beans, the majority of cafestol and kahweol are maintained in esterification state. To analyze cafestol and kahweol amount in extracted SCG, saponification is required to isolate cafestol and kahweol with fatty acids. The saponification procedure was performed as described previously [37]. Initially, two-milliliter KOH ethanol solution with concentration at 1M was mixed with SCG extract (~0.05 g) and heated in water bath for an hour at 80°C. Then, five-milliliter diethyl ether was put into mixed solution. Centrifugation at 3000 rpm for five-minute was carried out with mixed solution. Insoluble compounds in mixed solution were separated with organic solvents. Subsequently, the organic solvent was removed and another five-milliliter diethyl ether was put into centrifugation tube. Insoluble compounds remained were washed by diethyl ether. This washing procedure was repeated two to three times until the organic solvent became colorless. Then, three-milliliter NaCl water solution with concentration at 2 M was added to collected organic solvents, and organic layer in the upper phase was collected. Three to four times repetitions of this process were

performed until organic phase became colorless. Later, the collected organic solvent was dried in N_2 atmosphere. The obtained solid compounds after drying were dissolved in acetone. Finally, the insoluble compounds in the acetone solution were removed using No. 5 B filter paper (95 mm, Kiriyama, Tokyo, Japan) with a suction filter. The filtered acetone solution was diluted into a certain volume and injected into the HPLC system to get the quantification of cafestol and kahweol.

Determination of cafestol and kahweol

Reversed-phase chromatography was used to quantify cafestol and kahweol. A column comprising a Cosmosil-C_{18}-MS-II guard column (5 μm, 4.6ID × 10 mm, Cosmosil, Kyoto, Japan) and a Cosmosil 5C_{18}-PAQ packed column (5 μm, 4.6ID × 250 mm, Cosmosil, Kyoto, Japan) was applied. A diode array detector (SPD-M10A, Shimadzu, Kyoto, Japan), system controller (CBM-20A, Shimadzu, Kyoto, Japan), a pump (LC-20AD, Shimadzu, Kyoto, Japan), and an autosampler (SIL–10 AF, Shimadzu, Kyoto, Japan) were used. Solution of acetonitrile: water (45:55 v/v) was applied as the mobile phase at 1 mL/min. The temperature of HPLC column was maintained at 40 °C. Cafestol was detected at 230 nm and kahweol was detected at 285 nm [37]. To calculate the concentration of cafestol and kahweol in extract, standards (purity ≥ 98%) of these two compounds with five different concentrations were prepared and analyzed. Then, the calibration curves of peak areas as a function of the concentrations of cafestol and kahweol were drawn to calculate concentrations of them in the SCG extract. The correlation coefficients of both the calibration curves were greater than 0.99.

Determination of total phenolic content

Total phenolic content in SCG extract was determined by Folin-Ciocalteu assay according to our lab's earlier study by Chhouk K. et al. [38]. Briefly, SCG extract was dissolved in ethanol and concentration of it was set approximate ~0.1 mg/mL. Then, 1 mL Folin-Ciocalteu solution and 1 mL ethanol solution of the SCG extract were mixed. The prepared mixture solution was placed in dark for 5 min. Then, 1 mL of 7.5 wt.% Na_2CO_3 and 7 mL ethanol were put into previous solution, and the prepared solution was placed in place without light for 150 min. Finally, the absorbance of the mixed solution was measured at 750 nm using a spectrophotometer (V-550, Jasco Co., Tokyo,

Japan). The calibration curve for TPC calculation was drawn using gallic acid as a standard with five different concentrations ranging from 0 to 0.5 mg/mL.

2.2.5 Supercritical anti-solvent crystallization

A schematic of the SAS is shown in **Figure 2.2.2**. The experimental procedure and conditions of the SAS process were based on a previous experiment of Chhouk et al. [29]. The particles produced using the acetone: ethanol = 9:1 (v/v) solutions containing the PVP: SCG extracts (1:1, 10:1, 20:1, and 30:1) with a PVP concentration at 5 mg/mL. The temperature of the system was maintained at 40 °C by an oven (WFO-400, Tokyo Rikakikai, Tokyo, Japan). The pressure (15 MPa) of the system was controlled by the BPR (AKICO, Tokyo, Japan) and indicated by a pressure gauge meter (MIGISHITA SEIKIMFG. Co. Ltd., Hyogo, Japan). First, the liquefied CO_2 was pumped into the system using a CO_2 pump (PU-2086, JASCO, Tokyo, Japan) at a flow rate of 15 mL/min until the pressure of the system reached 15 MPa. Then, the CO_2 pump was stopped, and the system was maintained at 40 °C and 15 MPa for 30 min. Later, the solution (PU-980, JASCO, Tokyo, Japan) and CO_2 pumps were started simultaneously. The solution of the SCG extract and PVP was pumped into the system at 0.25 mL/min and mixed with SC-CO_2 in the solvent mixer (Swagelok, OH, USA). The precipitation of the solute occurred when the mixed solvent passed through the precipitation coil (SUS316 tube coil; GL Sciences, Tokyo, Japan). Subsequently, the solute was dispersed into a collection filter (SS-4F-K4-05, 0.5 μm, Swagelok, OH, USA) through a nozzle and collected by the filter. Precipitation was maintained for 60 minutes. Finally, the solution and CO_2 pumps were stopped and the pressure was released gradually through BPR.

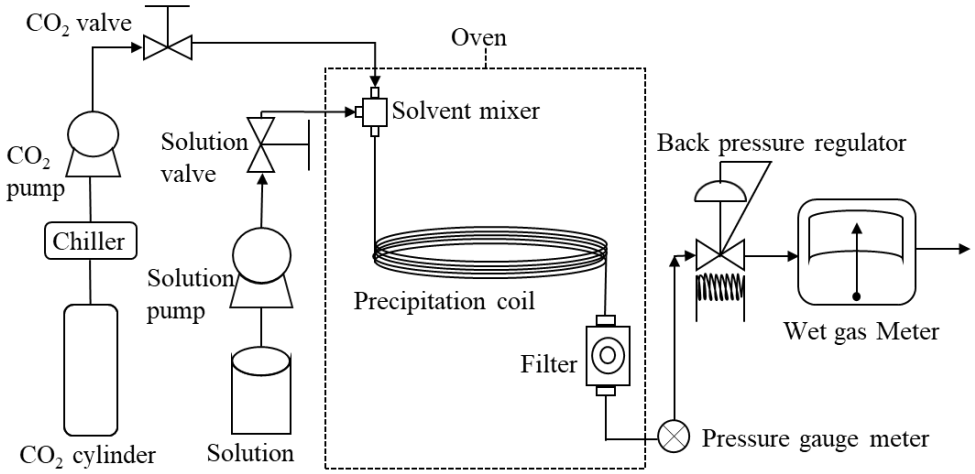

Figure 2.2.2 Schematic diagram of SAS process.

2.2.6 Characterization of produced particles

Surface morphology, particle size, and particle size distributions

Owing to the non-conductivity of the SCG and produced PVP particles, SCG and produced PVP particles were dispersed on a conductive double-sided tape and fixed to a sample stand for scanning electron microscopy (SEM; S4300, Hitachi, Tokyo, Japan). A vapor deposition device (IB-3, RMC Eiko Corp., Japan) was used to coat the experimental materials with gold. The accelerating voltage was set to 15 kV. The average particle sizes and particle size distributions obtained during the encapsulation process were determined using ImageJ software. More than 300 particles in each condition were counted to determine the particle size distribution.

Differential scanning calorimetry (DSC)

In this study, DSC (DSC-60A, Shimadzu, Japan) was used to determine the changes in the melting point of the produced particles to support the successful encapsulation of the SCG extract into PVP particles. The temperature of DSC ranged from −50 to 400 °C at a heat flow rate of 10 °C/min.

Fourier-transform infrared spectroscopy

Fourier-transform infrared spectroscopy (FTIR; Perkin-Elmer Ltd., Buckinghamshire, United Kingdom) with a wavenumber range of 4000–400 cm^{-1} was used to reveal the molecular structures of SCG and PVP particles.

2.3 Results and discussion

2.3.1 Analysis of variables (ANOVA) in extraction process

Design-Expert software (version 11, Stat-Ease, USA) was used for statistical analysis of the extraction results. The relationships between Y_1 and Y_2 and the independent variables (X_1, X_2, X_3) are represented by a second-order polynomial function (**Equation (3)**):

$$Y = b_0 + \sum_{i}^{3} b_i X_i + \sum_{i}^{3} b_{ii} X_i^2 + \sum_{i=1}^{2} \sum_{j=i+1}^{3} b_{ij} X_i X_j \qquad \textbf{Equation (3)}$$

Equation (4) and (5) define the predictive equations for Y_1 and Y_2, respectively. To evaluate the quality of the fit polynomial model, the coefficient of determination R^2 was used. Fisher's F-test of 95% confidence level and probability p were used to determine the statistical significance of the obtained models. Moreover, the p value can be used to show whether the model fits the data. In ANOVA, the p value of each independent variable and the interaction between each independent variable were determined as shown in **Table 2.3.1**.

$$Y_1 = 12.03 + 2.36X_2 + 4.56X_3 - 0.77\,X_1X_2 + 0.87\,X_1^2 \qquad \textbf{Equation(4)}$$

$$Y_2 = 66.38 + 20.09X_1 + 15.34X_1X_2 + 11.39X_1X_3 - 11.76\,X_2^2 - 11.24\,X_3^2 \qquad \textbf{Equation (5)}$$

Table 2.3.1 Analysis of variance for individual response; **(A)** ANOVA of extraction yield (Y_1), **(B)** ANOVA of total diterpene content (Y_2)

(A)

Source	Sum of squares	Degree of freedom	Mean square	F-value	p-value
Y_1 model	463.76	9	51.53	49.37	< 0.0001
X_1	3.54	1	3.54	3.40	0.0795
X_2	102.25	1	102.25	97.98	< 0.0001
X_3	342.52	1	342.52	328.20	< 0.0001
X_1X_2	5.13	1	5.13	4.91	0.0379
X_1X_3	0.21	1	0.21	0.20	0.6607
X_2X_3	3.54	1	3.54	3.39	0.0796
X_1^2	5.01	1	5.01	4.80	0.0398
X_2^2	0.18	1	0.18	0.17	0.6862
X_3^2	4.29	1	4.29	4.11	0.0555
Residual	21.92	21	1.04		
Lack of fit	12.55	7	1.79	2.68	0.0551
Pure error	9.36	14	0.67		
Cor total	485.68	30			

(B)

Source	Sum of squares	Degree of freedom	Mean square	F-value	p-value
Y_2 model	18914.47	9	2101.61	21.46	<0.0001
X_1	10703.10	1	10703.10	109.30	<0.0001
X_2	8.65	1	8.65	0.09	0.7673

X_3	64.39	1	64.39	0.66	0.4206
X_1X_2	2225.69	1	2225.69	22.73	<0.0001
X_1X_3	1620.97	1	1620.97	16.55	0.0001
X_2X_3	188.36	1	188.36	1.92	0.1705
X_1^2	5.20	1	5.20	0.05	0.8186
X_2^2	1760.62	1	1760.62	17.98	<0.0001
X_3^2	1704.45	1	1704.45	17.41	<0.0001
Residual	5973.37	61	97.92		
Lack of fit	2919.80	19	153.67	2.11	0.0218
Pure error	3053.58	42	72.70		
Cor total	24887.84	70			

p-value < 0.001 highly significant, 0.001 ≤ p-value <0.05 significant, p-value ≥ 0.05 not significant.

2.3.1.1 Effects of independent variables on extraction yield

The predicted model of the extraction yield (Y_1) is defined by **equation (4)**. The coefficient of determination (R^2) for this model is 0.9549. The ANOVA results for the individual responses to the extraction yield is summarized in **Table 2.2.1 (A)**. The p value of this model indicates that the model is highly significant. The linear terms of pressure (X_2) and ethanol ratio (X_3) equally and significantly affected the dependent variable Y_1 ($p < 0.0001$), followed by the interaction term of the temperature and pressure of the system (X_1X_2) and the quadratic term of temperature (X_1^2). Other factors including the linear term of temperature (X_1), interaction term of temperature and ethanol ratio (X_1X_3), interaction term of pressure and ethanol ratio (X_2X_3), quadratic term of pressure (X_2^2), and quadratic term of ethanol ratio (X_3^2) have p values higher than 0.05, indicating that these factors are insignificant.

2.3.1.2 Effects of independent variables on total diterpene content

The predicted model for the total diterpene content is defined in equation (5). Although the coefficient of determination (R^2) is 0.7600, the short difference between R^2_{adj}=0.7246 with R^2 and the small p value (less than 0.001) of this predictive model reveals the adequality and signification of this model in this research. According to **Table 2.3.1 (B)**, the linear term of temperature (X_1), as well as the interaction term of temperature and pressure (X_1X_2), the quadratic term of pressure (X_2^2), and the quadratic term of ethanol ratio (X_3^2), all show a high effect on the dependent variable (Y_2) with a low p value, followed by the interaction term of temperature and ethanol ratio (X_1X_3). The interaction term of pressure and ethanol ratio (X_2X_3), linear term of pressure (X_2), linear term of ethanol ratio (X_3), and quadratic term of temperature (X_1^2) show a p-value higher than 0.05, indicating that these factors are insignificant in this model.

2.3.2 Effects of experimental parameters on the extraction yield

Figures 2.3.1 (A) and **(B)** exhibit the interaction effects of the pressure and ethanol ratio with temperature at 40 °C and the interaction of pressure and temperature with ethanol ratio at 10% v/v on the extraction yield. It is reported that the distance between molecules can be shortened and the mass transfer can be enhanced in the extraction process as the pressure of the SC-CO_2 system increased, which can further increase the extraction yield using SC-CO_2 [39]. In this work, as pressure increased, the SCG extraction yield increased due to the increased mass transfer and the solvent power. Meanwhile, the ethanol ratio showed a significant and positive influence on the extraction yield, which contributed to the affinity increase of SC-CO_2 towards polar compounds by adding ethanol [9, 34, 40]. Moreover, the modifier ethanol can help to swell SCG matrix up and allow more solvents to penetrate inside the matrix to dissolve compounds. It is reported by Putra et al. that the addition of ethanol as a modifier noticeably increased the total tocopherol and carotene content [41]. Temperature is reported about its counteracting effects on the extraction result because temperature effects both the density corresponds to the solvent power and the vapor pressure of solutes corresponds to the solubility of solutes in SC-CO_2 [9, 34]. At the given pressure

range and ethanol ratio at 10% v/v in this work, from 40 °C to 60 °C, the negative effects of density decrease caused by temperature increase were the dominant factor influencing the extraction result. Thus, temperature increase in this range decreased the extraction yield due to the decrease in the solvent power of mixed solvents. Gracia et al. reported that the extraction yield decreased as temperature increased due to the dominancy of density reduction by increasing the temperature under a given pressure [42]. Moreover, a slight increase in the extraction yield was observed as the temperature increased from 60 °C to 80 °C, because the positive effect of solute vapor pressure prevailed over the adverse effect caused by the reduction of solvent power and led to the increase of extraction yield. It is also revealed that the solute vapor pressure dormancy of paprika extract in SC-CO_2 increased the extraction yield as temperature increased [43]. Compared with the effects of pressure and ethanol ratio on extraction yield, the effect of temperature was relatively small, and the lowest extraction yield was observed at 60 °C. Likewise, temperature was reported to be a less significant factor than pressure and ethanol ratio in carotene extraction from palm-pressured fibers using ethanol-modified SC-CO_2 [41].

Overall, changes of pressure and ethanol ratio showed significant and positive effects on the extraction yield. However, since temperature and pressure show adverse effect on extract yield, as revealed in Equation (4), a high extraction yield is obtained at low temperature with a high pressure and ethanol ratio. Similarly, this prediction agrees with the surface plots of the pressure and ethanol ratio at 40 °C (**Figures 2.3.1 (A)**).

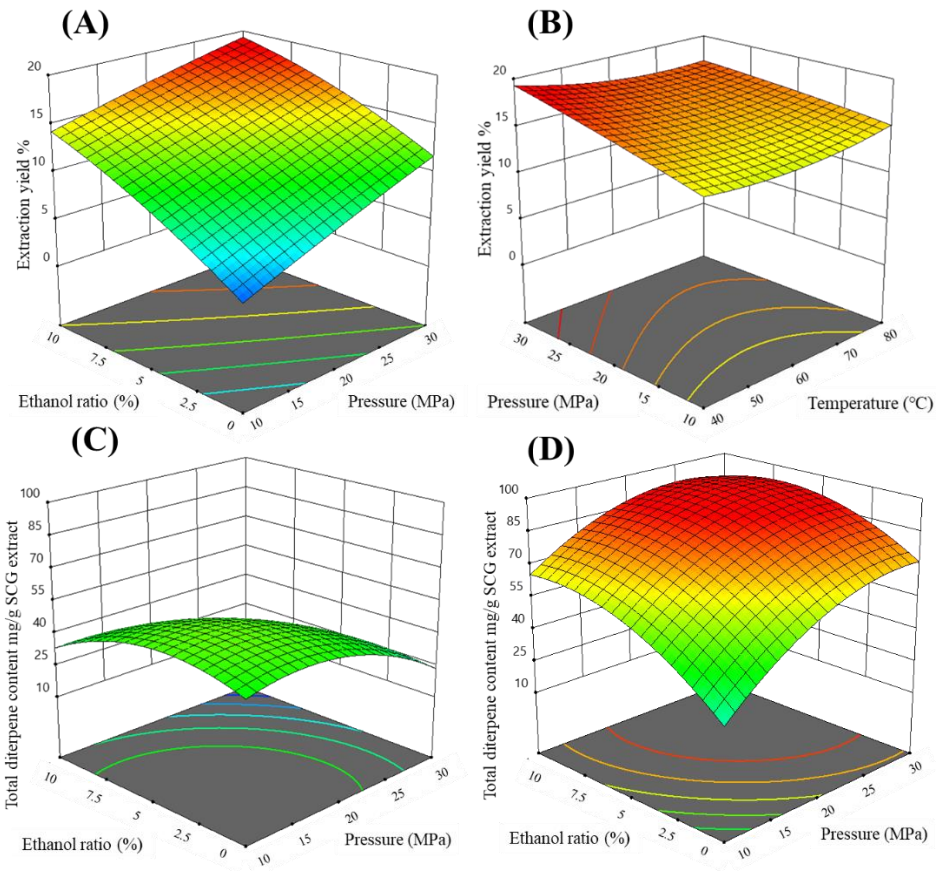

598

599 **Figure 2.3.1** The interaction effect of ethanol ratio and pressure on (**A**) extraction yield
600 at 40 ºC; (**B**)the interaction effect of pressure and temperature on extraction yield with
601 ethanol ratio at 10% v/v; the interaction of ethanol ratio and pressure on total diterpene
602 content at (**C**) 40 ºC and (**D**) 80 ºC.

603

604 **2.3.3 Effects of extraction parameters on the total diterpene content**

605 **Figures 2.3.1 (C)** and **(D)** show the effects of pressure and ethanol ratio on the total
606 diterpene content in the SCG extract at the two-end temperature in this work. In the
607 range of 40 °C to 80 °C, the total diterpene content in the SCG extract was significantly
608 and positively affected by temperature increase, which is attributed to the dormancy of
609 increase in the vapor pressure of diterpenes as the temperature increases. In the
610 extraction of β−carotene from oleoresin using SC-CO_2, temperature was considered to
611 be the most significant and positive factor, and the β−carotene content increased
612 approximately 48% as the temperature increased from 70 °C to 80 °C under the same

pressure (40 MPa) [44]. The affinity of ethanol-modified SC-CO_2 towards diterpenes increased as the addition of ethanol increased, and further the total diterpene content in the SCG extract was increased. Nonetheless, a high content of ethanol (>6%) led to a decrease in the diterpene content. Similarly, it can be found out that from Run 9 (SCG extract, 40 °C, 20 MPa, 0%; 69.17 mg/g SCG extract, 108.36 mg GAE/g SCG extract) to Run 10 (40 °C, 20 MPa, 10%; 4.01 mg/g SCG extract; 135.01 mg GAE/g SCG extract) in **Table 2.2.2**, under the same temperature and pressure, diterpenes content decreased but the phenolic compounds (exhibited as TPC value) in the SCG extract increased as ethanol ratio increased. Therefore, it can be inferred that the affinity of ethanol modified SC-CO_2 for other non-diterpenic polar compounds such as phenolic compounds was enhanced under the high ethanol ratio, and it directly decreased the diterpene content in the SCG extract. The reason of high ethanol ratio causing negative impact on the diterpenic compounds content in SCG extract is attributed to the increased affinity of ethanol modified SC-CO_2 toward other polar compounds revealed by Barbosa et al..[9] Although an increase in pressure can enhance the extraction yield by increasing its solvating power, excessive pressure can decrease the diffusivity of supercritical fluid and decrease the contact of supercritical fluid with compounds inside the pores of SCG matrix, leading to the decreased solute dissolution [45]. When the pressure varies in the range of 10–25 MPa, pressure increase shows positive effect on the total diterpene content owing to the increase of solvent power. However, in the range of 25–30 MPa, an increase in pressure reduced the total diterpene content in the SCG extract, which is attributed to the decreased mass transfer between the compounds inside the matrix and modified SC-CO_2 due to the increased pressure [38, 46]. In addition, as the pressure increases, the solid matrix becomes more packed which reduces the interaction of diterpenic compounds inside the matrix with SC-CO_2. The packing effect of the material was also reported to be the cause of the decrease of total tocopherols content from palm-pressured fibers using SC-CO_2 [41]. Therefore, the high temperature showed a significant and positive effect on total diterpene content in SCG extract as also revealed in **Equation (5)**. The pressure and ethanol ratio both showed positive effects on total diterpene content, but too high pressure and ethanol ratio turned to show negative effects on it. Thus, the optimal extraction conditions for total diterpene content can be obtained.

2.3.4 Optimization of experimental conditions on extraction results

The predicted optimal experimental conditions for extraction yield and total diterpene content are listed in **Table 2.3.2** based on extraction results. The optimal experimental conditions for extraction yield were 40 °C/30 MPa/10% v/v of ethanol. The predicted extraction yield is 19.31% with extremely low diterpene content, which is in accordance with the real result—an extraction yield of 19.55% and a total diterpene content of 2.83 mg/g SCG extract. High pressure and high ethanol ratio with low temperature provide high solvent power and high affinity for non-diterpenic polar compounds such as phenolic compounds of modified SC-CO_2, which leads to a high extraction yield. The optimal experimental conditions for the total diterpene content were 80 °C/25 MPa/6% v/v of ethanol. The predicted total diterpene content was 93.83 mg/g SCG extract with an extraction yield of 14.01%. The real total diterpene content under this condition was 66.89 mg/g SCG extract. The difference between the actual diterpene content and the predicted value can be attributed to the degradation of cafestol and kahweol during saponification at high temperature into other compounds such as dehydrocafestol and dehydrokahweol [13, 47, 48]. Additionally, the predicted diterpene value under optimal conditions was 15 times that of Soxhlet using hexane, confirming the selectivity of ethanol-modified SC-CO_2 for diterpenes.

Table 2.3.2 The predicted optimal extraction conditions for the extraction yield and total diterpene content.

Dependent responses	Independent Variables			Predicted values	Actual values
	X_1 (°C)	X_2 (MPa)	X_3(% v/v)		
Extraction yield (wt.%)	40	30	10	19.31	19.56
Total diterpene content (mg/g SCG extract)	80	25	6	93.82	66.89

2.3.5 Characterization of SCG extract and SCG residue

The FT−IR spectra of the SCG and extraction residues are shown in **Figure 2.3.2**. Compared with the raw SCG, the residues after extraction of unmodified and ethanol-modified SC-CO_2 exhibited a distinct decrease in absorbance intensity at 1742 cm^{-1} of C = O stretching. Moreover, the sharp absorbance decreases at 2918 and 2852 cm^{-1} of symmetrical and asymmetrical alkyl C–H stretching in the extraction residues indicates that compounds with alkyl C–H bonds were extracted. Combining these two findings, we think the compounds with ketone and carbonyl functional groups were extracted by SC-CO_2. The previous work carried out by Chhouk et al., also reported the declined intensity of the functional groups of Khmer medicinal plants after SC-CO_2 extraction [49]. Notably, there are stronger decreases in SCG residues of ethanol-modified SC-CO_2 in these regions than that of SCG residues extracted by only SC-CO_2. This phenomenon indicates the higher affinity of ethanol-modified SC-CO_2 showed higher affinity toward compounds with ketone or carbonyl groups. Furthermore, decreases in the absorbance of SCG residues at 1645 cm^{-1} of C = O stretching, 1447 cm^{-1} of O–H stretching of carboxylic acid, 1373 cm^{-1} corresponding to O–H stretching of alcohol, 1165 cm^{-1} of CH_3 stretching, and 813 cm^{-1} and 714 cm^{-1} of aromatic C–H stretching were observed. Accordingly, it could be inferred that lipid and phenolic compounds were extracted using unmodified and ethanol-modified SC-CO_2.

The SEM images of the raw SCG and SCG residues after extraction using ethanol-modified SC-CO_2 are shown in **Figure 2.3.3**. The oily surface of the raw SCG residue cannot be found in SCG residues after extraction. This might indicate that the compounds contained in the oily layers of SCG were extracted by SC-CO_2. Furthermore, it was observed that there were damaged structures in the SCG residue images, and it revealed the successful penetration of ethanol-modified SC-CO_2 into the matrix of SCG to extract compounds present inside. Yamamoto et al., reported the damaged surface morphology of *Vitellaria paradoxa* Gaertn seeds indicating that substances inside the matrix were extracted using SC-CO_2 [50]. Briefly speaking, the extraction of SCG using SC-CO_2 was successfully performed, and ethanol-modified SC-CO_2 showed higher affinity toward polar compounds in SCG than SC-CO_2.

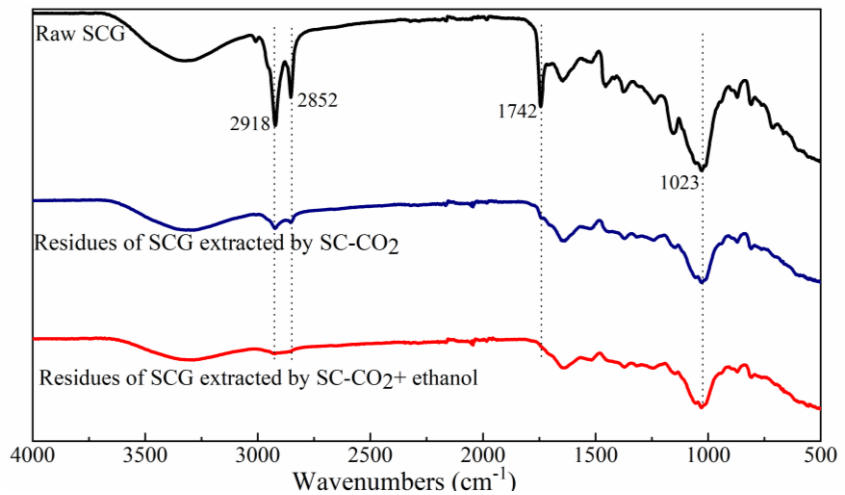

696

697 **Figure 2.3.2** FT−IR spectra of SCG and its solid residues extracted by unmodified and
698 ethanol modified SC-CO_2.

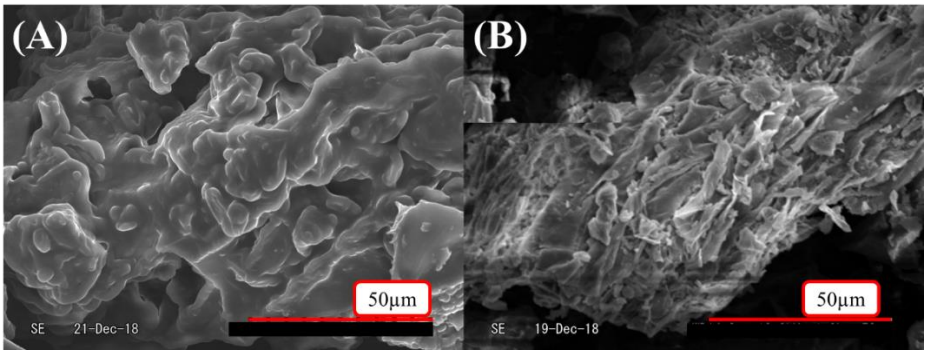

699

700 **Figure 2.3.3 (A)** SEM image of raw SCG; **(B)** SEM image of residues after extraction
701 by ethanol modified SC-CO_2.

702

703 **2.3.5 Morphology and particle size distribution of produced nanoparticles**

704 As has been introduced previously, to improve the stability and water dispersibility of
705 the oily SCG extract rich in diterpenes in water, the encapsulation of the SCG extract
706 into nanoparticles of the water-soluble polymer (PVP) was performed using the SAS
707 process. The morphology and particle size distribution of obtained particles were
708 analyzed by SEM, and the encapsulation of the SCG extract with PVP was determined
709 by DSC, FT–IR and UV–Vis.

The SEM images of produced particles with PVP:SCG extract ratios at 1:1, 10:1, 20:1, and 30:1 together with particle size distributions are shown in **Figure 2.3.4**. It can be found out that particle sizes were distributed in the range of 50–450 nm with majority of particles distributed in range of 100–300 nm. When the ratio of the PVP:SCG extract was 1:1, spherical particles together with some irregular particles were observed, but produced particles were strongly entangled with others. It is attributed to the low proportion of PVP which is insufficient to cover the SCG extract and harden nanoparticles into spherical shape. It has been reported that the low ratio of polymer led to the formation of irregular particles due to the insufficiency of polymers by several previous researches [29, 51]. As the PVP:SCG extract ratio increased from 1:1 to 30:1, the spherical outline of the particles was gradually and clearly observed, and the entanglement among particles became weaker. The mean average particle sizes of the PVP:SCG extract ratios of 1:1, 10:1, 20:1, and 30:1 were 162 ± 61 nm, 198 ± 62 nm, 186 ± 67 nm, and 140 ± 52 nm (standard ± deviation), respectively. The smaller average particle size with the PVP:SCG extract at 1:1 is attributed to the low PVP ratio, which is inadequate to cover a large amount of the SCG extract. Thus, the relatively small particles with ~60% particles being smaller than 150 nm were formed. When the PVP:SCG extract ratio was increased to 10:1, as the amount of PVP increased, the formation of larger particles with only ~50% particles being smaller than 150 nm became to form. The increase of particle size as PVP ratio increase was reported where the particle size significant amplified as PVP / fistein ratio increased from 2:1 to 5:1 [52]. When the PVP:SCG extract ratio was 30:1, the average particle size decreased to 140 nm, and relatively uniform-sized particles were formed where more than 80% particles are smaller than 150 nm. The reduction in particle size from 10:1 to 30:1 is attributed to the decrease in the PVP SCG/extract solution viscosity as the SCG extract concentration decreased. Chhouk et al. reported that the decrease of the feed solution viscosity led to the reduction of curcumin/PVP particle size [29]. To put it in another way, when the ratio of PVP:SCG extract was 30:1, particles with relatively uniform particles size and small average particle size were obtained.

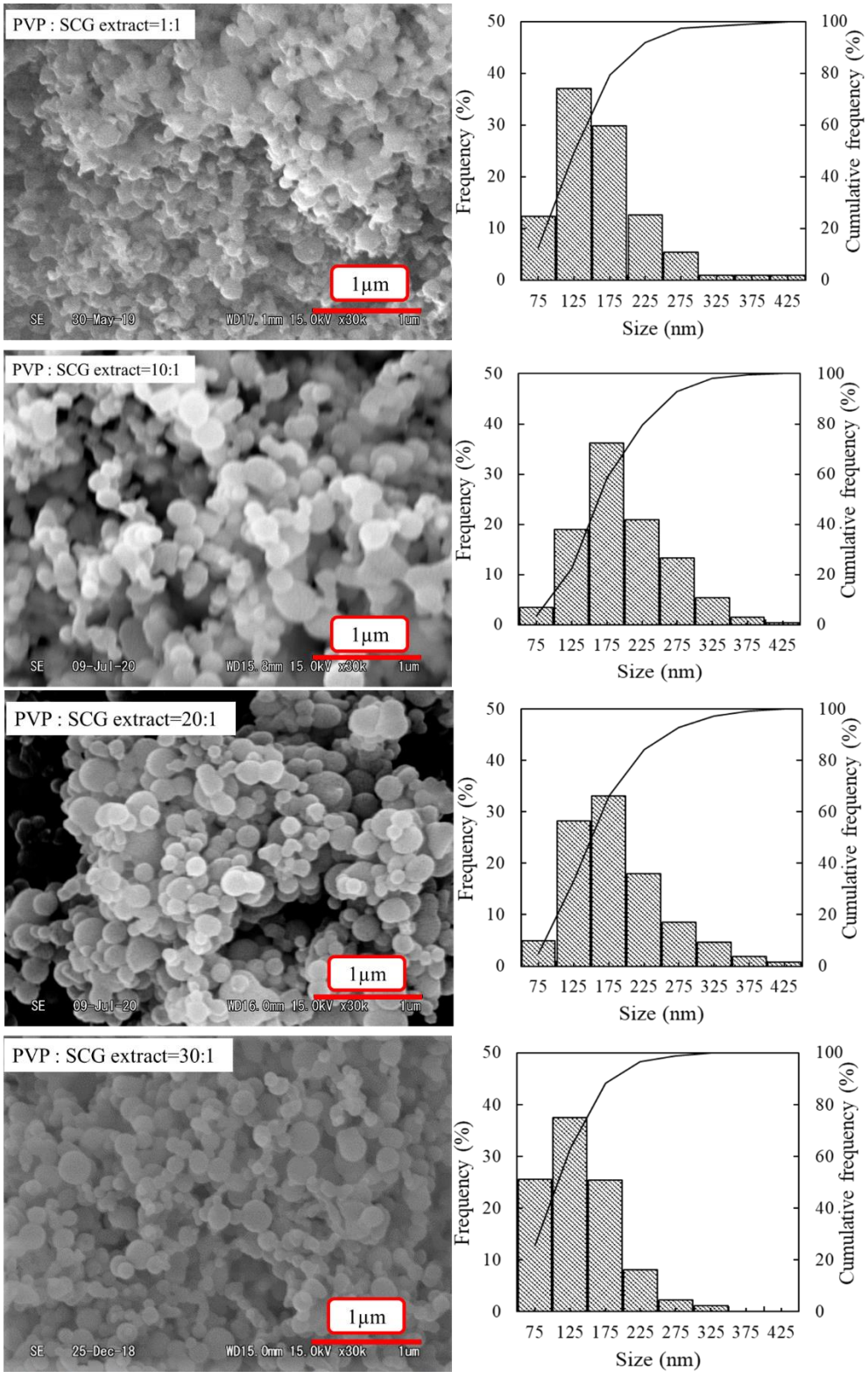

739

740 **Figure 2.3.4** SEM images and particle size distribution of produced particles under

741 PVP: SCG extract of 1:1, 10:1, 20:1 and 30:1.

2.3.6 Interaction between PVP and SCG extract in nanoparticles

To check the intermolecular structure between the PVP and SCG extract, the produced particles were characterized using the FT–IR spectroscopy (**Figure 2.3.5**). The SCG extract showed a characteristic absorption band at 3011 cm^{-1} for unsaturated = CH_n stretching, 2921 cm^{-1} for symmetrical, 2852 cm^{-1} for asymmetrical alkyl C–H stretching, and 1742 cm^{-1} for C = O stretching. Normally, the deformation of CH_2 and asymmetrical deformation of CH_3 at 1450 cm^{-1} exhibit two absorbances at 1460 and 1440 cm^{-1}, but owing to the overlap of these two absorption bands, the absorption peak is observed at 1460 cm^{-1} [53]. Moreover, absorbance band at 1645 cm^{-1} of C = O stretching, the symmetrical deformation of CH_3 stretching at 1380 cm^{-1}, 1165 cm^{-1} for CH_3 stretching, and 803 cm^{-1} together with 719 cm^{-1} of aromatic C–H stretching was observed in the FT–IR spectrum of the SCG extract. The spectrum of PVP particles shows a 3405 cm^{-1} absorption band of O–H stretching, 2955 cm^{-1} of symmetrical alkyl C–H stretching, 1645 cm^{-1} of C = O stretching, 1288 cm^{-1} of CH_2 stretching, and 576 cm^{-1} of N = O stretching [54]. The FT−IR spectrum of produced particles showed characteristic stretching like that of PVP particles. The disappearance of asymmetric CH_2 and CH_3 stretching and C = O stretching is caused by the encapsulation of the SCG extract into the PVP particles. Moreover, the small shift at 1645 cm^{-1}, and changed absorption at 1460 cm^{-1} and 1440 cm^{-1} in the FT–IR spectra of the produced particles are caused by the intermolecular bonding between C = O of PVP and C–H of the SCG extract, which also revealed the successful encapsulation of the SCG extract into nanoparticles.

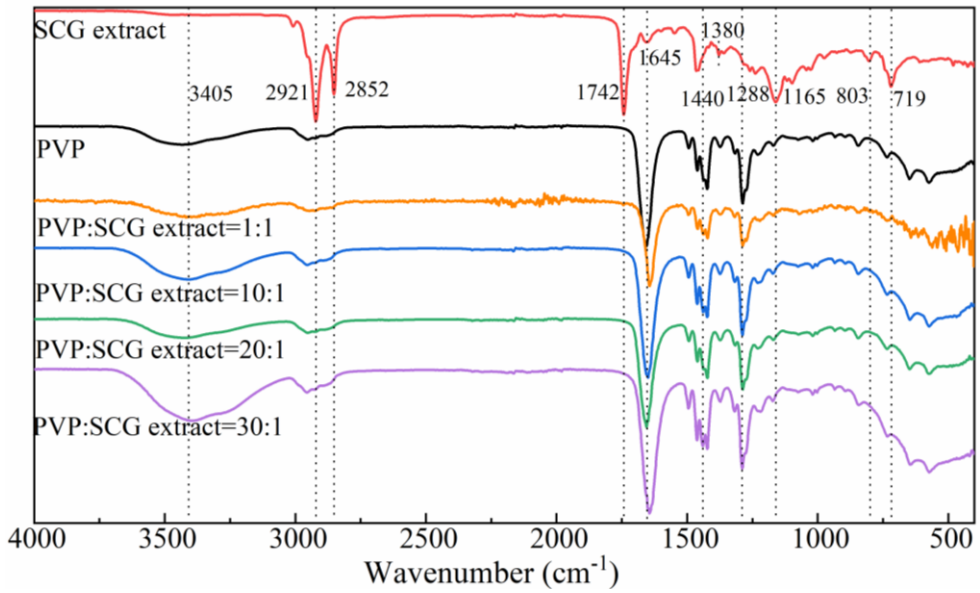

764

765 **Figure 2.3.5** FT−IR spectra of SCG extract, PVP particles, particles produced with the
766 ratio of PVP: SCG extract at 1:1, 10:1, 20:1 and 30:1.

767

768 The DSC curves of the produced particles exhibit the characteristic peak of PVP with a
769 characteristic broad endothermic peak of PVP ranging from 5 ℃ to 100 ℃ due to
770 dehydration (**Figure 2.3.6**). However, compared with the curve of pure PVP with a peak
771 around 63 ℃, the decreased DSC peak of the produced particles suggests that the SCG
772 extract inside the particles led to the reduction of DSC peak. Li et al. revealed the similar
773 DSC curves of borneol–PVP nanofiber and PVP which demonstrated the success
774 encapsulation of borneol into PVP nanofibers [55]. . The UV–Vis spectra of the produced
775 particles are shown in **Figure 2.3.6**. When the SCG extract was dissolved in water with
776 or without PVP addition, an absorbance peak was observed around 285 nm. It is because
777 polar and water-soluble compounds in SCG were also extracted out by ethanol-
778 modified SC-CO_2. Moreover, similar peaks were observed around 285 nm in the water
779 solution of particles produced under all the conditions. As the particles produced with
780 PVP:SCG extract ratio at 1:1 were strongly entangled with each other, in the following
781 parts, we focus on the comparison between nanoparticles produced with the PVP:SCG
782 extract ratio at 10:1, 20:1, and 30:1. In **Figure 2.3.7**, from the images of the physically

mixed SCG extract in water and the solution of dissolved nanoparticles in water, we obviously observed that produced nanoparticles dispersed in water fully and speedily forming a clear solution with light-yellow color. However, the performance of the physically mixed SCG extract in water was not favorable as the SCG extract kept insoluble in water. Thus, we believe produced nanoparticles exhibit enhanced water dispersibility of the SCG extract in water. From the FT–IR spectra, DSC curves and UV–Vis spectra, it was confirmed that the SCG extract rich in diterpenes was successfully encapsulated in PVP nanoparticles under all the experimental conditions. The smallest average particle size was obtained with PVP: SCG extract ratio at 30:1.

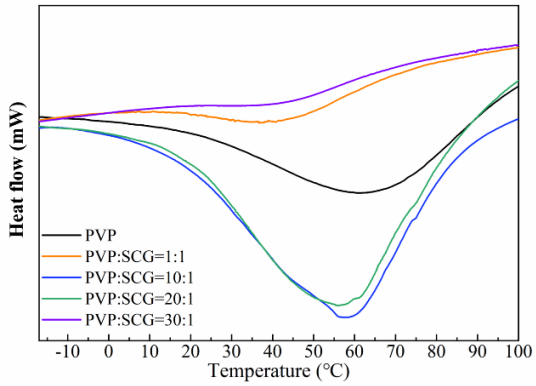

Figure 2.3.6 DSC curves of PVP, particles produced with the ratio of PVP:SCG extract at 1:1, 10:1, 20:1 and 30:1.

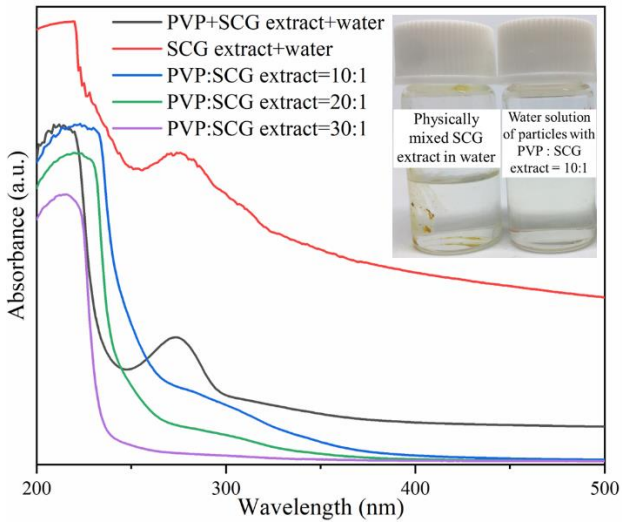

Figure 2.3.7 UV−Vis spectra of physically mixed PVP + SCG extract in water, SCG extract in water, and water dissolved particles produced under PVP:SCG extract= 10:1, 20:1 and 30:1; images of water solution of physically mixed SCG extract in water, and water dissolved particles produced under PVP:SCG extract = 10:1.

2.4 Conclusions

In this study, the Box–Behnken design of RSM and ANOVA was used to optimize the experimental conditions for the extraction of diterpenes using ethanol-modified SC-CO_2. The effects of three parameters (temperature: 40–80 °C, pressure: 10–30 MPa, and ethanol ratio: 0%–10% v/v) on the total extraction yield and total diterpene content in the SCG extract were demonstrated. Particularly, the predicted optimal condition of the total diterpene content was 80 ºC/25 MPa/6% v/v, where the predicted total diterpene content in the SCG extract was 15 times the results of conventional hexane extraction. This confirms the superiority of ethanol-modified SC-CO_2 toward diterpenes in SCGs than other methods. The encapsulation of the SCG extract rich in diterpenes into PVP nanoparticles was successfully performed. Based on the SEM images, particles with an average particle size of 140 nm were obtained with the ratio of PVP:SCG extract at 30:1. Notably, the successful encapsulation of the SCG extract rich in diterpenes into PVP nanoparticles was confirmed by DSC curves, FT–IR spectra, UV−Vis spectra, and the fast dispersion of produced nanoparticles in water was observed. The results of this study can serve as a reference for the separation of diterpenes from SCGs and the utilization of SCG extract with high water dispersibility.

References:

[1] International coffee organization. https://www.ico.org/ (accessed June 29, 2022).
[2] Campos-Vega, R.; Loarca-Piña, G.; Vergara-Castañeda, H. A.; Oomah, B. D., Spent coffee grounds: A review on current research and future prospects. *Trends in Food Science & Technology,* **2015**, *45* (1), 24-36.
[3] Leifa, F.; Pandey, A.; Soccol, C. R., Solid state cultivation — an efficient method to use toxic agro-industrial residues. *Journal of Basic Microbiology,* **2000**, *40* (3), 187-197.
[4] Lee, K. O. K., H.J.; Lee, H.J.; Hyeon, S.J. , Up-cycling natural dyeing using coffee sludge: Dyeability study of coffee pigment. *Fiber Technology and Industry,* **2017**, *21*, 82-92.

[5] Hong, K. H., Effects of tannin mordanting on coloring and functionalities of wool fabrics dyed with spent coffee grounds. *Fashion and Textiles,* **2018**, *5* (1), 33.
[6] Abdeltaif, S.; SirElkhatim, K.; Hassan, A., Estimation of Phenolic and Flavonoid Compounds and Antioxidant Activity of Spent Coffee and Black Tea (Processing) Waste for Potential Recovery and Reuse in Sudan. *Recycling,* **2018**, *3* (2), 27.
[7] Acevedo, F.; Rubilar, M.; Scheuermann, E.; Cancino, B.; Uquiche, E.; Garcés, M.; Inostroza, K.; Shene, C., Spent Coffee Grounds as a Renewable Source of Bioactive Compounds. *Journal of Biobased Materials and Bioenergy,* **2013**, *7* (3), 420-428.
[8] de Oliveira, P. M. A.; de Almeida, R. H.; de Oliveira, N. A.; Bostyn, S.; Gonçalves, C. B.; de Oliveira, A. L., Enrichment of diterpenes in green coffee oil using supercritical fluid extraction – Characterization and comparison with green coffee oil from pressing. *The Journal of Supercritical Fluids,* **2014**, *95*, 137-145.
[9] Barbosa, H. M. A.; de Melo, M. M. R.; Coimbra, M. A.; Passos, C. P.; Silva, C. M., Optimization of the supercritical fluid coextraction of oil and diterpenes from spent coffee grounds using experimental design and response surface methodology. *The Journal of Supercritical Fluids,* **2014**, *85*, 165-172.
[10] Regina Lago; Rosemar Antoniassi; Freitas, S. In *Centesimal composition and amino acids of raw, roasted and spent ground of soluble coffee*, Anais do II Simpósio de Pesquisa dos Cafés do Brasil Vitoria, Vitoria, 2001.
[11] Couto, R. M.; Fernandes, J.; da Silva, M. D. R. G.; Simões, P. C., Supercritical fluid extraction of lipids from spent coffee grounds. *The Journal of Supercritical Fluids,* **2009**, *51* (2), 159-166.
[12] Mussatto, S. I., Chapter 11 - Generating Biomedical Polyphenolic Compounds from Spent Coffee or Silverskin A2 - Preedy, Victor R. In *Coffee in Health and Disease Prevention*, Academic Press: San Diego, 2015; pp 93-106.
[13] Benassi, M. d. T.; Dias, R. C. E., Chapter 109 - Assay of Kahweol and Cafestol in Coffee. In *Coffee in Health and Disease Prevention*, Preedy, V. R., Ed. Academic Press: San Diego, 2015; pp 993-1004.
[14] Speer, K.; Kölling-Speer, I., The lipid fraction of the coffee bean. *Brazilian Journal of Plant Physiology,* **2006**, *18*, 201-216.
[15] Kurzrock, T.; Speer, K., DITERPENES AND DITERPENE ESTERS IN COFFEE. *Food Reviews International,* **2001**, *17* (4), 433-450.
[16] Ludwig, I. A.; Clifford, M. N.; Lean, M. E. J.; Ashihara, H.; Crozier, A., Coffee: biochemistry and potential impact on health. *Food & Function,* **2014**, *5* (8), 1695-1717.

[17] Murthy, P. S.; Naidu, M. M., Recovery of Phenolic Antioxidants and Functional Compounds from Coffee Industry By-Products. *Food and Bioprocess Technology,* **2012**, *5* (3), 897-903.
[18] Ren, Y.; Wang, C.; Xu, J.; Wang, S., Cafestol and Kahweol: A Review on Their Bioactivities and Pharmacological Properties. *International Journal of Molecular Sciences,* **2019**, *20* (17), 4238.
[19] Cavin, C.; Holzhaeuser, D.; Scharf, G.; Constable, A.; Huber, W. W.; Schilter, B., Cafestol and kahweol, two coffee specific diterpenes with anticarcinogenic activity. *Food and Chemical Toxicology,* **2002**, *40* (8), 1155-1163.
[20] Geow, C. H.; Tan, M. C.; Yeap, S. P.; Chin, N. L., A Review on Extraction Techniques and Its Future Applications in Industry. *European Journal of Lipid Science and Technology,* **2021**, *123* (4), 2000302.
[21] Fornari, T., Supercritical CO_2 Extraction: Relevance to Food Processing. In *Reference Module in Food Science*, Elsevier: 2016.
[22] Baldino, L.; Della Porta, G.; Reverchon, E., Supercritical CO_2 processing strategies for pyrethrins selective extraction. *Journal of CO2 Utilization,* **2017**, *20*, 14-19.
[23] Andrade, K. S.; Gonçalvez, R. T.; Maraschin, M.; Ribeiro-do-Valle, R. M.; Martínez, J.; Ferreira, S. R. S., Supercritical fluid extraction from spent coffee grounds and coffee husks: Antioxidant activity and effect of operational variables on extract composition. *Talanta,* **2012**, *88*, 544-552.
[24] Rabasco Alvarez, A. M.; González Rodríguez, M. L., Lipids in pharmaceutical and cosmetic preparations. *Grasas y Aceites,* **2000**, *51* (1-2), 74-96.
[25] Garmus, T. T.; Paviani, L. C.; Queiroga, C. L.; Magalhães, P. M.; Cabral, F. A., Extraction of phenolic compounds from pitanga (*Eugenia uniflora L.*) leaves by sequential extraction in fixed bed extractor using supercritical CO_2, ethanol and water as solvents. *The Journal of Supercritical Fluids,* **2014**, *86*, 4-14.
[26] Araújo, M. N.; Azevedo, A. Q. P. L.; Hamerski, F.; Voll, F. A. P.; Corazza, M. L., Enhanced extraction of spent coffee grounds oil using high-pressure CO_2 plus ethanol solvents. *Industrial crops and products,* **2019**, *141*, 111723.
[27] Froiio, F.; Mosaddik, A.; Morshed, M. T.; Paolino, D.; Fessi, H.; Elaissari, A., Edible Polymers for Essential Oils Encapsulation: Application in Food Preservation. *Industrial & Engineering Chemistry Research,* **2019**, *58* (46), 20932-20945.
[28] Nuchuchua, O.; Nejadnik, M. R.; Goulooze, S. C.; Lješković, N. J.; Every, H. A.; Jiskoot, W., Characterization of drug delivery particles produced by supercritical carbon dioxide technologies. *The Journal of Supercritical Fluids,* **2017**, *128*, 244-262.

[29] Chhouk, K.; Wahyudiono; Kanda, H.; Kawasaki, S.-I.; Goto, M., Micronization of curcumin with biodegradable polymer by supercritical anti-solvent using micro swirl mixer. *Frontiers of Chemical Science and Engineering,* **2018**, *12* (1), 184-193.
[30] Duta Lestari, S.; Machmudah, S.; Winardi, S.; Wahyudiono; Kanda, H.; Goto, M., Particle micronization of Curcuma mangga rhizomes ethanolic extract/biopolymer PVP using supercritical antisolvent process. *The Journal of Supercritical Fluids,* **2019**, *146*, 226-239.
[31] Araújo, J. M. A.; Sandi, D., Extraction of coffee diterpenes and coffee oil using supercritical carbon dioxide. *Food Chemistry,* **2007**, *101* (3), 1087-1094.
[32] Baş, D.; Boyacı, İ. H., Modeling and optimization I: Usability of response surface methodology. *Journal of Food Engineering,* **2007**, *78* (3), 836-845.
[33] Beg, Q. K.; Sahai, V.; Gupta, R., Statistical media optimization and alkaline protease production from *Bacillus mojavensis* in a bioreactor. *Process Biochemistry,* **2003**, *39* (2), 203-209.
[34] Jokić, S.; Molnar, M.; Cikoš, A.-M.; Jakovljević, M.; Šafranko, S.; Jerković, I., Separation of selected bioactive compounds from orange peel using the sequence of supercritical CO_2 extraction and ultrasound solvent extraction: optimization of limonene and hesperidin content. *Separation Science and Technology,* **2020**, *55* (15), 2799-2811.
[35] Putra, N. R.; Idham, Z. B.; Machmudah, S.; Ruslan, M. S. H. b.; Che Yunus, M. A., Extraction of peanut skin oil by modified supercritical carbon dioxide: Empirical modelling and optimization. *Separation Science and Technology,* **2018**, *53* (17), 2695-2703.
[36] Jerković, I.; Rajić, M.; Marijanović, Z.; Bilić, M.; Jokić, S., Optimization of supercritical CO_2 extraction of dried *Helichrysum italicum* flowers by response surface methodology: GC-MS profiles of the extracts and essential oil. *Separation Science and Technology,* **2016**, *51* (18), 2925-2931.
[37] Moeenfard, M.; Silva, J. A.; Borges, N.; Santos, A.; Alves, A., Quantification of Diterpenes and Their Palmitate Esters in Coffee Brews by HPLC-DAD. *International Journal of Food Properties,* **2015**, *18* (10), 2284-2299.
[38] Chhouk, K.; Quitain, A. T.; Gaspillo, P.-a. D.; Maridable, J. B.; Sasaki, M.; Shimoyama, Y.; Goto, M., Supercritical carbon dioxide-mediated hydrothermal extraction of bioactive compounds from Garcinia Mangostana pericarp. *The Journal of Supercritical Fluids,* **2016**, *110*, 167-175.

[39] Khaw, K.-Y.; Parat, M.-O.; Shaw, P. N.; Falconer, J. R., Solvent Supercritical Fluid Technologies to Extract Bioactive Compounds from Natural Sources: A Review. *Molecules (Basel, Switzerland),* **2017**, *22* (7), 1186.

[40] M.D. Luque de Castro, M. V., M.T. Tena, Analytical Supercritical Fluid Extraction. *Springer-Verlag,Berlin, Heidelberg, ,* **1994**, 135.

[41] Putra, N. R.; Wibobo, A. G.; Machmudah, S.; Winardi, S., Recovery of valuable compounds from palm-pressed fiber by using supercritical CO_2 assisted by ethanol: modeling and optimization. *Separation Science and Technology,* **2020**, *55* (17), 3126-3139.

[42] Gracia, I.; Garc; Iacute; A, M. T.; Rodr; Iacute; Guez, J. F.; Lucas, A. d., Application of Supercritical Fluid Extraction for the Recovery of Aroma Compounds to be Used in Fast Aged Rum Production. *Food Science and Technology Research,* **2009**, *15* (4), 353-360.

[43] Kostrzewa, D.; Dobrzyńska-Inger, A.; Turczyn, A., Experimental Data and Modelling of the Solubility of High-Carotenoid Paprika Extract in Supercritical Carbon Dioxide. *Molecules (Basel, Switzerland),* **2019**, *24* (22), 4174.

[44] Kehili, M.; Kammlott, M.; Choura, S.; Zammel, A.; Zetzl, C.; Smirnova, I.; Allouche, N.; Sayadi, S., Supercritical CO_2 extraction and antioxidant activity of lycopene and β-carotene-enriched oleoresin from tomato (*Lycopersicum esculentum L.*) peels by-product of a Tunisian industry. *Food and Bioproducts Processing,* **2017**, *102*, 340-349.

[45] Belwal, T.; Dhyani, P.; Bhatt, I. D.; Rawal, R. S.; Pande, V., Optimization extraction conditions for improving phenolic content and antioxidant activity in Berberis asiatica fruits using response surface methodology (RSM). *Food Chemistry,* **2016**, *207*, 115-124.

[46] Şanal, İ. S.; Bayraktar, E.; Mehmetoğlu, Ü.; Çalımlı, A., Determination of optimum conditions for SC-(CO_2 + ethanol) extraction of β-carotene from apricot pomace using response surface methodology. *The Journal of Supercritical Fluids,* **2005**, *34* (3), 331-338.

[47] Dias, R. C. E.; de Faria-Machado, A. F.; Mercadante, A. Z.; Bragagnolo, N.; Benassi, M. d. T., Roasting process affects the profile of diterpenes in coffee. *European Food Research and Technology,* **2014**, *239* (6), 961-970.

[48] Novaes, F. J. M.; Bayan, F. C.; Aquino Neto, F. R.; Resende, C. M., The occurrence of cafestol and kahweol diterpenes in different coffee brews. *Coffee Science - ISSN 1984-3909,* **2019**, *14* (2), 265 - 280.

[49] Chhouk, K.; Wahyudiono; Kanda, H.; Goto, M., Efficacy of supercritical carbon dioxide integrated hydrothermal extraction of Khmer medicinal plants with potential pharmaceutical activity. *Journal of Environmental Chemical Engineering,* **2018**, *6* (2), 2944-2956.

[50] N. Yamamoto, K. M., C. Kimthet, W. Wahyudiono, S. Onwona–Agyeman, H. Kanda, and M. Goto, Lipids from *Vitellaria paradoxa* Gaertn Seeds by Supercritical CO_2:Extraction and Optimization of Parameters by Response Surface Methodology. *Engineering Journal,* **2018.**, *22* (5), 31-44.

[51] Patomchaiviwat, V.; Paeratakul, O.; Kulvanich, P., Formation of Inhalable Rifampicin-Poly(L-lactide) Microparticles by Supercritical Anti-solvent Process. *AAPS PharmSciTech,* **2008**, *9* (4), 1119-1129.

[52] Chen, L.-F.; Xu, P.-Y.; Fu, C.-P.; Kankala, R. K.; Chen, A.-Z.; Wang, S.-B., Fabrication of Supercritical Antisolvent (SAS) Process-Assisted Fisetin-Encapsulated Poly (Vinyl Pyrrolidone) (PVP) Nanocomposites for Improved Anticancer Therapy. *Nanomaterials,* **2020**, *10* (2), 322.

[53] Agatonovic-Kustrin, S.; Ristivojevic, P.; Gegechkori, V.; Litvinova, T. M.; W. Morton, D., Essential Oil Quality and Purity Evaluation via FT–IR Spectroscopy and Pattern Recognition Techniques. *Applied Sciences,* **2020**, *10* (20), 7294.

[54] Machmudah, S.; Winardi, S.; Wahyudiono; Kanda, H.; Goto, M., Formation of Fine Particles from Curcumin/PVP by the Supercritical Antisolvent Process with a Coaxial Nozzle. *ACS Omega,* **2020**, *5* (12), 6705-6714.

[55] Li, X.-Y.; Wang, X.; Yu, D.-G.; Ye, S.; Kuang, Q.-K.; Yi, Q.-W.; Yao, X.-Z., Electrospun Borneol-PVP Nanocomposites. *Journal of Nanomaterials,* **2012**, *2012*, 731382.

Chapter 3 One-step preparation of *Z*-isomer-rich β-carotene nanodispersions using a natural catalyst, allyl isothiocyanate in ultrasound-assisted supercritical carbon dioxide

3.1 Introduction

3.1.1 Introduction of β-carotene nanodispersions

In recent years, due to the increasing consciousness about healthy lifestyle, the demand for natural and organic products are in demand. Especially, demands for carotenoids as a typical naturally-derived pigment are increasing annually. β-Carotene is a naturally-occurring hydrophobic carotenoid consists of 8 isoprene units categorized as tetraterpene **(Figure 3.1.1)**, abundantly existed in vegetables such as carrots and pumpkins with a deep orange-yellow color [1, 2]. In addition, due to its multiple health benefits, such as pro-vitamin A, antioxidant, and anti-atherosclerotic activities, β-carotene is considered as a safe and high value-added food colorant worldwide [3-5]. However, due to high hydrophobicity, high crystallinity, and poor solubility in water and various organic solvents of β-carotene, the utilization efficiency in food industry is reported to be not high [6, 7]. Additionally, In addition, fat-soluble components like carotenoids have a low dispersion in water, which could reduce its bioavailability in human body [8].

Generally, to enhance the bioavailability of carotenoids, fine pulverizing treatments and dispersion treatment using emulsifiers in water are carried out [9, 10]. Mahalakshmi et al. revealed that encapsulated β-carotene with average size at 653 nm showed a 1.8-fold increased permeability than that of microparticles with average size at 2104 nm in an *ex vivo* everted gut sac technique [9]. Therefore, in many cases of food processing, emulsifiers are generally used after water-soluble preparation (disperse processing) of β-carotene. Several studies have reported the successful obtaining of carotenoid nanodispersions by emulsification-evaporation technique. The specific operational steps are as follows: (1) dissolve carotenoids in an organic solvent; (2) distribute the

organic solvent solution into an aqueous solution containing an emulsifier; (3) evaporate the organic solvent by reduced pressure treatment (**Figure 3.1.2 (A)**) [11, 12].

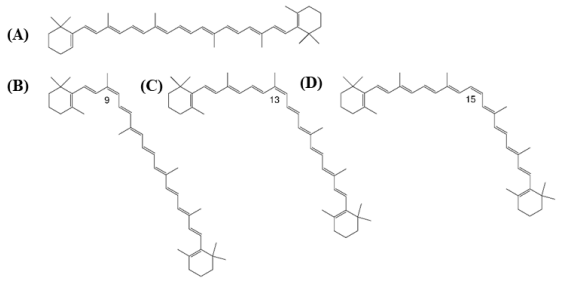

Figure 3.1.1 Chemical structures of typical β-carotene isomers: (**A**) (all-*E*)-β-carotene; (**B**) (9*Z*)-β-carotene; (**C**) (13*Z*)-β-carotene; (**D**) (15*Z*)-β-carotene.

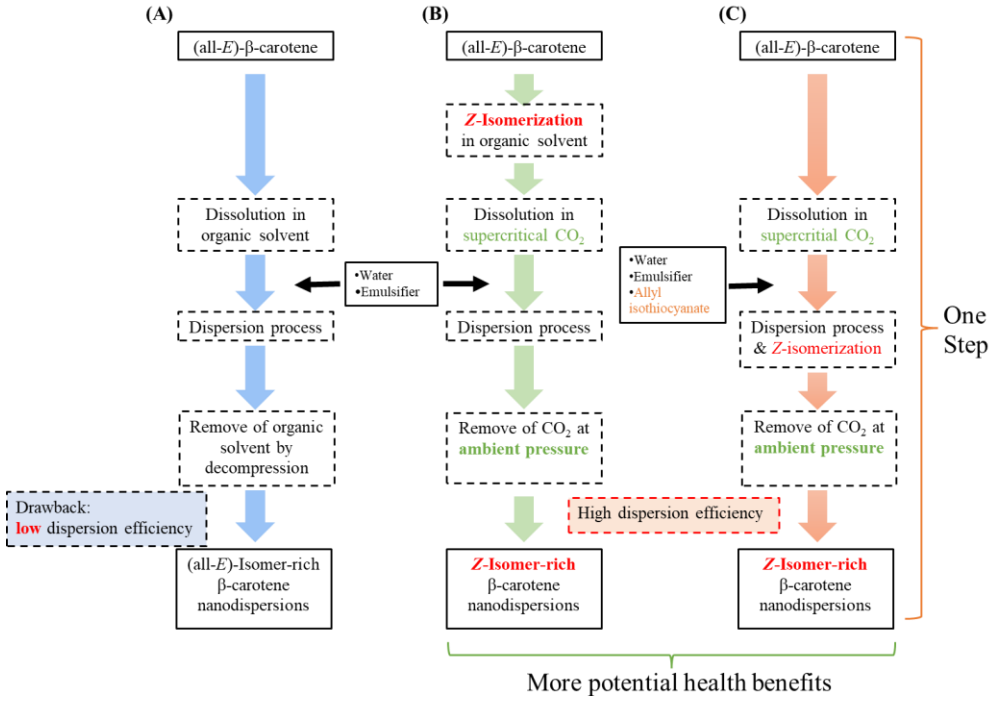

Figure 3.1.2 Solubility improvement by *Z*-isomerization and the improved production efficiency of aqueous solution distribution treatment: (**A**) general partitioning method for carotenoids (emulsification-evaporation technique using organic solvents) [11, 12]; (**B**) the emulsification-evaporation technique using SC-CO_2 instead of organic solution as the organic solution phase, where the *Z*-isomerization process is performed prior to the dispersion process [13]; (**C**) the emulsification-evaporation technique using SC-CO_2 as the organic phase performed by adding allyl isothiocyanate (a new and original method in this study) for simultaneous the *Z*-isomerization and the dispersion processes.

3.1.2 *Z*-Isomerization using allyl isothiocyanate

Since (all-*E*)-β-carotene (**Figure 3.1.1 (A)**) existing as the predominant geometric isomer in nature, exhibits extremely low solubility in SC-CO_2 and other organic solvents, which can greatly reduce the processes efficiency such as extraction, emulsification, and micronization. For instance, the lycopene extraction yield by ethanol from *Z*-isomer-rich tomato pulp was 12-fold that using all-*E*-isomer-rich tomato pulp, and the encapsulation efficiency using *Z*-isomer-rich β-carotene in emulsification process was 21.2 times that using all-*E*-isomer-rich β-carotene [7, 13, 14]. Additionally, several studies demonstrated that *Z*-isomerization of carotenoids can be a method to improve their bioavailability [15-17]. It has been reported that *Z*-isomers of carotenoid generated by the thermal treatment exhibit greater bioavailability and tissue accumulation efficiency than that of all-*E*-isomers [18-20]. For instance, compared with the results of all-*E*-isomer-rich β-carotene (total *Z*-isomer ratio at 2.2%), Honda et al. reported a 5.3-fold increase of β-carotene concentration in specific tissues, such as liver, adrenal, and testis of rats orally taking *Z*-isomer-rich β-carotene (total *Z*-isomer ratio at 83.6%) [20]. Moreover, several studies indicated that specific β-carotene *Z*-isomers have higher biological activities, such as antioxidant and antiatherogenesis activities, than that of all-*E*-isomer [21, 22].

Heat treatment is a common method to obtain the *Z*-isomer of β-carotene, and usually toxic organic solvents such as dichloromethane (CH_2Cl_2) and chloroform ($CHCl_3$) are used in the heat treatment [6, 13, 23]. Although all-*E*-carotenoids can be thermally isomerized to *Z*-isomers in SC-CO_2, this process is very inefficient and normally requires high temperature heating [14]. Honda et al. reported the decomposition ratio of β-carotene in ethyl acetate under 60-min heating at 60 °C was approximate 66% [23]. Recently, it has been discovered that some compounds of plant origin, such as isothiocyanates and polysulfides, can be used to promote the *Z*-isomerization reaction of all-*E*-carotenoids. [23-25].

3.1.3 *Z*-Isomer-rich β-carotene nanodispersions prepared using ultrasound-assisted SC-CO_2

In previous studies, supercritical carbon dioxide (SC-CO_2) was successfully used to produce β-carotene dispersions, and because of its non-toxic and gaseous nature at room temperature, it can be easily separated from the final product and is a good alternative to common organic solvents. [13]. In the production of β-carotene dispersions using SC-CO_2, a *Z*-isomerization treatment process was performed prior to the dispersion process. (**Figure 3.1.2 (B)**). The reason for the *Z*-isomerization pretreatment was that both the *Z*-isomers of β-carotene (**Figure 3.1.1 (B)–(D)**) in SC-CO_2 and the organic solvent possessed higher solubility than the all-*E*-isomer [6, 7, 26-28]. For instance, Honda et al. reported that the *Z*-isomers of β-carotene is 250 times more soluble in ethanol than the all-*E*-isomer [8]. The astaxanthin containing 63.2% *Z*-isomers exhibited approximately 700-fold higher solubility than that of all-*E*-astaxanthin in ethanol [6]. Recently, compared with *E*-isomer-rich astaxanthin feed, Honda et al. reported the increased bioavailability of *Z*-isomer-rich astaxanthin feed in specific crickets [17]. Moreover, it is revealed that (9*Z*)-β-carotene showed nearly four times higher solubility in SC-CO_2 than that of all-*E*-isomer [26]. Therefore, it is considered that the production efficiency of preparing β-carotene dispersion can be improved by using *Z*-isomer-rich β-carotene. Moreover, the enrichment of *Z*-isomers of β-carotene in nanodispersions is prospective to enhance the health benefits of the final product [22, 29]. However, previous method consists of relatively complicated processes as shown in **Figure 3.1.2 (B)**.

Therefore, we proposed that *Z*-isomerization accelerating catalyst was added into the reaction vessel to *Z*-isomerize (all-*E*)-β-carotene in SC-CO_2 during preparing β-carotene nanodispersions by emulsification-evaporation technique, to further improve the production efficiency of β-carotene nanodispersions (**Figure 3.1.2 (C)**). The aim of this study was to improve the production performance of β-carotene nanodispersions using a *Z*-isomerization-accelerating catalyst of plant origin during ultrasound-assisted SC-CO_2 nanodispersios production. Among them, allyl isothiocyanate (AITC) was used as the catalyst. AITC is abundantly present in mustard seeds and is marketed as a product available in high purity and relatively cheap price, and in addition, AITC is non-toxic and has several benefits for human health such as anti-cancer and anti-

inflammatory activities [30, 31]. Furthermore, due to the relatively low boiling point and high volatility of AITC, it can be easily removed from produced nanodispersions [32].

3.1.4 Research objectives

The solubility of *Z*-isomers of β-carotene in various solvents including SC-CO_2 are higher than that of all-*E*-isomer [6, 26]. In our previous work, the production efficiency of β-carotene nanodispersions was successfully improved utilizing the solubility improvement of β–carotene after *Z*-isomerization by using the emulsification-evaporation technique [13]. However, as noted before, toxic solvents (CH_2Cl_2 and methanol) were involved in *Z*-isomerization process of (all-*E*)-β-carotene, and relatively complicated processes were performed. In this study, we aimed to develop a one-step process containing both *Z*-isomerization and water-dispersion process using a naturally occurring *Z*-isomerization-accelerating catalyst, AITC, where there was no involvement of organic solvents in the whole process.

3.2 Materials and methods

3.2.1 Materials and chemicals

(All-*E*)-β-carotene (crystalline β-carotene) and high-performance liquid chromatography (HPLC) grade organic solvents (acetone, hexane, methanol, methyl tertiary butyl ether (MTBE) were purchased from FUJIFILM Wako Pure Chemical Company (Osaka, Japan). Polyoxyethylene sorbitan monolaurate (Tween 20) and AITC were purchased from Tokyo Chemical Industry Co. (Tokyo, Japan). Carbon dioxide was supplied by Tomoe Shokai Co. (Tokyo, Japan). Distilled water was used in all the experiments.

3.2.2 Nanodispersions production using ultrasound-assisted supercritical carbon dioxide

According to the previous method described [11, 13], the distributed processing of β-carotene was performed. **Figure 3.2.1** shows a schematic diagram of the dispersion process. 15 mg of crystalline β-carotene and 13.5 mL of distilled water containing 0.5 wt.% Tween 20 (emulsifier) were added into the 15 ml SUS-316 stainless-steel high-pressure vessel with two 2-μm filters (GL Sciences Inc., Tokyo, Japan). Carbon dioxide was introduced into the aqueous solution to remove the dissolved oxygen from the aqueous solution. After the removal of oxygen, AITC (50 or 100 mg) was added to the vessel. Afterwards, the reactor vessel containing the solution was connected to the system. The liquid CO_2 in the cylinder is cooled by a cooler (TBG020AA, Advantec Toyo Kaisha, Ltd., Tokyo, Japan) and pumped into the vessel by a high-pressure pump (PU-980, Jasco Co., Tokyo, Japan). Subsequently, the upper space of the vessel is filled with liquefied CO_2. The pressure of the system is maintained at 20 MPa by the back-pressure regulator (BPR; Akico Co., Ltd., Tokyo, Japan), and the vessel is preheated to 50 °C in a water bath for 30 minutes to transform the liquid CO_2 to the supercritical state. Afterwards, the volume ratio of SC-CO_2/water phase was maintained at 1:9 inside the vessel [12, 33]. After the dispersion treatment, the pressure of the system was slowly reduced to atmospheric pressure by BPR and the nanodispersions were taken out together with CO_2 passing through the 2 μm filter and collected in the recovery bottle. β-Carotene that was not encapsulated was removed from the produced aqueous solution and left inside the reaction vessel via the 2 μm filter. All the experiments were carried out for three times and the results are expressed as mean ± standard deviation.

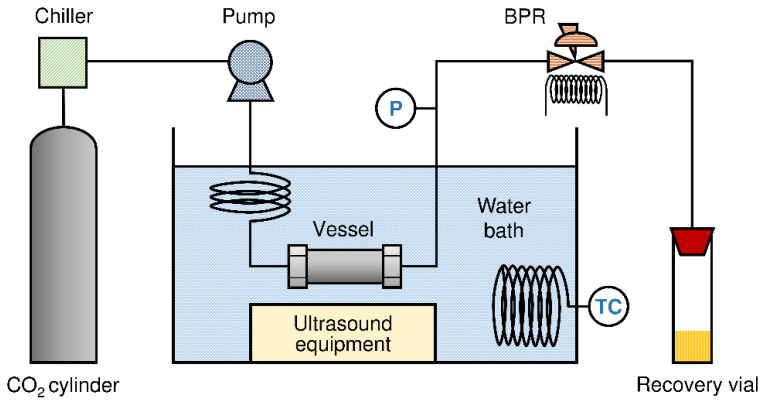

Figure 3.2.1 Schematic diagram of the β-carotene dispersion process. Two 2-μm filters were inserted to the two outlets of the vessel.

3.2.3 Encapsulated β-carotene content

As described previously, a UV–Vis spectrophotometer (V-550, Jasco Co., Tokyo, Japan) was used to determine the absorbance at 453 nm of the produced nanodispersions to determine the β-carotene content in it [11, 13, 34]. Only β-carotene that is successfully dispersed in the solution shows absorbance, and its concentration is proportional to the absorbance value. Therefore, undispersed crystalline β-carotene does not contribute to the absorbance value. We used five different concentrations of pure (all-*E*)-β-carotene dissolved in ethanol as calibration curves for concentration calculations in nanodispersions [13].

3.2.4 Absorption spectra of β-carotene nanodispersions

Reversed-phase HPLC with a C_{30} carotenoid column (250×4.6mm i.d., 5 mm, YMC Co., Ltd., Kyoto, Japan) was used to determine the total *Z*-isomer ratio of β-carotene in prepared nanodispersions [13, 35, 36]. The mixture of ethanol and hexane (1:1, v/v) were used to extract β-carotene isomers from produced nanodispersions. Mixed solution of MTBE/methanol (11:89, v/v) was applied as the mobile phase at 1 mL/min. The temperature of HPLC column was maintained at 40 °C. The β-carotene isomers were detected and quantified by the peak area at 453 nm with a UV–Vis detector (UV-2075

Plus, Jasco Co., Tokyo, Japan). The HPLC retention times, absorption maximum of the isomer, and relative intensities of the *Z*-peak as $\%D_B/D_{II}$ (Q-ratios) were used to identify the peaks of β-carotene isomers such as (all-*E*)-, (9*Z*)-, and (13*Z*)-isomers [13, 23, 35-37]. The total *Z*-isomer ratio (%) of β-carotene was calculated as equation (1) shown. the ratio of peak areas of *Z*-isomers of β-carotene to peak areas of all β-carotene isomer.

$$\text{Total } Z\text{- isomer ratio } \% = \frac{\text{Peak areas of } Z\text{-isomers of } \beta\text{-carotene}}{\text{Peak areas of all } \beta\text{-carotene}} \% \qquad \textbf{Equation (1)}$$

3.2.5 Analysis of the color of β-carotene nanodispersions

To evaluate the color of resulting β-carotene nanodispersions, the absorption spectra of nanodispersions as well as β-carotene crystalline, AITC, and tween 20 water solutions were measured by a UV–Vis spectrophotometer (V-550, Jasco Co., Tokyo, Japan) ranging from 300 nm to 800 nm. All the nanodispersions and reagents were dissolved in distilled water.

3.2.6 Analysis of the size of produced nanodispersions

The average diameters of prepared β-carotene nanodispersions were measured by dynamic light scattering (DLS) ranging from 0.3 nm to 10 μm (Zetasizer Nano ZS, Malvern Instruments, Ltd., Worcestershire, United Kingdom). The refractive index of β-carotene in water was set at 1.47 and every sample was measured for 3 times [13, 38].

3.3 Results and discussion

3.3.1 Effects of AITC amount on total *Z*-isomer ratio and β-carotene content in nanodispersions

The HPLC chromatograms of β-carotene isomers in produced nanodispersions as well as raw β-carotene material (crystalline β-carotene) are shown in **Figure 3.3.1**. In the intact crystalline β-carotene, more than 90% of β-carotene was detected as the all-*E*-isomer, whereas in produced nanodispersions, the detected peak numbers and the area

of β-carotene *Z*-isomers markedly increased. Ample studies have revealed that (all-*E*)-carotenoids can be thermally isomerized to *Z*-isomers in solvents including SC-CO_2 [14, 23]. Thus, we believed that thermal *Z*-isomerization of (all-*E*)-β-carotene proceeded in this nanodispersion preparation process, and it led to the generation of some unidentified *Z*-isomers and 13*Z*-isomer as shown in **Figure 3.3.1 (B)**. It is worth mentioning that no 9*Z*-isomer of β-carotene was produced with no addition of AITC, but when AITC was added, a large amount of the 9*Z*-isomer was produced. It might be because the relatively higher activation reaction energy is required to transform all-*E*-isomer of β–carotene to 9*Z*-isomer compared with the relatively lower activation reaction energy of *Z*-isomerizing all-*E*-isomer to 13*Z*-isomer as reported by Guo et al. [39]. Therefore, under low heating temperature at 50 °C, only 13*Z*-isomer was found. This phenomenon also indicated that AITC as a catalyst did help with the *Z*-isomerization from all-*E*-isomer to *Z*-isomer normally requiring relatively high temperature under mild thermal treatment. Moreover, several researches disclosed that (9*Z*)-β-carotene exhibited greater antiatherosclerotic and antiatherogenic activities than all-*E*-isomer [22, 29]. Hence, the pharmacological activity of produced β-carotene nanodispersions could be improved by AITC addition.

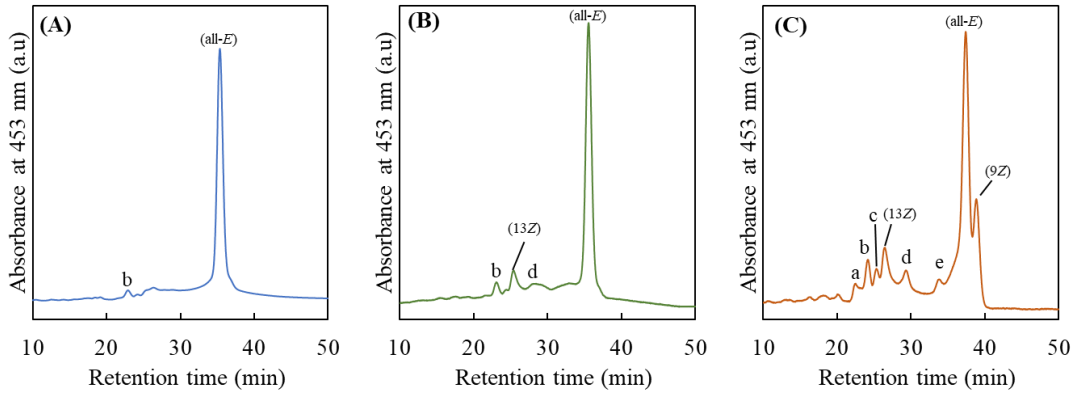

Figure 3.3.1 Chromatograms of (**A**) crystalline β-carotene and various isomers in the nanodispersions produced (**B**) without AITC addition and (**C**) with 100 mg AITC addition detected by reversed-phase HPLC. The nanodispersions were obtained by the 180-min ultrasound treatment at 50 °C and 20 MPa. (All-*E*)-, (9*Z*)-, and (13*Z*) designated in the chromatograms were identified according to previous studies [13, 23, 35-37]. Some of the peaks (a–e) were tentatively identified as shown in **Table 3.3.1**.

In **Table 3.3.2**, the total *Z*-isomer ratio and β-carotene content in prepared nanodispersions are summarized. In brief, the addition of 50 mg or more amounts of AITC successfully enhanced the total *Z*-isomer ratio of β-carotene in the prepared nanodispersions. In addition, the β-carotene encapsulation content of the prepared nanodispersions was significantly enhanced. For instance, when 100 mg of AITC was added, the amount of β-carotene that was internally encapsulated was four times that with no AITC addition. This is since the solubility of β-carotene in SC-CO_2 was greatly increased after *Z*-isomerization [13, 14, 23]. This study is the first success example of performing isomerization and dispersion in one step without using any organic solvents in the whole process. Although produced nanodispersions had the smell of AITC, since AITC is highly volatile, it could be easily removed by further decompression treatment [32]. On the other hand, since AITC has several useful bioactivities such as anticancer and anti-inflammatory activities [30, 31], a synergistic health effect could be expected when it is taken together with β-carotene.

Table 3.3.1 Absorption maxima (λ_{max}) and relative intensities of *Z*-peak (%D_B/D_{II}) of geometrical β-carotene isomers separated and observed in reversed-phase HPLC analysis.

Peak	β-Carotene isomer	λ_{max} (nm)		% D_B/D_{II}	
		Observed	Reported[a]	Observed	Reported[a]
a	U*Z*	336,458,483,582	–	56.7	–
b	U*Z*	342,434,452,484	–	55.6	–
c	U*Z*	329,393,442,486	–	64.1	–
	(13*Z*)	336,425,442,472	339,420,445,470	44.2	37.1
d	U*Z*	332,412,442,484	–	70.1	–
e	U*Z*	338,442,462,473	–	61.7	–
	(all-*E*)	423,450,473	426,452,478	ND	ND
	(9*Z*)	338,420,446,470	340,422,447,473	6.6	9.4

Values and peak designations were obtained from the chromatograms in **Figure 3.3.1**.
–, not assigned. U*Z*, unidentified *Z*-isomer of β-carotene. ND, not detected substantially.
[a] Tentatively assigned in the literatures [13, 23, 35-37].

Table 3.3.2 Total *Z*-isomer ratio (%) and β-carotene content (mg/L) in nanodispersions.

Addition mount of AITC added (mg)	Total *Z*-isomer ratio (%)	β-Carotene content (mg/L)
0	15.0 ± 2.0	29.6 ± 9.8
50	31.1 ± 0.7	69.6± 5.1
100	37.4 ± 1.5	116.4 ± 11.2

3.3.2 Characterization of β-carotene nanodispersions

3.3.2.1 Color of nanodispersions

The colors of prepared β-carotene nanodispersions with or without AITC addition were evaluated by the appearances and absorption spectra (**Figure 3.3.2**). In the case of no AITC addition, the appearance of β-carotene nanodispersions showed light reddish yellow. When 100 mg of AITC was added in the dispersion process, the prepared nanodispersions was deep yellow. Silva et al. reported that β-carotene nanodispersions obtained by organic solvent-used emulsification-evaporation technique showed that similar color appearance [33].

Notably, the absorption spectrum detected by UV–Vis also confirmed the successful encapsulation of β-carotene with AITC addition. As it can be found easily, there was no absorption in range of 350–700 nm of the dispersions of β-carotene, AITC, and Tween 20 water solution. This phenomenon is in consonance with previously described fact that the unencapsulated β-carotene crystalline keeps aqueously insoluble and doesn't attribute to the absorption around 453 nm as the encapsulated and well-dispersed β-carotene. β-Carotene nanodispersions produced without AITC addition showed a slight absorption in the range of 400–550 nm because the slight thermal *Z*-isomerization of some β-carotene increase the encapsulated β-carotene content in it. β-Carotene nanodispersions with 100 mg AITC addition showed strong absorption in the range of 400–550 nm due to the high encapsulated β-carotene content. The absorption spectrum around 400–550 nm is a characteristic range of β-carotene, and the observed absorption around this range indicated that β-carotene is well-dispersed in water and exhibits color [13, 34, 40].

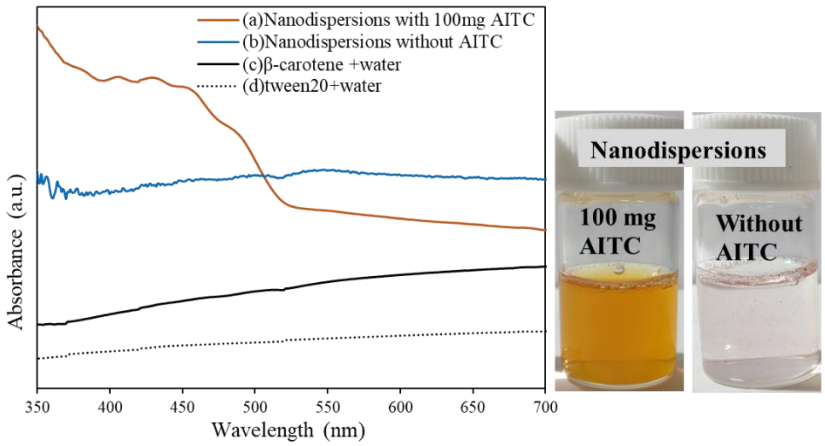

Figure 3.3.2 Absorption spectra of β-carotene nanodispersions with and without 100 mg of AITC as well as water dispersions of β-carotene, AITC, and Tween 20; appearances of produced β-carotene nanodispersions.

3.3.2.2 Size distribution of nanodispersions

The size distributions of prepared β-carotene nanodispersions in this work are shown in **Figure 3.3.3**. It is obvious that there are two peaks at around 100 and 700 nm separately in both nanodispersions. Similar size distribution pattern is also observed in our previous study [13]. We think that crystalline β-carotene encapsulated in tween 20 micelle exhibited the size peak around 700 nm and it is because high crystallinity of all-*E*-isomer making it easier to form large crystals to further increase nanodispersions size. The dissolved *Z*-isomers of β-carotene in SC-CO_2 help with the formation of nanodispersions with size peak around 100 nm. The reason is that amorphous *Z*-isomers could be efficiently dispersed into relatively small size by the cavitation effect of ultrasound and the *Z*-isomers existence inhibited the crystallinity of β-carotene from forming large crystal via steric hindrance. In previous work, nanodispersions produced with approximate 80% *Z*-isomers ratio of β-carotene showed only one sharp peak around 100 nm with only few existences of large nanodispersions around 700 nm [13]. Moreover, Tan and Nakajima reported that when prepared β-carotene dispersions by organic solvent-used emulsification-evaporation technique, the particle size of the resulting dispersions was at around 100 nm [11]. Furthermore, the addition of AITC helped to produced relatively uniform size of nanodispersions as a shaper size peak was

found in nanodispersions with 100 mg AITC addition compared with that without AITC addition.

The mean diameters of prepared β-carotene nanodispersions without AITC and with 50 and 100 mg of AITC were 212.1 ± 33.2, 186.1 ± 28.4, and 101.1 ± 47.9 nm respectively. AITC addition significantly reduced the diameters of β-carotene nanodispersions. It is attributed to the *Z*-isomers ratio increase after AITC addition which helped to inhibited the crystal formation of β-carotene [6, 7]. It has been indicated that nano-sized carotenoid suspensions with size around 100 nm showed enhanced bioavailability [41, 42]. Therefore, the use of AITC in this method could contribute to improve the β-carotene bioavailability.

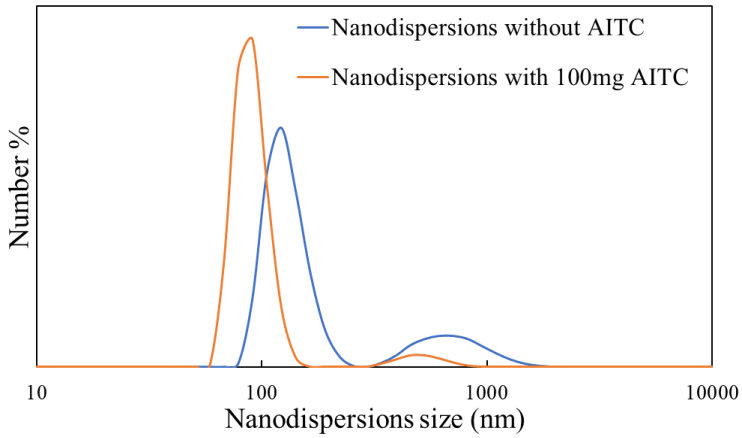

Figure 3.3.3 Size distributions of β-carotene nanodispersions produced with and without AITC addition.

3.4 Conclusions

Z-Isomer-rich β-carotene nanodispersions with average size around 100 nm were successfully prepared using ultrasound-assisted SC-CO_2 with the addition of AITC as a *Z*-isomerization-accelerating catalyst. Notably, in this work, we succeeded in developing one-step process for producing *Z*-isomer-rich β-carotene nanodispersions with no involvement of any organic solvents in the whole process. The successful development of this system can be expected to solve the previously reported problems of residual organic solvents in final product and complicated operation processes. The

improvement of process efficiency by adding AITC was confirmed, because β-carotene content in nanodispersions produced with 100 mg AITC addition was approximately 4 times and the average diameter was half that produced without AITC addition. Moreover, in the conditions of this work, we found out that AITC addition could mainly enhance the transformation of all-*E*-isomer to 9*Z*-isomer which shows greater antiatherosclerotic and antiatherogenic activities than all-*E*-isomer. Concluded, this one-step dispersion method is very efficient not only for production β-carotene nanodispersions without organic solvents involvement, but also for the enhancement of β-carotene bioactivity.

References:

[1] Jaswir, I.; Noviendri, D.; Fitri Hasrini, R.; Octavianti, F., Carotenoids: Sources, medicinal properties and their application in food and nutraceutical industry. *Journal of Medicinal Plants Research,* **2011**, *5* (33), 7119-7131.

[2] Seo, J. S.; Burri, B. J.; Quan, Z.; Neidlinger, T. R., Extraction and chromatography of carotenoids from pumpkin. *Journal of Chromatography A,* **2005**, *1073* (1), 371-375.

[3] Qian, C.; Decker, E. A.; Xiao, H.; McClements, D. J., Inhibition of β-carotene degradation in oil-in-water nanoemulsions: Influence of oil-soluble and water-soluble antioxidants. *Food Chemistry,* **2012**, *135* (3), 1036-1043.

[4] Gul, K.; Tak, A.; Singh, A. K.; Singh, P.; Yousuf, B.; Wani, A. A., Chemistry, encapsulation, and health benefits of β-carotene - A review. *Cogent Food & Agriculture,* **2015**, *1* (1), 1018696.

[5] D'Odorico, A.; Martines, D.; Kiechl, S.; Egger, G.; Oberhollenzer, F.; Bonvicini, P.; Sturniolo, G. C.; Naccarato, R.; Willeit, J., High plasma levels of α- and β-carotene are associated with a lower risk of atherosclerosis: Results from the Bruneck study. *Atherosclerosis,* **2000**, *153* (1), 231-239.

[6] Honda, M.; Kodama, T.; Kageyama, H.; Hibino, T.; , W.; Kanda, H.; Goto, M., Enhanced Solubility and Reduced Crystallinity of Carotenoids, β-Carotene and Astaxanthin, by *Z*-Isomerization. *European Journal of Lipid Science and Technology,* **2018**, *120* (11), 1800191.

[7] Honda, M.; Kageyama, H.; Hibino, T.; Zhang, Y.; Diono, W.; Kanda, H.; Yamaguchi, R.; Takemura, R.; Fukaya, T.; Goto, M., Improved Carotenoid

Processing with Sustainable Solvents Utilizing *Z*-Isomerization-Induced Alteration in Physicochemical Properties: A Review and Future Directions. *Molecules (Basel, Switzerland),* **2019**, *24* (11), 2149.

[8] Ribeiro, H. S.; Cruz, R. C. D., Highly Concentrated Carotenoid-Containing Emulsions. *Engineering in Life Sciences,* **2005**, *5* (1), 84-88.

[9] Mahalakshmi, L.; Leena, M. M.; Moses, J. A.; Anandharamakrishnan, C., Micro- and nano-encapsulation of β-carotene in zein protein: size-dependent release and absorption behavior. *Food & Function,* **2020**, *11* (2), 1647-1660.

[10] Salvia-Trujillo, L.; Qian, C.; Martín-Belloso, O.; McClements, D. J., Influence of particle size on lipid digestion and β-carotene bioaccessibility in emulsions and nanoemulsions. *Food Chemistry,* **2013**, *141* (2), 1472-80.

[11] Tan, C. P.; Nakajima, M., β-Carotene nanodispersions: preparation, characterization and stability evaluation. *Food Chemistry,* **2005**, *92* (4), 661-671.

[12] de Paz, E.; Martín, Á.; Mateos, E.; Cocero, M. J., Production of water-soluble β-carotene micellar formulations by novel emulsion techniques. *Chemical Engineering and Processing: Process Intensification,* **2013**, *74*, 90-96.

[13] Ono, M.; Honda, M.; Wahyudiono; Yasuda, K.; Kanda, H.; Goto, M., Production of β-carotene nanosuspensions using supercritical CO_2 and improvement of its efficiency by *Z*-isomerization pre-treatment. *The Journal of Supercritical Fluids,* **2018**, *138*, 124-131.

[14] Watanabe, Y.; Honda, M.; Higashiura, T.; Fukaya, T.; Machmudah, S.; Wahyudiono; Kanda, H.; Motonobu, G., Rapid and Selective Concentration of Lycopene *Z*-isomers from Tomato Pulp by Supercritical CO_2 with Co-solvents. *Solvent Extraction Research and Development Japan,* **2018**, *25* (1), 47-57.

[15] Honda, M., Chapter 5 - Carotenoid isomers: A systematic review of the analysis, biological activity, physicochemical property, and methods for isomerization. In *Studies in Natural Products Chemistry*, Atta ur, R., Ed. Elsevier: 2021; Vol. 68, pp 173-220.

[16] Cheng, Y.; Lianfu, Z.; Rong, T., Chemistry and biochemistry of dietary carotenoids: bioaccessibility, bioavailability and bioactivities. *Journal of Food Bioactives,* **2020**, *10* (0).

[17] Honda, M.; Hirota, K.; Zhang, Y.; Yoshiaki, H.; Sugahara, R., Effect of astaxanthin isomer supplementation on their accumulation in edible orthopterans: migratory locusts and two-spotted crickets. In *Journal of Insects as Food and Feed*, (Accepted).

[18] Unlu, N. Z.; Bohn, T.; Francis, D. M.; Nagaraja, H. N.; Clinton, S. K.; Schwartz, S. J., Lycopene from heat-induced *cis*-isomer-rich tomato sauce is more bioavailable than from all-*trans*-rich tomato sauce in human subjects. *British Journal of Nutrition,* **2007**, *98* (1), 140-6.
[19] Honda, M.; Murakami, K.; Osawa, Y.; Kawashima, Y.; Hirasawa, K.; Kuroda, I., *Z*-Isomers of Astaxanthin Exhibit Greater Bioavailability and Tissue Accumulation Efficiency than the All-*E*-Isomer. *Journal of Agricultural and Food Chemistry,* **2021**, *69* (11), 3489-3495.
[20] Honda, M.; Takasu, S.; Nakagawa, K.; Tsuda, T., Differences in bioavailability and tissue accumulation efficiency of (all-*E*)- and (*Z*)-carotenoids: A comparative study. *Food Chemistry,* **2021**, *361*, 130119.
[21] Jimenez, C.; Pick, U., Differential Reactivity of β-Carotene Isomers from Dunaliella bardawil Toward Oxygen Radicals. *Plant Physiology,* **1993**, *101* (2), 385-390.
[22] Harari, A.; Harats, D.; Marko, D.; Cohen, H.; Barshack, I.; Kamari, Y.; Gonen, A.; Gerber, Y.; Ben-Amotz, A.; Shaish, A., A 9-cis β-Carotene–Enriched Diet Inhibits Atherogenesis and Fatty Liver Formation in LDL Receptor Knockout Mice. *The Journal of Nutrition,* **2008**, *138* (10), 1923-1930.
[23] Honda, M.; Kageyama, H.; Hibino, T.; Ichihashi, K.; Takada, W.; Goto, M., Isomerization of Commercially Important Carotenoids (Lycopene, β-Carotene, and Astaxanthin) by Natural Catalysts: Isothiocyanates and Polysulfides. *Journal of Agricultural and Food Chemistry,* **2020**, *68* (10), 3228-3237.
[24] Honda, M.; Kageyama, H.; Hibino, T.; Takemura, R.; Goto, M.; Fukaya, T., Enhanced *Z*-isomerization of tomato lycopene through the optimal combination of food ingredients. *Scientific Reports,* **2019**, *9* (1), 7979.
[25] Honda, M.; Zhang, Y.; Goto, M., Isothiocyanate-functionalized silica as an efficient heterogeneous catalyst for carotenoid isomerization. *Food Chemistry,* **2023**, *410*, 135388.
[26] Gamlieli-Bonshtein, I.; Korin, E.; Cohen, S., Selective separation of cis-trans geometrical isomers of β-carotene via CO_2 supercritical fluid extraction. *Biotechnology and Bioengineering,* **2002**, *80* (2), 169-174.
[27] Murakami, K.; Honda, M.; Takemura, R.; Fukaya, T.; Kubota, M.; Wahyudiono; Kanda, H.; Goto, M., The thermal *Z*-isomerization-induced change in solubility and physical properties of (all-*E*)-lycopene. *Biochemical and Biophysical Research Communications,* **2017**, *491* (2), 317-322.

[28] Honda, M.; Watanabe, Y.; Murakami, K.; Hoang, N. N.; diono, W.; Kanda, H.; Goto, M., Enhanced Lycopene Extraction from Gac (Momordica cochinchinensis Spreng.) by the *Z*-Isomerization Induced with Microwave Irradiation Pre-Treatment. *European Journal of Lipid Science and Technology,* **2018**, *120* (2), 1700293.
[29] Relevy, N. Z.; Rühl, R.; Harari, A.; Grosskopf, I.; Barshack, I.; Ben-Amotz, A.; Nir, U.; Gottlieb, H.; Kamari, Y.; Harats, D.; Shaish, A., 9-cis β-carotene Inhibits Atherosclerosis Development in Female LDLR-/- Mice. *Functional Foods in Health and Disease,* **2015**, *5*, 67-79.
[30] Wagner, A. E.; Boesch-Saadatmandi, C.; Dose, J.; Schultheiss, G.; Rimbach, G., Anti-inflammatory potential of allyl-isothiocyanate—role of Nrf2, NF-κB and microRNA-155. *Journal of Cellular and Molecular Medicine,* **2012**, *16* (4), 836-43.
[31] Zhang, Y., Allyl isothiocyanate as a cancer chemopreventive phytochemical. *Molecular Nutrition & Food Research,* **2010**, *54* (1), 127-35.
[32] Kamihira, M.; Asai, T.; Yamagata, Y.; Taniguchi, M.; Kobayashi, T., Formation of inclusion complexes between cyclodextrins and aromatic compounds under pressurized carbon dioxide. *Journal of Fermentation and Bioengineering,* **1990**, *69* (6), 350-353.
[33] Silva, H. D.; Cerqueira, M. A.; Souza, B. W. S.; Ribeiro, C.; Avides, M. C.; Quintas, M. A. C.; Coimbra, J. S. R.; Carneiro-da-Cunha, M. G.; Vicente, A. A., Nanoemulsions of β-carotene using a high-energy emulsification–evaporation technique. *Journal of Food Engineering,* **2011**, *102* (2), 130-135.
[34] de Paz, E.; Martín, Á.; Estrella, A.; Rodríguez-Rojo, S.; Matias, A. A.; Duarte, C. M. M.; Cocero, M. J., Formulation of β-carotene by precipitation from pressurized ethyl acetate-on-water emulsions for application as natural colorant. *Food Hydrocolloids,* **2012**, *26* (1), 17-27.
[35] Emenhiser, C.; Simunovic, N.; Sander, L. C.; Schwartz, S. J., Separation of Geometrical Carotenoid Isomers in Biological Extracts Using a Polymeric C_{30} Column in Reversed-Phase Liquid Chromatography. *Journal of Agricultural and Food Chemistry,* **1996**, *44* (12), 3887-3893.
[36] Imsic, M.; Winkler, S.; Tomkins, B.; Jones, R., Effect of Storage and Cooking on β-Carotene Isomers in Carrots (*Daucus carota* L. cv. 'Stefano'). *Journal of Agricultural and Food Chemistry,* **2010**, *58* (8), 5109-5113.
[37] Böhm, V.; Puspitasari-Nienaber, N. L.; Ferruzzi, M. G.; Schwartz, S. J., Trolox Equivalent Antioxidant Capacity of Different Geometrical Isomers of α-Carotene, β-

Carotene, Lycopene, and Zeaxanthin. *Journal of Agricultural and Food Chemistry,* **2002**, *50* (1), 221-226.
[38] Tanaka, Y.; Uemori, C.; Kon, T.; Honda, M.; Wahyudiono; Machmudah, S.; Kanda, H.; Goto, M., Preparation of liposomes encapsulating β–carotene using supercritical carbon dioxide with ultrasonication. *The Journal of Supercritical Fluids,* **2020**, *161*, 104848.
[39] Guo, W.-H.; Tu, C.-Y.; Hu, C.-H., Cis−Trans Isomerizations of β-Carotene and Lycopene: A Theoretical Study. *The Journal of Physical Chemistry B,* **2008**, *112* (38), 12158-12167.
[40] Kaga, K.; Honda, M.; Adachi, T.; Honjo, M.; Wahyudiono; Kanda, H.; Goto, M., Nanoparticle formation of PVP/astaxanthin inclusion complex by solution-enhanced dispersion by supercritical fluids (SEDS): Effect of PVP and astaxanthin Z-isomer content. *The Journal of Supercritical Fluids,* **2018**, *136*, 44-51.
[41] Rohini Vishwanathan; Wilson, T. A.; Nicolosi, R. J., Bioavailability of a Nanoemulsion of Lutein Is Greater than a Lutein Supplement. *Nano Biomedicine and Engineering,* **2009**, *1* (1), 38-49.
[42] Affandi, M. M. R. M. M.; Julianto, T.; Majeed, A. B. A., Enhanced Oral Bioavailability of Astaxanthin with Droplet Size Reduction. *Food Science and Technology Research,* **2012**, *18* (4), 549-554.

Chapter 4 Continuous production of *Z*-isomer-rich β-carotene nanodispersions using subcritical ethyl acetate and a swirl-type mixer

4.1 Introduction

4.1.1 Continuous production process

In previous work, we succeeded in producing *Z*-isomer-rich β-carotene nanodispersions with one-step batch process using ultrasound-assisted SC-CO_2. Unlike batch process where human operation is required to take product of one process to the next process, in the continuous production process, produced material of each process will be sent to the next process directly [1]. Therefore, continuous production technology is attracting increasing attention, because it involves less human operation relating to higher efficiency and accuracy, and has lower containment probability and less scale-up effects than traditional batch processes. Especially, in medicine production process, continuous process development is prospective to meet the further demand for small-scale production of personalized medicine with high efficiency and accuracy.

4.1.2 Thermal *Z*-isomerization under high temperature

The most documented method for *Z*-isomerization of (all-*E*)-carotenoids is the thermal method, but the efficiency of this method is reported to be not high [2, 3]. The iodine and heavy metal catalyst are often used, but many of these catalysts are highly toxic which is not allowed to be used in food, cosmetic and pharmaceutical products [3-6]. Therefore, in this work, we aimed to investigate whether the *Z*-isomerization efficiency of carotenoid can be improved under extreme high temperature in range of 140–200 °C without the involvement of any types of catalyst. Precisely, ethyl acetate was used to dissolve (all-*E*)-β-carotene, and the prepared solution was continuously thermally-

treated under high temperature for certain time. However, due to the low boiling point (77.1 °C) of ethyl acetate, the thermal treatment of *Z*-isomerization in ethyl acetate was carried out under high pressure (10 MPa) where ethyl acetate is kept in subcritical state.

4.1.3 Introduction of swirl-type mixer

In recent years, many types of dispersion mixers have been developed, such as Y-shape, coaxial nozzle, and central-collision [7-9]. Initially, to solve unwanted stagnant at mixing point inside some conventional mixers (such as T-type mixer) in nanoparticles production using supercritical water, the idea of swirl-type mixer, which can help (1) to prevent the contact of adhesive fluid with mixer wall and inhibit stagnant flow inside it, (2) instantaneous mixing of main flow fluid with two sub fluids to produce relatively small and uniformed particles, was proposed and utilized for metal oxide nanoparticles production using supercritical water [7, 8]. Except for the metal oxide nanoparticles production, Chhouk et al. used swirl-type mixer for the nanoparticles production of curcumin/PVP with average particle size of 90 nm showing enhanced water dispersibility [9]. According to the previous studies, swirl-type mixer showed excellent mixing effect and helped in the formation of sharp particles distribution. As the mixing efficiency and size distribution show significant influence on the production efficiency of nanodispersions, and the stability and bioavailability of core compounds, we exploited the use of the swirl-type mixer in developing a continuous production process of *Z*-isomer-rich β-carotene nanodispersions.

4.1.4 Research objectives

Overall speaking, the objective of this work is to develop a continuous process for producing *Z*-isomer-rich β-carotene nanodispersions. The experimental scheme was showed in **Figure 4.1.1**. Items investigated in this work were as follows:

1. Effects of thermal treatment temperature, time, and the addition of antioxidant compounds on the *Z*-isomer-rich β-carotene solution;

2. Effects of the ratio of emulsifier water solution/β-carotene solution, temperature, and pressure on produced β-carotene nanodispersions using a swirl-type mixer.

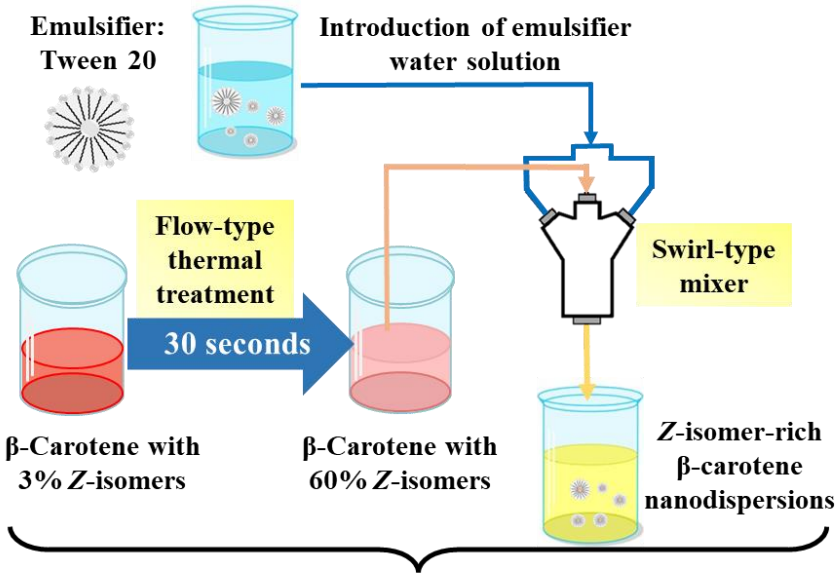

Figure 4.1.1 Schematic graph for *Z*-isomer-rich β–carotene nanodispersions production.

4.2 Materials and methods

4.2.1 Materials and chemicals

(All-*E*)-β-carotene was purchased from FUJIFILM Wako Pure Chemical Corp. (Osaka, Japan). High-performance liquid chromatography (HPLC)-grade organic solvents [methanol, ethanol, ethyl acetate, methyl tert-butyl ether (MTBE), and hexane], and polyoxyethylene (20) sorbitan monolaurate (Tween 20) were purchased from Kanto Chemical Co., Inc. (Tokyo, Japan). α-Tocopherol was obtained from Tokyo Chemical Industry Co., Ltd. (Tokyo, Japan).

4.2.2 Continuous β-carotene *Z*-isomerization in subcritical ethyl acetate

(All-*E*)-β-carotene solutions in ethyl acetate (0.1 mg/mL) were thermally treated by a continuous-flow reactor, as shown in **Figure 4.2.1 (Scheme 1)** for *Z*-isomerization. The reactor consisted of a liquid feed piping (SUS-316, inside diameter 0.5 mm; Shimadzu Co., Ltd., Kyoto, Japan), high-pressure pump (LC-20AD, Shimadzu Co., Ltd., Kyoto, Japan), heating chamber (DX 302, Yamato Scientific Co., Ltd., Tokyo, Japan), water tank for cooling, and back-pressure regulator (HPB-500, Akico Co., Ltd., Tokyo, Japan). Thermal processing was conducted in a heating chamber at 140–200 ℃ and 10 MPa for 30 s–5 min. To suppress the thermal degradation of β-carotene isomers under high temperature during processing, the experiment with addition of antioxidant compound—α-tocopherol (1 mg/mL) was also carried out [10-12].

4.2.3 Continuous production of *Z*-isomer-rich β-carotene nanodispersions

The β-carotene solution in ethyl acetate with or without thermal treatment (**Figure 4.2.1**; **Scheme 1**) was continuously introduced and then mixed with distilled water containing 0.5 wt.% Tween 20 inside the swirl-type mixer (4-1/16YSM-0.8-0.5-S, Sugiyama Shoji Co., Ltd., Kanagawa, Japan) as shown in **Figure 4.2.1** (**Scheme 2**) [13, 14]. The tube diameters of swirl-type mixer main flow and side flow were 0.8 and 0.5 mm, respectively. The prepared β-carotene solution was fed to the main flow passage

at a flow rate of 0.5 mL/min; meanwhile, the water solution was fed to the side flow passage of the mixer with flow rate in range of 2.5–10 mL/min to adjust the ratio of the β-carotene solution/the water solution from 1:5 to 1:20 (v/v) [8, 9]. The effects of temperature and pressure of dispersion process were also investigated in range of 40–70 °C and 0–20 MPa, respectively. The produced β-carotene dispersion solution was collected after the back-pressure regulator, and ethyl acetate was immediately removed from the dispersion liquid using a rotary evaporator under reduced pressure at 40 °C. Finally, *Z*-isomer-rich β-carotene nanodispersions were obtained. This dispersion method of fat-soluble compounds using organic solvents is called the emulsification–evaporation technique [13, 14].

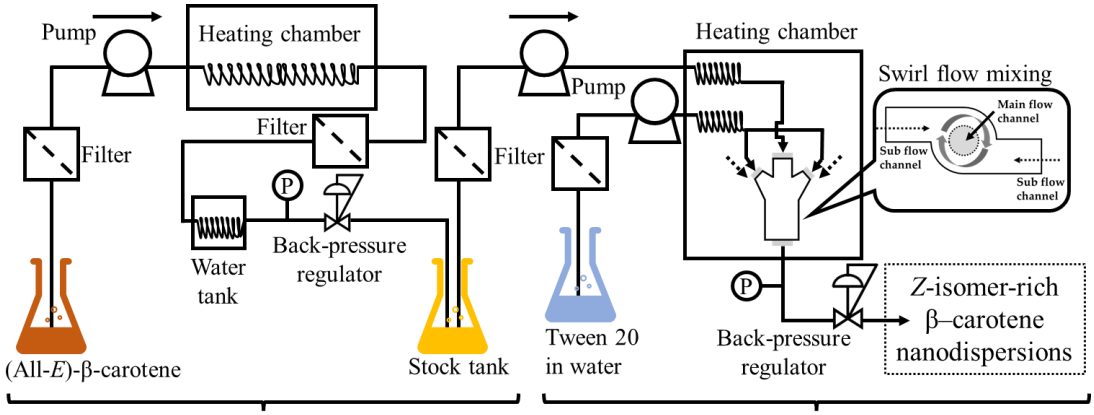

Scheme 1: *Z*-isomerization process **Scheme 2**: Nanodispersions process

Figure 4.2.1 Schematic graph of *Z*-isomer-rich β-carotene nanodispersions production process.

4.2.4 Characterization of *Z*-isomer-rich β-carotene nanodispersions

4.2.4.1 HPLC analysis

β-Carotene isomers were analyzed using reversed-phase HPLC with a photodiode array detector (SPD-M20A; Shimadzu Corp., Kyoto, Japan) as described in previous methods [15-18]. Briefly, to separate β-carotene isomers, a C_{30} column as the stationary phase (250 mm length, 4.6 mm inner diameter, 5 μm particle size; YMC Co., Ltd., Kyoto, Japan) and mobile phase consisting of mixed methanol/MTBE/water (60:35:5,

v/v/v) were used. Mobile phase was pumped at 1 mL/min and the temperature of separation column was kept at 40 °C, respectively. The quantification of β-carotene isomers was performed by peak area integration at 450 nm. HPLC retention times, spectral data, and relative intensities of the *Z*-peak to the absorption maximum peak of the isomer (*Q*-ratio), as shown in **Table 4.3.1** were used to identify peaks originating from β-carotene isomers [15-18]. The total (or individual) *Z*-isomer ratio of β-carotene was assessed as follows:

$$\text{Total (or individual) } Z\text{– isomer ratio (\%)} = \frac{\text{total (or individual) peak area of β-carotene } Z\text{–isomers}}{\text{total peak area of β-carotene isomers including the all–}E\text{–isomer}} \times 100 \qquad \textbf{Equation (1)}$$

$$\text{Residual β-carotene (\%)} = \frac{\text{total peak area of β-carotene isomers after thermal treatment}}{\text{total peak area of β-carotene isomers before thermal treatment}} \times 100 \qquad \textbf{Equation (2)}$$

4.2.4.2 Characterization of β-carotene nanodispersions

The color, particle size distribution, encapsulated β-carotene content, and *Z*-isomer ratio of β-carotene in produced nanodispersions were evaluated as described in previous works [13, 14, 19, 20]. In brief, the color of the produced β-carotene nanodispersions was characterized by the absorption spectrum detected using UV–Vis spectrophotometer (UV-1280, Shimadzu Corp., Kyoto, Japan). Particle size distribution was calculated using a dynamic light scattering particle size analyzer (NanoSAQLA, Otsuka Electronics Co., Ltd., Osaka, Japan). Mean particle size was calculated based on the detected size of nanodispersions in the range of 1–1000 nm; the general mean particle size of the carotenoid dispersions produced by the emulsification–evaporation technique is distributed in range of 10–300 nm [13, 14, 19, 20]. The encapsulated β-carotene content in produced nanodispersions was determined by the absorbance of its water solutions at 452 nm detected by a UV–Vis spectrophotometer [14, 19, 20]. The amount of encapsulated β-carotene is proportional to its absorbance, whereas crystalline non-encapsulated β-carotene does not contribute to the absorbance (**Figure 4.2.2**). The encapsulation efficiency (%) was calculated using the following equation [19, 20]:

$$\text{Encapsulation efficiency (\%)} = \frac{\text{total amount of encapsulated } \beta\text{−carotene}}{\text{total amount of introduced } \beta\text{−carotene}} \times 100 \qquad \textbf{Equation (3)}$$

The isomer ratio of encapsulated β-carotene was determined by reversed-phase HPLC [14, 16, 20]. β-Carotene isomers were extracted from the nanodispersions using a mixture of ethanol and hexane (3:4, v/v), and the hexane layer was carefully collected and evaporated to dryness under reduced pressure at 35 °C. The resulting solid was dissolved in a mixture of methanol/MTBE/water (60:35:5, v/v/v) for the HPLC analysis.

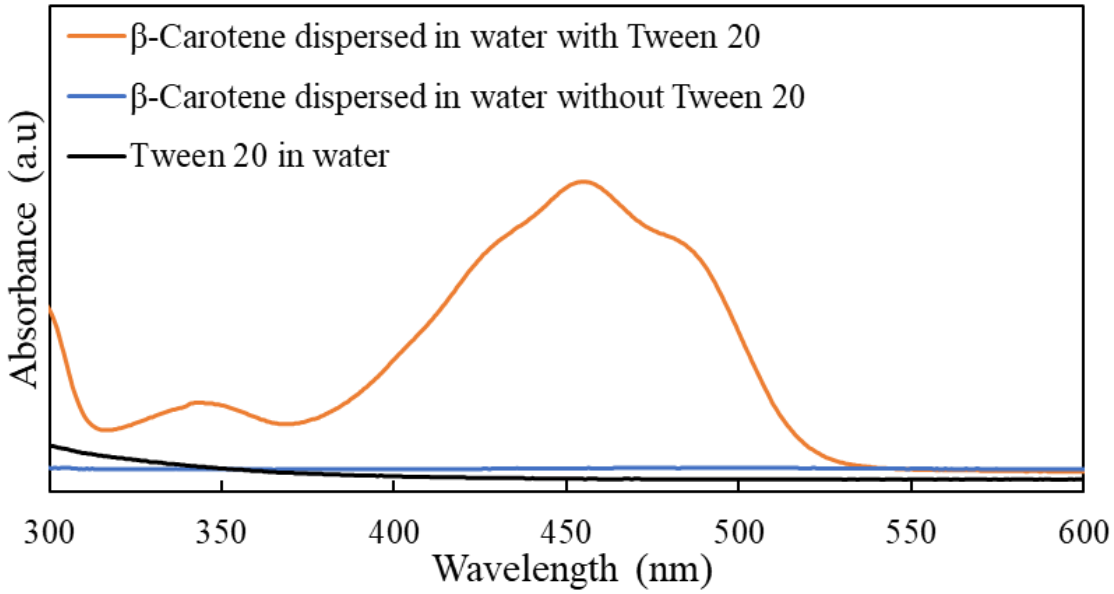

Figure 4.2.2 Absorption spectra of β-carotene dispersed in water with or without Tween 20, and Tween 20 water solution.

4.2.4.3 Statistical Analysis

All experiments were performed more than three times, and the data are presented as the mean ± standard deviation. Statistical analysis was conducted using Tukey's multiple comparison test or Welch's *t*-test using the EZR software program (version 1.54; Saitama Medical Center, Jichi Medical University, Saitama, Japan), and significant differences were calculated at $p < 0.05$ or $p < 0.01$.

4.3 Results and discussion

4.3.1 Effects of *Z*-isomerization temperature and time on total *Z*-isomer ratio

Typical HPLC chromatograms of the intact β-carotene standard and thermally treated β-carotene in a continuous-flow reactor at 200 °C for 30 seconds are shown in **Figure 4.3.1**. Most β-carotene in the standard was the (all-*E*)-β-carotene (> 97%). Eight peaks originating from β-carotene *Z*-isomers were observed after thermal treatment (**Table 4.3.1**), and the predominant isomers are 9*Z*- and 13*Z*-isomer [15-18]. Except the high antiatherogeneis activity of 9*Z*-isomer as previously described, it is recently reported that the feeding of a (13*Z*)-β-carotene-rich diet to rats resulted in higher β-carotene concentrations in plasma and tissues than the (all-*E*)-β-carotene-rich diet [16]. Therefore, the continuous-flow thermal treatment using subcritical ethyl acetate is a prospective method for obtaining β-carotene with enhanced bioavailability and biological activities.

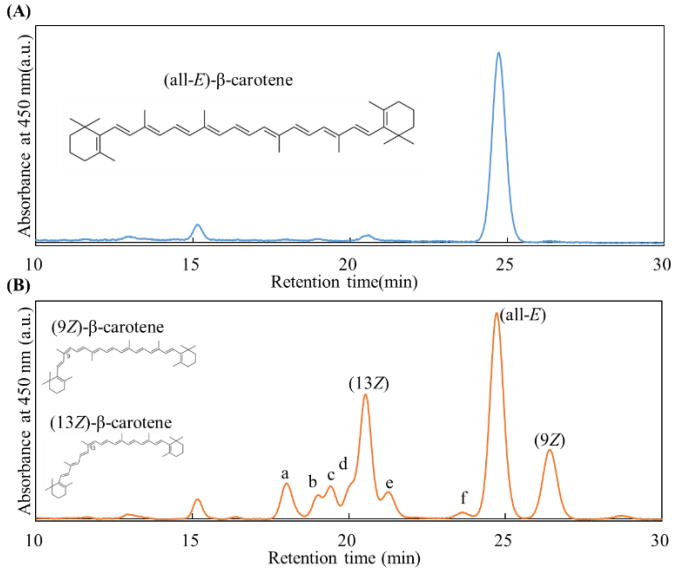

Figure 4.3.1 Reversed-phase HPLC chromatograms of β-carotene isomers (**A**) before and (**B**) after treatment at 200 °C and 10 MPa for 30 seconds with α-tocopherol addition. (all-*E*)-, (9*Z*)-, and (13*Z*)-β-Carotene designated in the chromatograms were identified according to the previous literature [15-18]. The peaks (a–f) were tentatively identified as shown in **Table 4.3.1**.

Table 4.3.1 Absorption maxima (λ_{max}) and relative intensities of the *Z*-peaks (*Q*-ratio) for geometrical β-carotene isomers separated and observed using reversed-phase high-performance liquid chromatography.

		λ_{max} (nm)		*Q*-ratio	
Peak	Isomer[a]	Observed	Reported[a]	Observed	Reported[a]
a	(x*Z*)-β-Carotene	342, 425, 433, 456	–	0.14	–
b	(x*Z*)-β-Carotene	342, 416, 436, 460	–	0.09	–
c	(x*Z*)-β-Carotene	343, 416, 436, 460	–	0.15	–
d	(x*Z*)-β-Carotene	340, 422, 455, 468	–	0.36	–
(13*Z*)	(13*Z*)-β-Carotene	340, 422, 442, 466	338, 423, 445, 468	0.42	0.44
e	(x*Z*)-β-Carotene	340, 418, 437, 461	–	0.15	–
f	(x*Z*)-β-Carotene	343, 417, 440, 465	–	0.06	–
(all-*E*)	(all-*E*)-β-Carotene	428, 450, 476	426, 452, 478	ND	ND
(9*Z*)	(9*Z*)-β-Carotene	343, 422, 444, 470	340, 422, 447, 473	0.08	0.05

Values and peak designations are obtained from the chromatograms in Figure 4.2.2. –, Not assigned. ND, Not detected substantially. [a]Tentatively assigned in the literature [15-18].

In **Figure 4.3.2**, it shows the *Z*-isomer ratio after thermal treatment by a flow-type reactor using subcritical ethyl acetate with temperature in the range of 140–200 °C for 30 s–5 min with pressure at 10 MPa. To note that several studies reported that the pressure has little effect on the isomerization reaction of carotenoids [21-23]. From **Figure 4.3.2** (**A**) to (**D**), as thermal treatment temperature increased, the total *Z*-isomer ratio after the *Z*-isomerization process increased. When the β-carotene solution was treated at 200 °C, the total *Z*-isomer ratio increased to approximately 60% after only 30-second thermal treatment. To the best of our knowledge, it could be the first work which succeeded in achieving this level of total *Z*-isomer ratio (> 40%) via *Z*-isomerization

within such a short time and without involvement of toxic catalysts [3, 5, 6, 15] . As thermal treatment temperature and time increased, the ratio of (13*Z*)-isomer decreased as the ratio of (9*Z*)-isomer increased gradually. It can be ascribed to the difference in activation energy from (all-*E*)-β-carotene to *Z*-isomers (9*Z*- > 15*Z*- > 13*Z*-), and potential energy of each isomer (15*Z*- > 13*Z*- > 9*Z*- > (all-*E*)-) [24, 25]. Briefly, relatively low activation energy from (all-*E*)-β-carotene to 13*Z*-isomer led to the rapid increase of 13*Z*-isomer initially, and as 9*Z*-isomer is more stable than 13*Z*-isomer, it led to the increase of thermodynamically stable 9*Z*-isomer as the thermal treatment temperature and time increased. The reason of total *Z*-isomer ratio decreases in 200 ℃ after 2 minutes was attributed to the extremely high-speed decomposition of β-carotene, especially the decomposition of some thermally-unstable *Z*-isomers, which led to the slight increase in the ratio of relatively-stable all-*E*-isomer. To be concluded, thermal treatment of β-carotene under 200 °C in this work, 30-second treatment increased total *Z*-isomer ratio into around 60% which is extremely more efficient than other conventional methods.

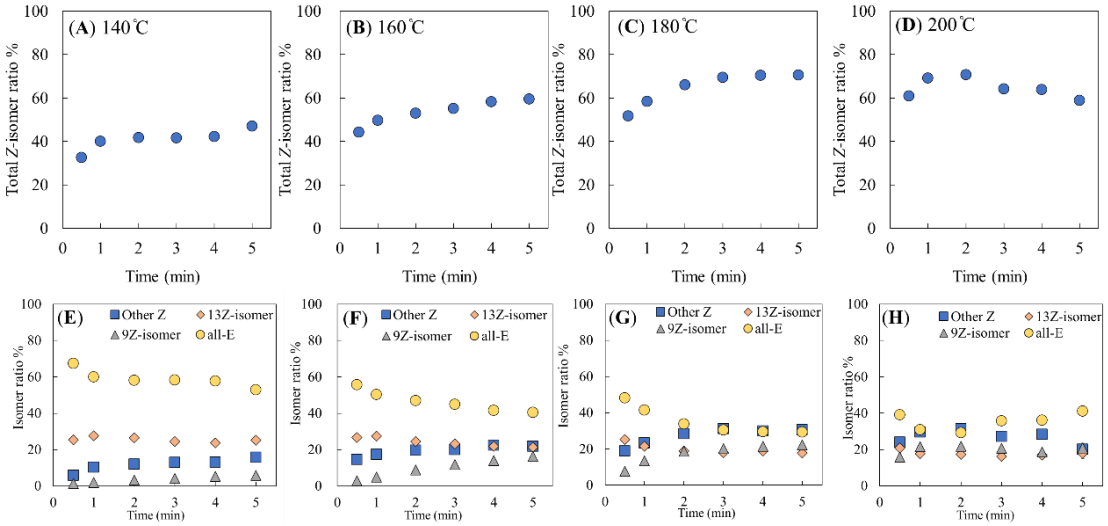

Figure 4.3.2 Effects of thermal treatment temperature and time on (**A**–**D**) total *Z*-isomer ratio and (**E**–**H**) each isomer ratio of β-carotene. Experiments were performed at (**A**, **E**) 140 °C, (**B**, **F**) 160 °C, (**C**, **G**) 180 °C, and (**D**,**H**) 200 °C and 10 MPa. Error bars show standard deviation (n = 3).

4.3.2 Effects of *Z*-isomerization temperature and time on residual ratio

Although high temperature processing helped to produce *Z*-isomer-rich β-carotene, high temperature with ethyl acetate led high degradation of β-carotene even after very short thermal treatment. Especially, when the β-carotene solution was treated at 200 °C, more than 40% of β-carotene decomposed after only 30-second thermal treatment.

To evaluate the degradation characteristic of β-carotene in the continuous-flow reactor using subcritical ethyl acetate, the rate constant (k; min^{-1}) and activation energy (E_a; kJ/mol) of β-carotene were determined. The following first-order kinetic model was employed to assess the degradation rate constant of β-carotene [26, 27]:

$$\ln\left(\frac{C}{C_0}\right) = -kt \qquad \textbf{Equation (4)}$$

where C_0 is the initial amount of β-carotene, C is the total amount of β-carotene after certain time thermal treatment, k is the β-carotene degradation rate constant, and t is the thermal treatment time. The rate constants calculated based on the results of showed in **Figure 4.3.3 (A)–(D)** were as follows: 1.5×10^{-1} min^{-1} (140 °C), 2.0×10^{-1} min^{-1} (160 °C), 3.0×10^{-1} min^{-1} (180 °C), and 1.8 min^{-1} (200 °C) (showed in **Figure 4.3.4**). In the thermal treatment under 200 °C, only the first two-minute data was used due to high decomposition ratio of β-carotene which might affect the accuracy of calculation. The activation energy of β-carotene degradation was determined using the Arrhenius equation as follows [26, 27]:

$$\ln(k) = -\frac{E_a}{R}\cdot\frac{1}{T} + \ln(A) \qquad \textbf{Equation (5)}$$

where k is the degradation rate constant of β-carotene, E_a is activation energy, R is the ideal gas constant (8.3148 J K^{-1} mol^{-1}), T is the absolute temperature, and A is the Arrhenius factor. The activation energy of β-carotene in the subcritical ethyl acetate was calculated to be 62.3 kJ/mol. This value is very close to previously reported values of 64.2 kJ/mol and 62.1 kJ/mol by Bechoff et al. and Lim et al., respectively [28, 29]. The clarification of this basic property of β-carotene is useful in considering the processing conditions for practical applications. By comparing activation energy of β-carotene in freeze-dried single-layer and layer-by-layer emulsion, Lim et al. revealed that the decomposition of β-carotene in single-layer is much more temperature-dependent than that in layer-by-layer emulsion [29].

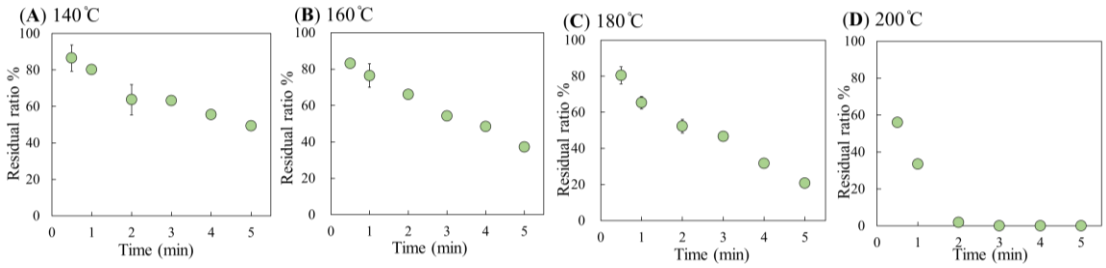

Figure 4.3.3 Effects of thermal treatment temperature and time on residual ratio of β-carotene under (**A**) 140 °C, (**B**) 160 °C, (**C**) 180 °C, (**D**) 200 °C.

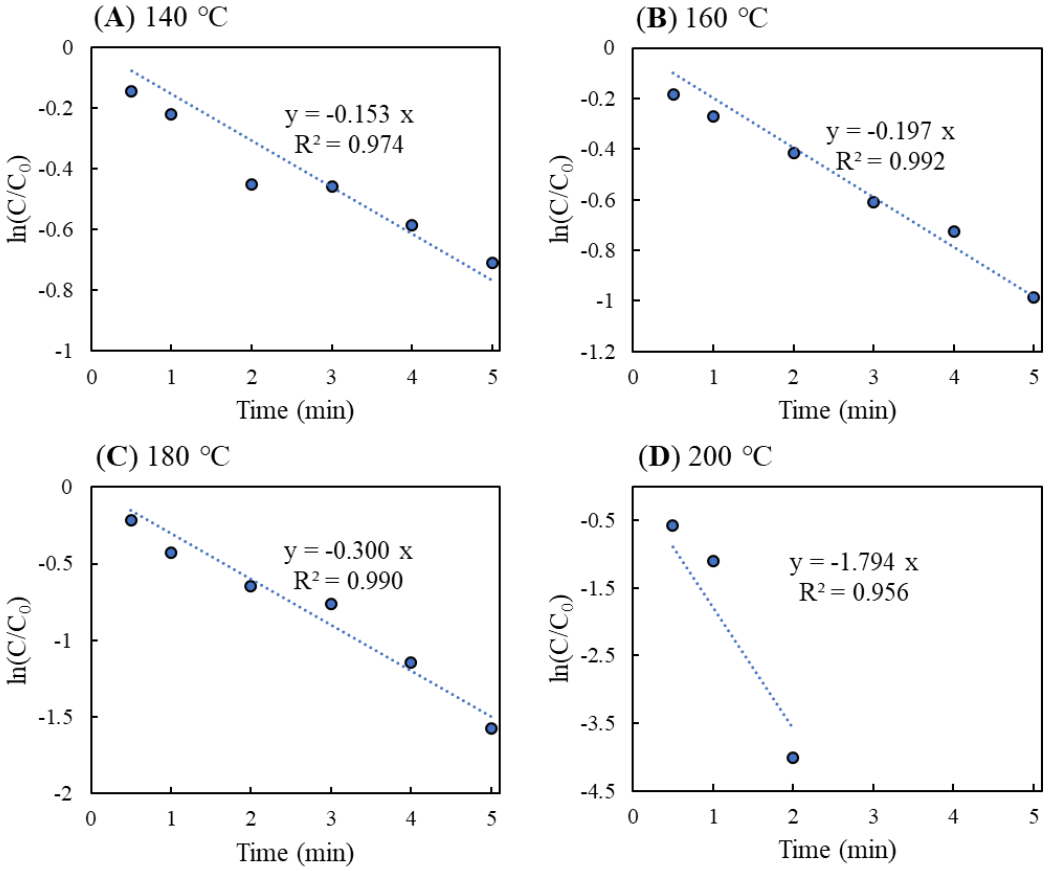

Figure 4.3.4 The degradation kinetic curves of β-carotene in the continuous-flow reactor under (**A**) 140 °C, (**B**) 160 °C, (**C**) 180 °C, (**D**) 200 °C and 10 MPa.

4.3.3 Effects of α-tocopherol addition on *Z*-isomer-rich β-carotene solution

Obviously, it can be observed that the total *Z*-isomer ratio increased to 60% after 30-second thermal treatment at 200 °C, but the residual ratio of β-carotene greatly decreased to 60%. Therefore, to enhance the practical application of this continuous flow-type *Z*-isomerization technology, the inhibition of β-carotene decomposition was investigated. The antioxidant abilities of α-tocopherol and ascorbic acid have been reported to be able to inhibit thermal degradation of β-carotene [10-12]. α-Tocopherol, a natural antioxidant, is one of the generally used antioxidants in the food industry and exhibits a particularly high inhibition effect for the thermal degradation of β-carotene [10, 11]. Hence, to inhibit the degradation of β-carotene in the continuous-flow process at high temperatures, the effect of α-tocopherol addition on the thermal stability of β-carotene was investigated. Specifically, α-tocopherol was added to the β-carotene solution with concentration at 1 mg/mL, and the solution was treated at 200 °C and 10 MPa. The addition of α-tocopherol showed slight effect on the total *Z*-isomer ratio and individual isomer ratio, whereas the residual ratio of β-carotene was markedly improved (**Figure 4.3.5**). At 200 °C without α-tocopherol, all the β-carotene degraded within 3 min. However, when α-tocopherol was added, 69.3% of β-carotene remained after 5-minute processing. This result strongly indicates that α-tocopherol effectively inhibits the β-carotene degradation in subcritical ethyl acetate. Consequently, the following dispersion process with the swirl-type mixer (**Figure 4.2.1; Scheme 2**) was performed with α-tocopherol addition.

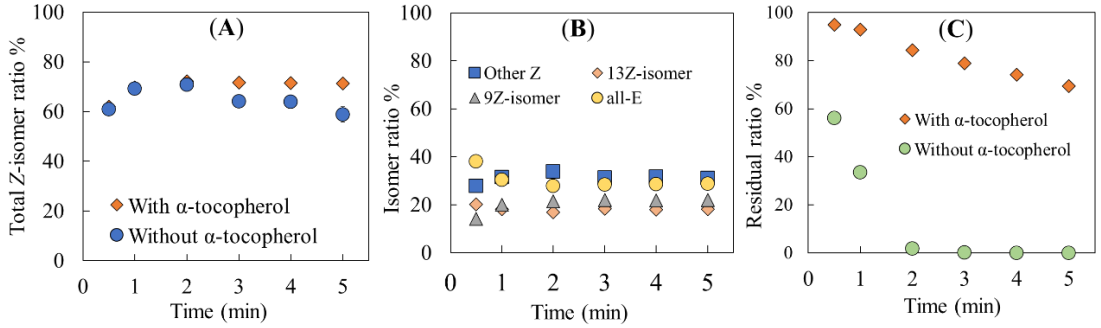

Figure 4.3.5 Effects of thermal treatment with and without 1 mg/mL α-tocopherol addition on (**A**) total *Z*-isomer ratio, (**B**) the ratio of each *Z*-isomer of β-carotene with α-tocopherol, (**C**) the residual ratio of β-carotene under 200 °C.

4.3.4 Effects of flow rate ratio of β-carotene/emulsifier solution on nanodispersions

The *Z*-isomer-rich β-carotene solution used for sequent nanodispersions was prepared under 30-second thermal treatment at 200 °C with α-tocopherol addition, and the total *Z*-isomer ratio and the residual ratio of β-carotene after the processing were 58.6% and 96.1%, respectively. The thermally treated β-carotene solution was dispersed in distilled water containing emulsifier—tween 20 (emulsifier water solution) via a swirl-type mixer (**Figure 4.2.1**; **Scheme 2**). The effects of the flow rate ratio of β-carotene solution/emulsifier water solution, temperature, and pressure on the encapsulation efficiency of β-carotene, total *Z*-isomer ratio, and mean size of produced β-carotene nanodispersions were investigated.

Initially, the effect of the flow rate ratio of the β-carotene solution/emulsifier water solution was evaluated with its ratio varying from 1:5 to 1:20 (v/v) where *Z*-isomer-rich β-carotene solution was kept at 0.5 mL/min, and the dispersion temperature and pressure were set at 50 °C and 5 MPa, respectively. The results were shown in **Figure 4.3.6** and **Table 4.3.2**, the encapsulation efficiency of β-carotene using swirl-type mixer was slightly affected by the flow rate ratio. However, as the ratio of the water solution increased (increase in the flow rate of emulsifier water solution), the average encapsulation efficiency showed a slightly increasing trend; for example, when the flow rate ratio increased from 1:5 to 1:15, the average encapsulation efficiency increased from 79.8 to 84.3% gradually. This is likely because the increase in the side flow (the emulsifier water solution) volume enhances the swirl motion in the mixer [8, 30], which improved the contact of emulsifier with β-carotene and further enhanced the encapsulation efficiency. Thus, a flow rate ratio of 1:10 or 1:15 is appropriate for higher encapsulation efficiency and productivity in this dispersion system. The average size of produced nanodispersions were approximately distributed in range of 10–300 nm by high-speed shearing, ultrasound, and high-pressure homogenizer [13-15, 19, 20, 31]. Impressively, the utilization of swirl-type mixer succeeded in producing nanodispersions with average size lower than 10 nm, which proves its splendid ability for producing smaller size particle.

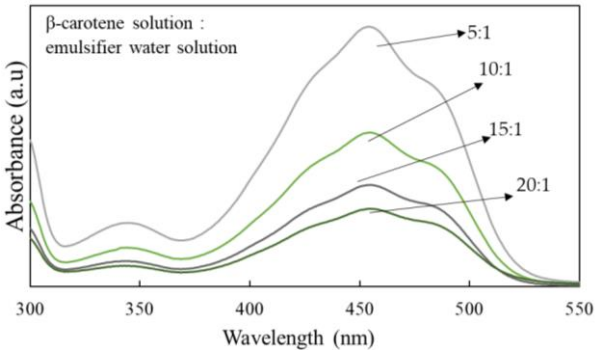

Figure 4.3.6 UV–Vis spectra of produced β-carotene nanodispersions at different flow rate ratio of β-carotene solution/emulsifier water solution with temperature at 50 °C and pressure at 5MPa.

Table 4.3.2 Effects of the flow rate ratio of β-carotene solution to water solution on β-carotene dispersion.

BC/W ratio[a)] (v/v)	Encapsulation efficiency (%)	Total *Z*-isomer ratio (%)	Mean size (nm)
1:5	79.8 ± 0.6[a]	56.2 ± 0.2[a]	6.0 ± 0.9[a]
1:10	82.8 ± 4.0[a]	55.5 ± 0.5[b]	6.3 ± 0.5[a]
1:15	84.3 ± 0.6[a]	55.7 ± 0.3[ab]	6.8 ± 1.2[a]
1:20	83.9 ± 0.5[a]	56.8 ± 0.2[a]	7.4 ± 0.1[a]

Values are presented as mean ± standard deviation (n = 3–6). Within a column, different superscript means significant difference between mean values (p < 0.05). The β-carotene dispersion was performed at 50 °C and 5 MPa.

[a)] Volume ratio of the β-carotene solution (BC) to emulsifier water solution (W).

4.3.5 Effects of temperature on nanodispersions

The impact of temperature (40–70 °C) on the dispersion process was evaluated at a 1:15 flow rate ratio of the β-carotene solution/emulsifier water solution at 5 MPa. As showed in **Figure 4.3.7** and **Table 4.3.3**, the dispersion temperature significantly affected the encapsulation efficiency and total *Z*-isomer ratio of encapsulated β-carotene. As temperature increased, the increase in the mass transfer and decrease in the liquid viscosity could enhance the agitation efficiency in the swirl-type mixer and contributed to the improvement of encapsulation efficiency. However, when dispersion process was conducted at 70 °C, the total *Z*-isomer ratio of encapsulated β-carotene significantly decreased. As several studies have revealed the transformation of *Z*-isomers of carotenoids to the all-*E*-isomers even in modest heating conditions [15, 32, 33]. As shown in **Figure 4.3.8**, it could be referred that some thermally-unstable *Z*-isomers transformed to relatively stable all-*E*-isomer, as it can be found out that the other *Z*-isomer ratio decreased as temperature increased from 60 °C to 70 °C. Based on encapsulation efficiency and total *Z*-isomer ratio, the dispersion process is preferable at 60 °C.

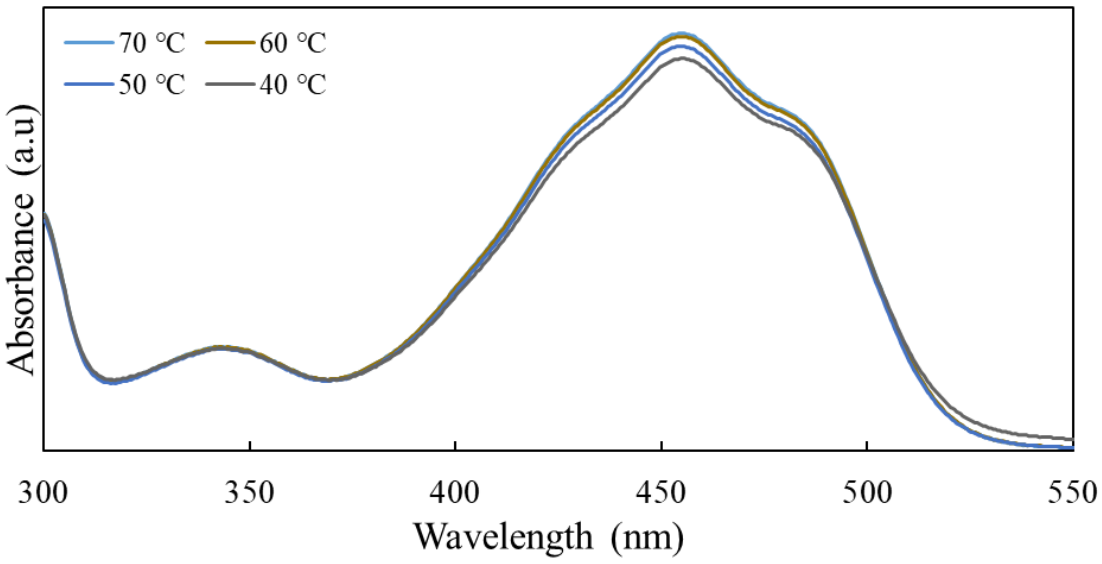

Figure 4.3.7 UV–Vis spectra of produced β-carotene nanodispersions at different dispersions temperature with flow rate ratio of β-carotene solution / emulsifier water solution at 1:15 and pressure at 5 MPa.

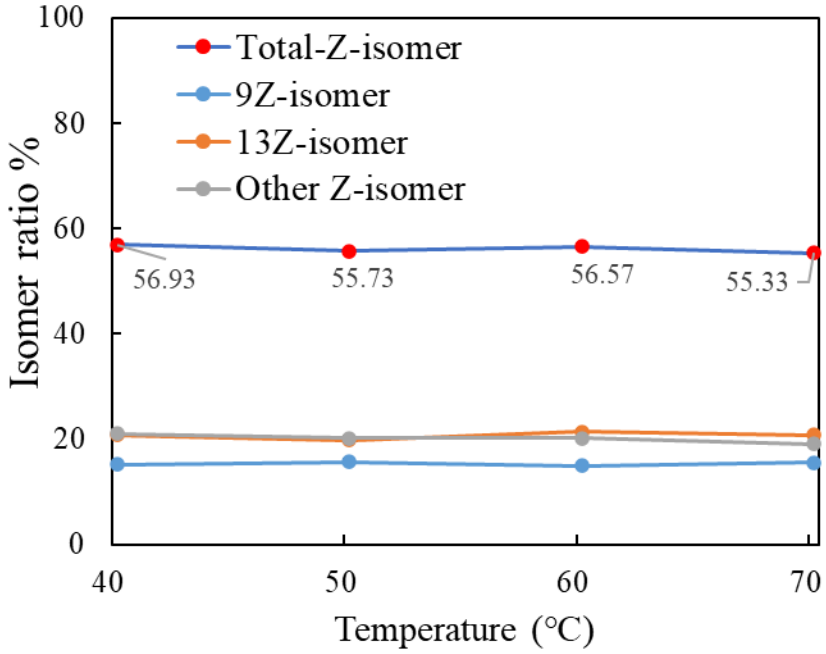

1822

1823 **Figure 4.3.8** The ratio of each *Z*-isomer of β-carotene in produced nanodispersions at
1824 different dispersion temperatures with flow rate ratio of β-carotene solution/emulsifier
1825 water solution at 1:15 and pressure at 5 MPa.

1826 **Table 4.3.3** Effects of temperature on β-carotene nanodispersions.

Temperature (°C)	Encapsulation efficiency (%)	Total *Z*-isomer ratio (%)	Mean particle size (nm)
40	81.8 ± 1.0^{c}	56.9 ± 0.3^{a}	5.6 ± 0.3^{a}
50	84.3 ± 0.6^{b}	55.7 ± 0.3^{bc}	6.8 ± 1.2^{a}
60	86.4 ± 0.5^{a}	56.6 ± 0.4^{ab}	6.2 ± 0.4^{a}
70	86.6 ± 0.4^{a}	55.3 ± 0.3^{c}	6.2 ± 0.2^{a}

1827 Values are presented as mean ± standard deviation (n = 3–6). The β-carotene dispersion
1828 was performed at 1:15 of the flow ratio of β-carotene solution to water solution and 5
1829 MPa.

1830

1831

4.3.6 Effects of pressure on nanodispersions

The effect of the pressure (0–20 MPa) on the β-carotene nanodispersion was investigated at a 1:15 flow rate ratio of the β-carotene solution/emulsifier water solution at 50 °C. As the dispersion pressure increased, the encapsulation efficiency showed an increasing trend as shown in **Figure 4.3.9**, with a plateau at 15 MPa. When the dispersion was conducted at 0 MPa (no pressure loaded via BPR) and 15 MPa, the efficiencies were 79.8 and 87.1%, respectively. This improvement might be due to the increase in the solubility of β-carotene and ethyl acetate in the water phase at high pressures [34, 35], which could enhance the encapsulation efficiency in the swirl-type mixer. Further research is needed to clarify the reason of this phenomenon. However, the pressure showed little effect on the total *Z*-isomer ratio of β-carotene and the mean particle size of produced nanodispersions. Thus, in terms of the encapsulation efficiency, it might be preferable to conduct dispersions process with a pressure load of at least 15 MPa, but taking the high cost of equipment and operation of high-pressure system during practical applications into consideration, low-pressure conditions might be alternative to achieve adequate performance for producing *Z*-isomer-rich β-carotene nanodispersions. Under all the conditions in this study, there is no difference in the average sizes of produced nanodispersions and they are mainly distributed in the range of 5–8 nm as shown in **Table 4.3.2**, **4.3.3**, **4.3.4** and **Figure 4.3.12 (B)**. It has been previously demonstrated that micelle-based encapsulation technology produced micelle with size in the range of 5–20 nm [36].

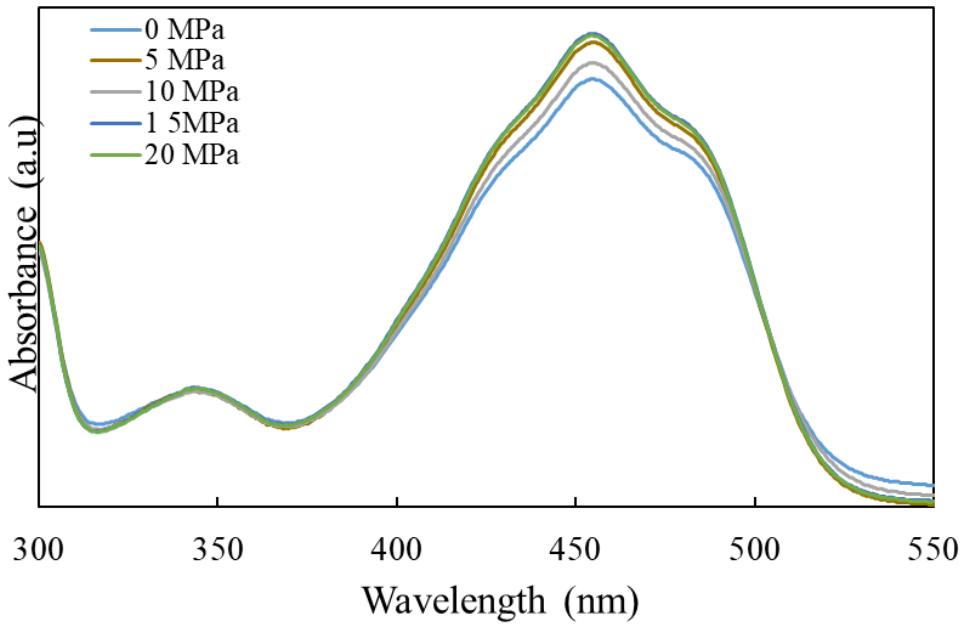

Figure 4.3.9 UV–Vis spectra of produced β-carotene nanodispersions at different dispersions pressure with flow rate ratio of β-carotene solution/emulsifier water solution at 1:15 and temperature at 50 °C.

Table 4.3.4 Effects of pressure on β-carotene dispersion.

Pressure (MPa)	Encapsulation efficiency (%)	Total *Z*-isomer ratio (%)	Mean particle size (nm)
0	79.8 ± 1.1^{c}	56.5 ± 0.1^{a}	5.4 ± 0.9^{a}
5	84.3 ± 0.6^{b}	55.7 ± 0.3^{ab}	6.8 ± 1.2^{a}
10	83.2 ± 0.9^{b}	55.6 ± 0.2^{b}	6.1 ± 0.9^{a}
15	87.1 ± 0.5^{a}	55.7 ± 0.3^{b}	5.6 ± 0.6^{a}
20	87.3 ± 0.5^{a}	55.2 ± 0.3^{b}	5.3 ± 0.3^{a}

Values are presented as mean ± standard deviation (n = 3–6). The β-carotene dispersion was performed at 1:15 of the flow ratio of β-carotene solution to water solution and 50 °C.

4.3.7 Effects of *Z*-isomerization on β-carotene nanodispersions

The dispersion efficiency and characteristics of the produced nanodispersions using (all-*E*)-β-carotene and *Z*-isomer-rich β-carotene solution in this continuous nanodispersion production system were compared. The *Z*-isomer-rich β-carotene was prepared from the all-*E*-isomer (total *Z*-isomer ratio: 2.7%) by 30-second thermal treatment at 200 °C with α-tocopherol addition (total *Z*-isomer ratio: 58.6%) using continuous flow-type reactor. The all-*E*-isomer-rich and *Z*-isomer-rich β-carotene ethyl acetate solution were dispersed using the swirl-type mixer with the flow rate ratio of β-carotene solution to emulsifier water solution at 1:10, temperature at 60 °C without pressure at 0 MPa. When the dispersion was performed using *Z*-isomer-rich β-carotene, the encapsulation efficiency and total *Z*-isomer ratio of encapsulated β-carotene in the nanodispersions were significantly higher than those of (all-*E*)-β-carotene, and the particle size was smaller than that produced using all-*E*-isomer (**Figure 4.3.10**). These improved performance in the nanodispersions produced with *Z*-isomer-rich β-carotene solution can be attributed to the enhanced solubility of *Z*-isomer-rich β-carotene in the mixed ethyl acetate and water solution. The decreased crystallinity of *Z*-isomer-rich β-carotene made it possible to disperse β-carotene ethyl acetate solution into small droplet by swirl-type mixer and further decreased the size of produced nanodispersions. Multiple studies have reported that the *Z*-isomerization of (all-*E*)-carotenoids, including β-carotene, enhanced the solubility and reduced the crystallinity [37, 38]. In fact, Ono et al. reported that when comparing the encapsulation efficiency and dispersion particle size of (all-*E*)-β-carotene and *Z*-isomer-rich β-carotene via the emulsification–evaporation technique with ultrasound treatment, the latter showed higher encapsulation efficiency and smaller particle size than the former [14]. In **Figure 4.3.10 (E)**, the absorption spectra of β-carotene nanodispersions rich in the all-*E*- and *Z*-isomers are shown. The absorption spectrum of the *Z*-isomer-rich nanodispersions shifted toward shorter wavelength than that of all-*E*-isomer-rich one and exihibted a maximum absorption wavelength of approximately 340 nm which is accordance with *Z*-isomers typical absorption in the ultraviolet A (UV-A, 315−400 nm) region. Therefore, *Z*-isomer-rich β-carotene nanodispersions is prospective to be used in sunscreens. These results strongly proved that *Z*-isomer-rich β-carotene nanodispersion

are superior to the all-*E*-isomer rich one, because the former potentially show greater bioavailability, biological activity, and productivity.

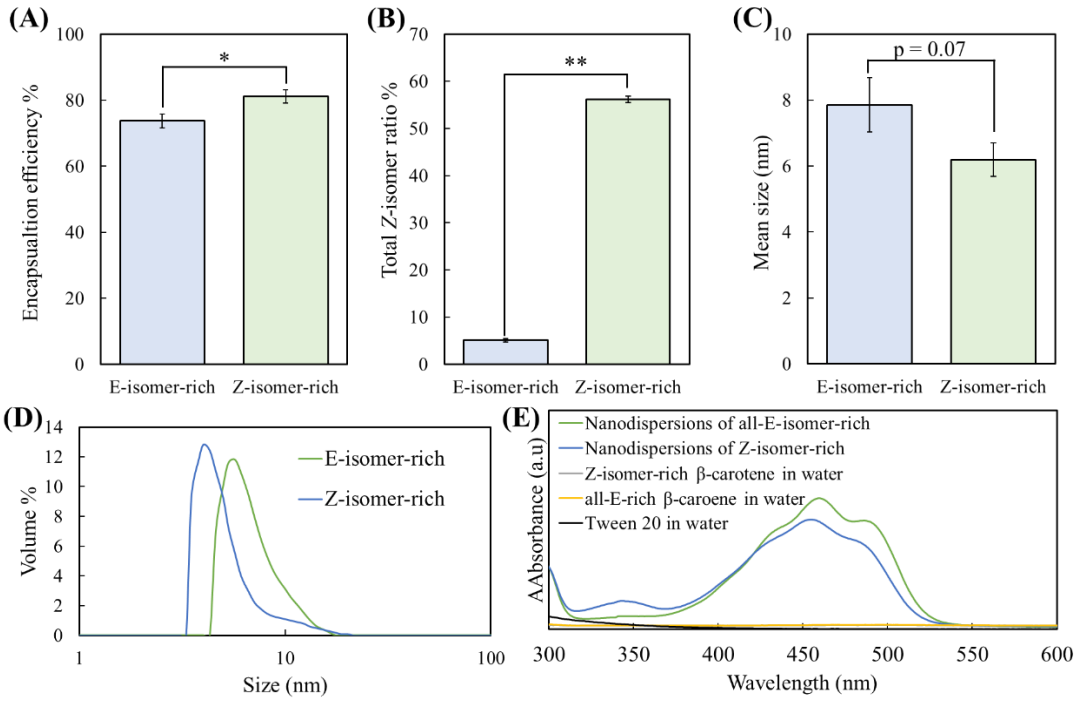

Figure 4.3.10 Effects of isomer ratio (total *Z*-isomer ratio: 2.7 or 58.6%) of β-carotene solution on **(A)** the encapsulation efficiency, **(B)** total *Z*-isomer ratio of encapsulated β-carotene, **(C)** mean size, **(D)** size distribution, and **(E)** absorption spectra. The dispersion was conducted at 60 °C without the pressure via the swirl mixer. Error bars show standard deviation (n = 3). Asterisks (*) indicate a statistically significant difference in each group (*$p < 0.05$, **$p < 0.01$, Student's t-test).

4.3.8 Storage stability of produced nanodispersions

The storage stability test was carried out using β-carotene nanodispersions with initial total *Z*-isomer ratio at 2.7% (*E*-isomer-rich) and 58.6% (*Z*-isomer-rich) prepared using the swirl-type mixer with the flow rate ratio of β-carotene solution to emulsifier water solution at 1:10, temperature at 50 °C and pressure at 15 MPa. Both the all-*E*-isomer-rich and *Z*-isomer-rich β-carotene nanodispersions were stored in dark at 4 °C for 21 days, and the changes of those nanodispersions during storage were determined and shown in **Figure 4.3.11 (A-C) and Figure 4.3.12 (A)**. The previous storage data was taken from Ono et al., where the residual ratio of β-carotene nanodispersions decreased to 50.9% of *E*-isomer-rich nanodispersion and 14.3% of *Z*-isomer-rich nanodispersions after 14-day storage at 4 °C in dark shown in **Figure 4.3.11 (B)** [14].

After 21-day storage at 4 °C, there was almost no changes of total *Z*-isomer ratio and average size, and the residual ratio of β-carotene remained at 92% of both *E*-isomer-rich nanodispersions and *Z*-isomer-rich nanodispersions produced in this work. The residual ratio of this work was much mor higher than previous work, and especially, the residual ratio of *Z*-isomer-rich nanodispersions was significantly improved. It revealed that this continuous nanodispersions production system exhibits excellent performance in producing highly-stable β-carotene nanodispersions solution. We think this high stability can be attributed to the strong mixing effects and superiority in producing small size particles of swirl-type mixer, which enhanced the interaction between emulsifier and encapsulated β-carotene and further improved its stability. Previous research also revealed the enhanced stability of core compounds by encapsulating it with emulsifier or surfactant [39]. Therefore, the continuous nanodispersions system via swirl-type mixer exhibits excellent performance and can be expected to be utilized for nanodispersions production of other bioactive compounds.

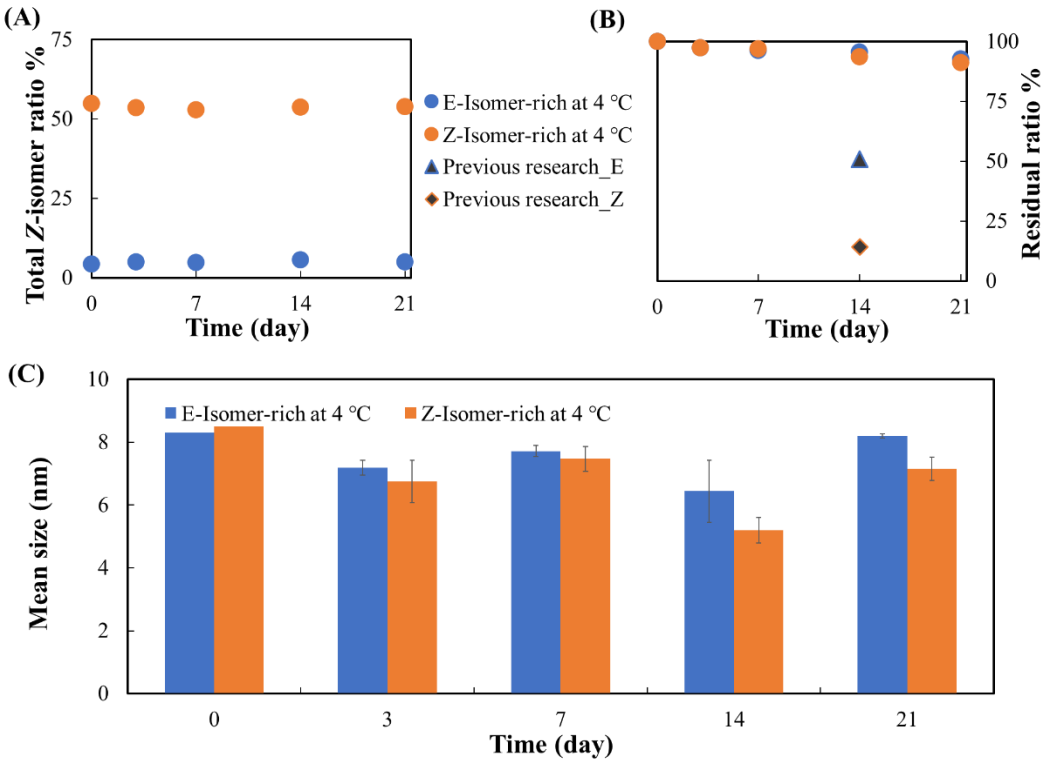

1936

1937 **Figure 4.3.11** The changes of **(A)** total *Z*-isomer ratio, **(B)** residual ratio of β-carotene,
1938 **(C)** mean size of prepared β-carotene nanodispersions with initial total *Z*-isomer ratio
1939 at 2.7% (*E*-isomer-rich) and 58.6% (*Z*-isomer-rich) after being stored in dark for 21-
1940 day at 4 °C. The previous storage data was taken from Ono et al., where the residual
1941 ratio of β-carotene nanodispersions decreased to 50.9% of *E*-isomer-rich
1942 nanodispersion (Previous research_*E*) and 14.3% of *Z*-isomer-rich nanodispersions
1943 (Previous research_*Z*) after 14-day storage at 4 °C [14].

1944

1945

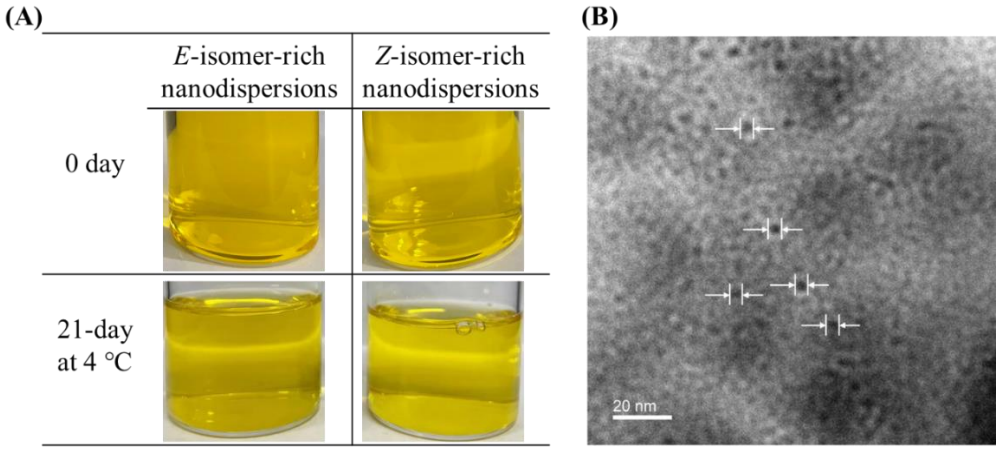

Figure 4.3.12 Images of produced β-carotene nanodispersions with **(A)** initial total *Z*-isomer ratio at 2.7% (*E*-isomer-rich) and 58.6% (*Z*-isomer-rich) and its images after 21-day storage at 4 °C in dark, (**B**) transmission electron microscopy (TEM) image of *Z*-isomer-rich β-carotene nanodispersions.

4.4 Conclusions

Z-Isomer-rich β-carotene nanodispersions were successfully prepared by the continuous production system developed in this work. By using the continuous flow-type heating reactor in subcritical ethyl acetate condition, (all-*E*)-β-carotene solution was efficiently isomerized to *Z*-isomer-rich solution with 60% *Z*-isomers after barely 30-second thermal treatment. Moreover, the sequent use of a swirl-type mixer continuously produced β-carotene nanodispersions with a mean particle size of approximate 5 nm, which is far smaller than the average water-soluble carotenoid particles produced in previous studies. When (all-*E*)-β-carotene and *Z*-isomer-rich β-carotene were treated in this continuous dispersion process, the latter showed greater encapsulation efficiency and smaller particle size. Moreover, the *Z*-isomer-rich β-carotene nanodispersions exhibited high stability. Hence, this continuous production system for producing *Z*-isomer-rich β-carotene nanodispersions is superior to previous production methods in terms of both productivity and the functionality of the produced nanodispersions.

References:

[1] Arden, N. S.; Fisher, A. C.; Tyner, K.; Yu, L. X.; Lee, S. L.; Kopcha, M., Industry 4.0 for pharmaceutical manufacturing: Preparing for the smart factories of the future. *International Journal of Pharmaceutics,* **2021**, *602*, 120554.

[2] Honda, M.; Kageyama, H.; Hibino, T.; Zhang, Y.; Diono, W.; Kanda, H.; Yamaguchi, R.; Takemura, R.; Fukaya, T.; Goto, M., Improved Carotenoid Processing with Sustainable Solvents Utilizing *Z*-Isomerization-Induced Alteration in Physicochemical Properties: A Review and Future Directions. *Molecules (Basel, Switzerland),* **2019**, *24* (11), 2149.

[3] Honda, M.; Kageyama, H.; Hibino, T.; Ichihashi, K.; Takada, W.; Goto, M., Isomerization of Commercially Important Carotenoids (Lycopene, β-Carotene, and Astaxanthin) by Natural Catalysts: Isothiocyanates and Polysulfides. *Journal of Agricultural and Food Chemistry,* **2020**, *68* (10), 3228-3237.

[4] Schierle, J.; Schellenberger, T.; Fizet, C.; Betz, R., A simple spectrophotometric determination of total β-carotene in food additives with varying *E*/*Z*-isomer ratios using an isobestic wavelength. *European Food Research and Technology,* **2002**, *215* (3), 268-274.

[5] Gao, Y.; Kispert, L. D., Reaction of Carotenoids and Ferric Chloride: Equilibria, Isomerization, and Products. *The Journal of Physical Chemistry B,* **2003**, *107* (22), 5333-5338.

[6] Rajendran, V.; Chen, B. H., Isomerization of β-carotene by titanium tetrachloride catalyst. *Journal of Chemical Sciences,* **2007**, *119* (3), 253-258.

[7] Wakashima, Y.; Suzuki, A.; Kawasaki, S.-i.; Matsui, K.; Hakuta, Y., Development of a New Swirling Micro Mixer for Continuous Hydrothermal Synthesis of Nano-Size Particles. *Journal of Chemical Engineering of Japan,* **2007**, *40* (8), 622-629.

[8] Kawasaki, S.; Sue, K.; Ookawara, R.; Wakashima, Y.; Suzuki, A., Development of novel micro swirl mixer for producing fine metal oxide nanoparticles by continuous supercritical hydrothermal method. *Journal of Oleo Science,* **2010**, *59* (10), 557-62.

[9] Chhouk, K.; Wahyudiono; Kanda, H.; Kawasaki, S.-I.; Goto, M., Micronization of curcumin with biodegradable polymer by supercritical anti-solvent using micro swirl mixer. *Frontiers of Chemical Science and Engineering,* **2018**, *12* (1), 184-193.

[10] Liu, Y.; Hou, Z.; Yang, J.; Gao, Y., Effects of antioxidants on the stability of β-Carotene in O/W emulsions stabilized by Gum Arabic. *Journal of Food Science and Technology,* **2015**, *52* (6), 3300-11.
[11] Yi, J.; Fan, Y.; Yokoyama, W.; Zhang, Y.; Zhao, L., Thermal Degradation and Isomerization of β-Carotene in Oil-in-Water Nanoemulsions Supplemented with Natural Antioxidants. *Journal of Agricultural and Food Chemistry,* **2016**, *64* (9), 1970-1976.
[12] Qian, C.; Decker, E. A.; Xiao, H.; McClements, D. J., Inhibition of β-carotene degradation in oil-in-water nanoemulsions: Influence of oil-soluble and water-soluble antioxidants. *Food Chemistry,* **2012**, *135* (3), 1036-1043.
[13] Tan, C. P.; Nakajima, M., β-Carotene nanodispersions: preparation, characterization and stability evaluation. *Food Chemistry,* **2005**, *92* (4), 661-671.
[14] Ono, M.; Honda, M.; Wahyudiono; Yasuda, K.; Kanda, H.; Goto, M., Production of β-carotene nanosuspensions using supercritical CO_2 and improvement of its efficiency by *Z*-isomerization pre-treatment. *The Journal of Supercritical Fluids,* **2018**, *138*, 124-131.
[15] Yang, C.; Yan, H.; Jiang, X.; Xu, H.; Tsao, R.; Zhang, L., Preparation of 9*Z*-β-Carotene and 9*Z*-β-Carotene High-Loaded Nanostructured Lipid Carriers: Characterization and Storage Stability. *Journal of Agricultural and Food Chemistry,* **2020**, *68* (47), 13844-13853.
[16] Honda, M.; Takasu, S.; Nakagawa, K.; Tsuda, T., Differences in bioavailability and tissue accumulation efficiency of (all-*E*)- and (*Z*)-carotenoids: A comparative study. *Food Chemistry,* **2021**, *361*, 130119.
[17] Böhm, V.; Puspitasari-Nienaber, N. L.; Ferruzzi, M. G.; Schwartz, S. J., Trolox Equivalent Antioxidant Capacity of Different Geometrical Isomers of α-Carotene, β-Carotene, Lycopene, and Zeaxanthin. *Journal of Agricultural and Food Chemistry,* **2002**, *50* (1), 221-226.
[18] Imsic, M.; Winkler, S.; Tomkins, B.; Jones, R., Effect of Storage and Cooking on β-Carotene Isomers in Carrots (*Daucus carota* L. cv. 'Stefano'). *Journal of Agricultural and Food Chemistry,* **2010**, *58* (8), 5109-5113.
[19] de Paz, E.; Martín, Á.; Estrella, A.; Rodríguez-Rojo, S.; Matias, A. A.; Duarte, C. M. M.; Cocero, M. J., Formulation of β-carotene by precipitation from pressurized ethyl acetate-on-water emulsions for application as natural colorant. *Food Hydrocolloids,* **2012**, *26* (1), 17-27.
[20] Zhang, Y.; Honda, M.; Fukaya, T.; Wahyudiono; Kanda, H.; Goto, M., One-Step Preparation of *Z*-Isomer-Rich β-Carotene Nanosuspensions Utilizing a

Natural Catalyst, Allyl Isothiocyanate, via Supercritical CO_2. *Symmetry,* **2020**, *12* (5), 777.
[21] Lerfall, J.; Birkeland, S., Effect of high pressure processing on astaxanthin stability. *International Journal of Food Science & Technology,* **2014**, *49* (1), 294-297.
[22] Qiu, W.; Jiang, H.; Wang, H.; Gao, Y., Effect of high hydrostatic pressure on lycopene stability. *Food Chemistry,* **2006**, *97* (3), 516-523.
[23] Honda, M.; Murakami, K.; Zhang, Y.; Goto, M., Rapid and Continuous Astaxanthin Isomerization in Subcritical Ethanol. *Industrial & Engineering Chemistry Research,* **2021**, *60* (39), 14060-14068.
[24] Guo, W.-H.; Tu, C.-Y.; Hu, C.-H., Cis−Trans Isomerizations of β-Carotene and Lycopene: A Theoretical Study. *The Journal of Physical Chemistry B,* **2008**, *112* (38), 12158-12167.
[25] Honda, M.; Kudo, T.; Kuwa, T.; Higashiura, T.; Fukaya, T.; Inoue, Y.; Kitamura, C.; Takehara, M., Isolation and spectral characterization of thermally generated multi-*Z*-isomers of lycopene and the theoretically preferred pathway to di-*Z*-isomers. *Bioscience, Biotechnology, and Biochemistry,* **2017**, *81* (2), 365-371.
[26] Demiray, E.; Tulek, Y., Degradation kinetics of β-carotene in carrot slices during convective drying. *International Journal of Food Properties,* **2017**, *20* (1), 151-156.
[27] Aparicio-Ruiz, R.; Mínguez-Mosquera, M. I.; Gandul-Rojas, B., Thermal degradation kinetics of lutein, β-carotene and β-cryptoxanthin in virgin olive oils. *Journal of Food Composition and Analysis,* **2011**, *24* (6), 811-820.
[28] Bechoff, A.; Dhuique-Mayer, C.; Dornier, M.; Tomlins, K. I.; Boulanger, R.; Dufour, D.; Westby, A., Relationship between the kinetics of β-carotene degradation and formation of norisoprenoids in the storage of dried sweet potato chips. *Food Chemistry,* **2010**, *121* (2), 348-357.
[29] Lim, A. S. L.; Griffin, C.; Roos, Y. H., Stability and loss kinetics of lutein and β-carotene encapsulated in freeze-dried emulsions with layered interface and trehalose as glass former. *Food Research International,* **2014**, *62*, 403-409.
[30] Ji, Y.; Bellettre, J.; Montillet, A.; Massoli, P., Fast oil-in-water emulsification in microchannel using head-on impinging configuration: Effect of swirl motion. *International Journal of Multiphase Flow,* **2020**, *131*, 103402.
[31] Chu, B.-S.; Ichikawa, S.; Kanafusa, S.; Nakajima, M., Preparation and Characterization of β-Carotene Nanodispersions Prepared by Solvent Displacement Technique. *Journal of Agricultural and Food Chemistry,* **2007**, *55* (16), 6754-6760.
[32] Honda, M.; Sowa, T.; Kawashima, Y., Thermal- and Photo-Induced Isomerization of All-*E*- and *Z*-Isomer-Rich Xanthophylls: Astaxanthin and Its

Structurally-Related Xanthophylls, Adonirubin, and Adonixanthin. *European Journal of Lipid Science and Technology,* **2020**, *122* (5), 1900462.
[33] Murakami, K.; Honda, M.; Takemura, R.; Fukaya, T.; Wahyudiono; Kanda, H.; Goto, M., Effect of thermal treatment and light irradiation on the stability of lycopene with high *Z*-isomers content. *Food Chemistry,* **2018**, *250*, 253-258.
[34] Baysal, T.; Ersus, S.; Starmans, D. A. J., Supercritical CO_2 Extraction of β-Carotene and Lycopene from Tomato Paste Waste. *Journal of Agricultural and Food Chemistry,* **2000**, *48* (11), 5507-5511.
[35] Gnayfeed, M. H.; Daood, H. G.; Illés, V.; Biacs, P. A., Supercritical CO_2 and Subcritical Propane Extraction of Pungent Paprika and Quantification of Carotenoids, Tocopherols, and Capsaicinoids. *Journal of Agricultural and Food Chemistry,* **2001**, *49* (6), 2761-2766.
[36] Ozkan, G.; Franco, P.; De Marco, I.; Xiao, J.; Capanoglu, E., A review of microencapsulation methods for food antioxidants: Principles, advantages, drawbacks and applications. *Food Chemistry,* **2019**, *272*, 494-506.
[37] Honda, M.; Kodama, T.; Kageyama, H.; Hibino, T.; , W.; Kanda, H.; Goto, M., Enhanced Solubility and Reduced Crystallinity of Carotenoids, β-Carotene and Astaxanthin, by *Z*-Isomerization. *European Journal of Lipid Science and Technology,* **2018**, *120* (11), 1800191.
[38] Murakami, K.; Honda, M.; Takemura, R.; Fukaya, T.; Kubota, M.; Wahyudiono; Kanda, H.; Goto, M., The thermal *Z*-isomerization-induced change in solubility and physical properties of (all-*E*)-lycopene. *Biochemical and Biophysical Research Communications,* **2017**, *491* (2), 317-322.
[39] Benelli, L.; Oliveira, W. P., Fluidized bed coating of inert cores with a lipid-based system loaded with a polyphenol-rich Rosmarinus officinalis extract. *Food and Bioproducts Processing,* **2019**, *114*, 216-226.

Chapter 5 Summary

Terpenoids as the secondary metabolite compounds, are responsible for various activities of living things, such as the activities relating to amor, taste, and color of plants. Terpenoids possess various physiological effects depending on its structures, such as anti-inflammatory, anti-cancer, anti-bacterial, and anticonvulsant activities. Due to these properties, terpenoids are universally used in food, cosmetic and pharmaceutical industries. However, as described previously, the majority of terpenoids are water-insoluble and further treatment are required to improve its water performance to further improve its absorption ratio in the human body. In this research, we focused on the improvement of water dispersibility of two types of terpenoids—diterpenes (cafestol and kahweol) and tetraterpene (β-carotene), and they are successfully encapsulated by the nanoencapsulation technologies using supercritical CO_2 and subcritical ethyl acetate.

Extraction of diterpenes from spent coffee grounds and encapsulation into polyvinylpyrrolidone particles using supercritical carbon dioxide

As most diterpenes are esterified with various water-insoluble fatty acids in coffee beans, there are plenty of esterified diterpenes remained in SCGs after coffee brewing. Therefore, we focused on the valuable and typical diterpenes—cafestol and kahweol contained in SCG. Primarily, to obtain SCG extract with high total diterpene content, we optimized the extraction of diterpenes from SCG using ethanol-modified SC-CO_2 due to the high solubilities of fatty acids in ethanol. Box-Behnken design of response surface methodology was used to get full understanding about the effects of temperature (40–80 °C), pressure (10–30 MPa), and ethanol ratio (0%–10% v/v) on SCG extraction. Notably, the predicted optimal condition of the total diterpene content was 80 ºC/25 MPa/6% v/v, where the predicted total diterpene content in the SCG extract was about 15 times the result of conventional hexane extraction. The superiority of ethanol-modified SC-CO_2 towards diterpenes extraction from SCG was confirmed.

Subsequently, the encapsulation of SCG extract rich in diterpenes into water-soluble polyvinylpyrrolidone (abbreviated as PVP) nanoparticles was successfully performed

by supercritical anti-solvent crystallization method. In this method, using SC-CO_2 as the anti-solvent helps to reduce organic solvents amount used, and organic solvent can be removed from final particles by SC-CO_2. The effect of the concentration ratio of PVP:SCG extract on produced nanoparticles was investigated. As a result, nanoparticles with the average size around 140 nm were prepared with the concentration ratio of PVP:SCG extract at 30:1. The successful encapsulation of the SCG extract into PVP nanoparticles was confirmed by DSC curves, FT–IR spectra, and UV–Vis spectra, and the fast dispersion of produced nanoparticles in water was observed. The results of this study can serve as a reference for the separation of diterpenes from SCG and the production of nanoparticles of SCG extract rich in diterpenes with high water dispersibility.

One-step preparation of *Z*-isomer-rich β-carotene nanodispersions using a natural catalyst, allyl isothiocyanate in ultrasound-assisted supercritical carbon dioxide

β-Carotene owns eight isoprene units known as tetraterpene, and is commonly used as the food pigment. Due to its antioxidant and antiatherosclerotic activities as well as provitamin A activity, it is expected to be used in various supplementary products. To obtain high bioavailability and high production efficiency of β-carotene product, two processes are commonly performed—water-dispersion process and *Z*-isomerization process. First, the water-dispersion process using hydrophilic emulsifier is normally carried out to improve the water dispersibility of hydrophobic β-carotene using ultrasound-assisted SC-CO_2. Due to the high crystallinity and low solubility of (all-*E*)-β-carotene in various organic solvents, the water-dispersion production efficiency using it is not high. Therefore, the purpose of the other process—*Z*-isomerization process is to *Z*-isomerize crystal (all-*E*)-β-carotene into *Z*-isomers with lower crystallinity and higher solubility to further enhance the production efficiency of the water-dispersion process. In previous study, the pretreatment of *Z*-isomerization process is performed, but complicated processes and the involvement of toxic organic solvents inhibited its utilization in food industry as shown in **Figure 3.1.2 (B)**.

This work aimed to develop a simple process for producing *Z*-isomer-rich β-carotene nanodispersions using ultrasound-assisted SC-CO_2. We came up with the idea of adding

Z-isomerization-accelerating catalyst—allyl isothiocyanate (AITC) into the reaction vessel to simultaneously *Z*-isomerize and disperse β-carotene to produce *Z*-isomer-rich β-carotene nanodispersions. The effects of AITC addition amount on the total *Z*-isomer ratio, β-carotene content, and average size of produced β-carotene nanodispersions were investigated. To be concluded, *Z*-isomer-rich β-carotene nanodispersions with the average size around 100 nm were successfully prepared using ultrasound-assisted SC-CO_2 with the addition of AITC. Notably, in this work, we first succeeded in developing one-step process for producing *Z*-isomer-rich β-carotene nanodispersions with no involvement of any organic solvents. The improvement of the process efficiency by adding AITC was confirmed, because 100 mg AITC addition led to the approximately 4-fold β-carotene content of that produced without AITC addition. The successful development of this system is prospective to solve the problems of residual organic solvents and complicated operation processes found in conventional processes.

Continuous production of *Z*-isomer-rich β-carotene nanodispersions using subcritical ethyl acetate and a swirl-type mixer

Unlike batch process, continuous production process is attracting increasing attention because it involves less human operation relating with higher efficiency and accuracy, and has lower containment probability and less scale-up effect than traditional batch process. Therefore, this work aimed to develop a continuous production process of *Z*-isomer-rich β-carotene nanodispersions, and the process can be further divided into two connected continuous process—*Z*-isomerization process and dispersion process.

In the *Z*-isomerization process, we challenged to *Z*-isomerize all-*E*-isomer-rich β-carotene into *Z*-isomer-rich β-carotene by thermal treatment in high temperature using subcritical ethyl acetate as the dissolving solvent. The effects of thermal treatment temperature (140–200 °C), thermal treatment time (30 s–5 min) and on the *Z*-isomer ratio and decomposition ratio of β-carotene were investigated. Due to the high decomposition ratio of β-carotene under high temperature treatment, the effects of the antioxidant α-tocopherol addition on the *Z*-isomer ratio and residual ratio of β-carotene were investigated. To be concluded, β-carotene with 60% *Z*-isomer was prepared after

extremely short-time treatment—30 seconds, and by adding α-tocopherol, the residual ratio of β-carotene was maintained at about 95%. To our best knowledge, this *Z*-isomerization method is more efficient than most reported methods. Additionally, the activation energy of β-carotene decomposition in subcritical ethyl acetate was calculated to help to understand the thermal decomposition property of β-carotene in subcritical ethyl acetate during practical use.

Z-Isomer-rich β-carotene solution produced in previous process was directly introduced into subsequent dispersion process. In the dispersion process, we exploited the use of swirl-type mixer which was designed and proved to be effective in producing uniform and small metal oxide nanoparticles in supercritical water as mentioned in **Chapter 4.1.3**. We used swirl-type mixer to disperse *Z*-isomer-rich β-carotene ethyl acetate solution into the water solution containing hydrophilic emulsifier. The effects of flow rate ratio of β-carotene/emulsifier solution, dispersion temperature, and dispersion pressure on β-carotene encapsulation efficiency, total *Z*-isomer ratio, and the average size of produced nanodispersions were investigated. Concluded, the flow rate ratio of 1:10 or 1:15, temperature of 60 °C and high pressure over than 15 MPa is appropriate for higher encapsulation efficiency and productivity in this dispersion system. However, these three parameters showed little influence on the average size of produced nanodispersions, where the produced nanodispersions all showed average particle size in range of 5–8 nm. The effects of *Z*-isomerization were investigated by comparing produced nanodispersions using *E*-isomer-rich and *Z*-isomer-rich β-carotene solution in this continuous system. *Z*-Isomerization significantly improved the encapsulation efficiency and total *Z*-isomer ratio, and reduced the average size of the produced nanodispersions. The produced *Z*-isomer-rich β-carotene nanodispersions showed much higher stability with the residual ratio of β-carotene remained up to 92% after 21-day storage at 4°C. Concluded, this continuous production system for producing *Z*-isomer-rich β-carotene nanodispersions is efficient in terms of both productivity and the functionality of produced nanodispersions, and it can be further used for other bioactive compounds nanodispersions production.

Acknowledgements

I would like to express my gratitude to my present supervisor—*Professor Seiichi Takami* and my previous supervisor—*Emeritus Professor Motonobu Goto* (Graduate School of Engineering, Nagoya University) for giving me this precious opportunity to pursue doctor degree in Nagoya University. Moreover, I would like to thank them for giving me support and professional suggestions on my doctoral thesis.

Then, I would like to give my appreciation to *Professor Armando T. Quitain* (International Research Organization for Advanced Science and Technology (IROAST), Kumamoto University), *Professor Kawajiri Yoshiaki* (Graduate School of Engineering, Nagoya University) who gave previous suggestions on my doctoral thesis. I want to express my gratitude to *Dr. Masaki Honda* (Faculty of Science & Technology, Meijo University) who provided me invaluable opportunity to do researches in his lab for several months, and gave me countless suggestions on my research and doctoral thesis.

Furthermore, I sincerely want to express my gratitude to *Dr. Hideki Kanda* (Graduate School of Engineering, Nagoya University) and *Dr. Wahyudiono* (Institute of Multidisciplinary Research for Advanced Materials, Tohoku University) for their kind suggestions on my research work and invaluable support to my research during my stay in Nagoya University.

Finally, I would like to express my gratitude to present Takami laboratory's members and previous Goto laboratory's members for showing inclusion to me and giving many precious advices in various aspects during my stay in Nagoya University.

ZHANG Yelin